العنوان:	CONTINUOUS SPATIAL DOMAIN IMAGE IDENTIFICATION AND RESTORATION WITH MULTICHANNEL APPLICATIONS
المؤلف الرئيسي:	Al Suwailem, Umar A.
مؤلفين آخرين:	Keller, James E.(super)
التاريخ الميلادي:	1996
موقع:	كولومبيا
الصفحات:	1 - 183
رقم MD:	616175
نوع المحتوى:	رسائل جامعية
اللغة:	English
الدرجة العلمية:	رسالة دكتوراه
الجامعة:	University of Missouri
الكلية:	The Graduate School
الدولة:	الولايات المتحدة الأمريكية
قواعد المعلومات:	Dissertations
مواضيع:	الهندسة الإلكترونية ، تطبيقات الحاسب ، ترميم الصور ، النمذجة ، الحركات الضبابية
رابط:	https://search.mandumah.com/Record/616175

CONTINUOUS SPATIAL DOMAIN
IMAGE IDENTIFICATION AND RESTORATION
WITH MULTICHANNEL APPLICATIONS

A Dissertation

presented to

the Faculty of the Graduate School

University of Missouri-Columbia

In Partial Fulfillment

of the Requirements for the Degree

Doctor of Philosophy

in Electrical and Computer Engineering

by

UMAR A. AL-SUWAILEM

Prof. James Keller, Dissertation Adviser

JULY, 1996

العنوان:	CONTINUOUS SPATIAL DOMAIN IMAGE IDENTIFICATION AND RESTORATION WITH MULTICHANNEL APPLICATIONS
المؤلف الرئيسي:	Al Suwailem, Umar A.
مؤلفين آخرين:	Keller, James E.(super)
التاريخ الميلادي:	1996
موقع:	كولومبيا
الصفحات:	1 - 183
رقم MD:	616175
نوع المحتوى:	رسائل جامعية
اللغة:	English
الدرجة العلمية:	رسالة دكتوراه
الجامعة:	University of Missouri
الكلية:	The Graduate School
الدولة:	الولايات المتحدة الأمريكية
قواعد المعلومات:	Dissertations
مواضيع:	الهندسة الإلكترونية ، تطبيقات الحاسب ، ترميم الصور ، النمذجة ، الحركات الضبابية
رابط:	https://search.mandumah.com/Record/616175

CHAPTER 1

INTRODUCTION

Images are produced for the purpose of recording, displaying, and analyzing useful information. Image processing is an essential and useful subject that has entered various fields in the real life today. It has important applications in the areas of education, medicine, industry, military, etc. The field of digital image processing can be divided into the following categories [73]:

1- Digitization and compression: Representing the image in a suitable and efficient format for further processing and manipulation.

2- Enhancement, identification, restoration, and reconstruction: Upgrading and improving the distorted data by reducing artifacts and corruption.

3- Matching, description, and recognition: Measuring properties and relationships between images or different parts of an image, and classifying image objects.

The subject of this thesis deals mainly with the second category, namely, blur identification and image restoration. The field of image restoration, sometimes

1

referred to as image deblurring, is concerned with the construction or estimation of the original image from a corrupted one. Basically, it tries to perform an inverting operation that will produce an image that is "as close as possible" to the original one. In doing so, the restoration methods assume that the characteristics of the degrading system and the noise are known *a priori*. However, in practice, one usually has hardly enough knowledge to obtain this information directly from the image formation process. The aim of the other related field, image identification, is to estimate the properties of the imperfect imaging system from the observed image itself prior to the restoration process [42]. Thus, the two problems are related to each other in the sense that good restoration results depend on how accurate the identified parameters are to the actual situation.

The available literature indicates that the field of image restoration has gained much more attention than the field of identification. Although this is true for the monochrome case, neither of the two fields has adequately been studied in the multichannel case, i.e., the parameter identification and restoration of, say, color or multispectral images. In fact, there is not any comprehensive study today that discusses the identification process in the multichannel case. One of the main purposes of this research is to investigate some novel identification techniques and their implementations in the monochrome and multichannel image processing.

1.1 Image Restoration

The process of image restoration is the process of obtaining the original image from a distorted and noisy one. This process involves using *a priori* knowledge available about the original image, mainly the point spread function (PSF) and the

noise statistics, which are either assumed or given. The PSF describes the characteristics of the degradation in the imaging system. For example, it may be known that an image has gone through a certain degradation, or it can be assumed from its appearance to have suffered from a well-known degradation.

Suppose that the image formation can be adequately described by a linear spatially invariant relation and that the noise is additive. The observed image $r(m,n)$ is then given as

$$r(m,n) = s(m,n)*h(m,n) + v(m,n) \tag{1.1}$$

where (*) denotes 2-D convolution, $s(m,n)$ represent the original (ideal) image, $h(m,n)$ is the degradation point spread function of the image formation system, and $v(m,n)$ is the noise in the observed image. This modeling will be fully discussed in chapter 2. The restoration scheme is represented in the Figure (1.1) where $\hat{s}(m,n)$ is the restored or estimated image.
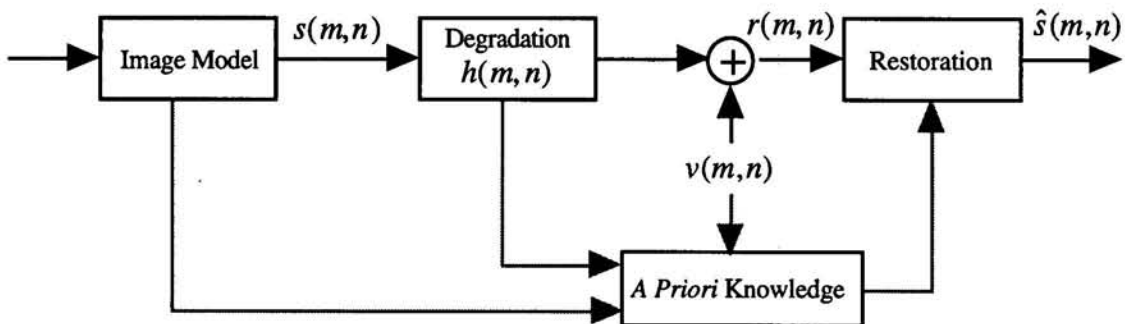
Figure 1.1 *A priori* restoration scheme. Knowledge about the image formation model, degradation, and noise is used in the restoration process.

1.2 Image Identification

Image identification (sometimes called blur identification or image-blur identification) refers to the process of estimating the parameters of the blur, noise and the original image in order to use them in restoring the original image. The combined process of identification and restoration of the image is sometimes referred to as *a posteriori* restoration. Figure 1.2 shows the schematic representation of this process. In the figure it is shown that prior to the restoration process, the characteristic of the blur (i.e. the PSF = $h(i,j)$), and some statistical properties of the noise and the original image must be estimated.
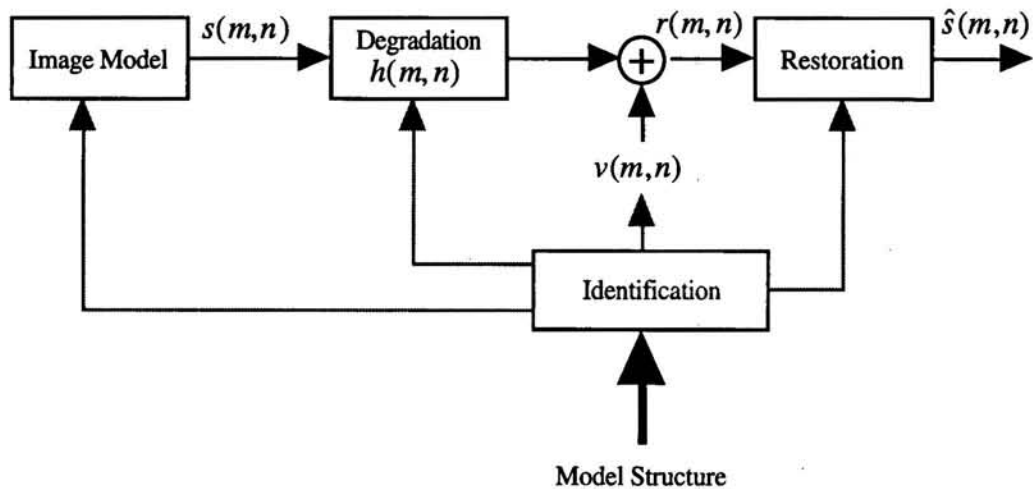
Figure 1.2 A *posteriori* identification and restoration scheme. The image model, blur, and noise are estimated prior to the restoration.

4

The quality of the estimated parameters and the performance of the identification algorithm can only be evaluated after the restoration is done. This is due to the fact that each parameter contains some estimation errors. Thus, the overall image identification process must be conjunct with the restoration problem for accurate evaluation.

The success of the restoration process in a given application depends on how close the assumed mathematical model is to the real degradation. In most real applications, the cause of the blur is not known. Thus, the first step is to identify the kind of blur the image has suffered. This is very difficult if the a priori information about the source of the blur and noise is not available.

In practice, it is assumed that the blur is either due to out-of-focus or relative motion between the object and the camera, since they are the most common causes of blur in image processing [61]. These blurs can be modeled as a function of one parameter. In other cases, blur can be modeled as a function of a number of parameters, in which case, the blur identification problem reduces to the estimation of these parameters [61].

1.3 The Degradations

During the process of image formation, some types of distortion and degradation alter the original image. There are many causes of this degradation that can be categorized mainly as blurs and noise. Normally, blurs are due to lens aberrations, diffraction effects of finite apertures, atmospheric turbulence, and/or relative motion(s) between object and the optical system. A blurred image is usually modeled as the linear convolution of the ideal image with the point spread function

(PSF) of the blur. On the other hand, noise is due to imperfections in the transmission medium, the recording medium, measurement errors, and/or quantization. The observation noise is usually assumed to be additive white Gaussian noise that is independent of the signal. Mathematically, degradation can be classified as point (e.g. additive noise), and spatial degradation (e.g. loss of resolution due to the integration of the imaging system) [19]. In chapter 2 we will discuss the modeling of the blur and noise in more detail.

1.4 Literature Review

In this section we review the research and development in the field of image restoration and identification. First we mention the available studies in this field for the single channel or monochrome images, then we provide a similar review for the multichannel and color imaging.

1.4.1 Restoration Methods

In the past three decades, a considerable amount of research has been performed on developing restoration filters and algorithms based on using *a priori* knowledge. The restoration process is an ill-posed problem where the solution involves finding the inverse of the imaging process [3,17,19,56]. Among the simplest approaches for image restoration is inverse filtering [3,29]. In this case, the restoration process is implemented simply by convolving the observed blurred image with the inverse of the PSF of the blur (or in the frequency domain multiplying it by

6

the transfer function of the inverse of the PSF). Unfortunately, this method can only be used if the inverse of the blur PSF exists and the noise is negligible. These conditions make this approach, in practice, limited to few applications.

A more practical approach is the linear minimum mean square error (LMMSE) methods, in which the mean square error between the estimate and the ideal image is minimized. One class of these filters is the famous Wiener filter in which the power spectrum of the ideal image is assumed to be known [3,24]. Another class is the constrained least square filters which are usually implemented in the frequency domain [26]. A third class that is extensively used is the recursive Kalman filter in 2-D which is implemented in the spatial domain [12,95,96].

Iterative techniques use a more practical approach in which the restoration scheme is terminated prior to convergence. The advantages of such techniques is that no matrix inversion is required, extension to more complex models is attainable, and they allow the possibility of inspecting the results in steps [35].

Spatially adaptive techniques are used to restore images that are dependent on the local image content [30]. In [52], a minimum-error minimum correlation criterion is implemented in conjunction with an adaptive windowing technique to restore noisy images adaptively. A different approach using generalized cross-validation criterion (GCV) is implemented [69,70]. In this approach, space-variant regularization and data error terms are incorporated and an efficient method for estimating the GCV criterion using image restoration techniques is presented. Tekalp and Kaufman [84] provide an extensive review of some adaptive restoration methods.

In such adaptive techniques, the artifacts of ringing (the undesired regular patterns that normally appear in the image after the restoration process) can be significantly reduced, as demonstrated by [43,86]. In [55], a regularized

7

constrained total least squares approach is used to solve a set of perturbed linear equations that describes the distorted image. In a recent paper [1], the ringing problem is tackled by padding the image with a reflected version of itself which produces visually accepted results.

Deterministic approaches in image restoration involve the use of *deterministic a priori* knowledge about the original image and the noise. This knowledge is formulated as (nonlinear) constraints on the restored image [80,99]. Then, by using an iterative technique known as the method of projection onto convex sets (POCS), an image is found satisfying all the a priori constraints [91]. The use of deterministic knowledge with spatial adaptivity have been proposed in [43,46] where a constrained iterative optimization strategy is employed.

In summary, restoration filters or processes can be categorized as stochastic or deterministic. Stochastic restoration assumes the signal involved in the system as random processes. The minimum mean square error (MMSE), the maximum entropy (ME) are just two examples of such restoration filters. Deterministic restoration assumes the signals involved as deterministic with some constraints as in the methods of least square criterion and POCS.

Computationally, the above filters can be categorized as linear/nonlinear, iterative/noniterative, and recursive/nonrecursive, depending on the implementation method. For example, Wiener filters which are based on the MMSE criterion can be implemented both iteratively and noniteratively. Andrews and Hunt, and Jain [3,29] provide an intensive review of the above classification. Sezan and Tekalp [81] discus recent developments of the above techniques.

Image restoration has also been approached by fairly new emerging technologies such as fuzzy sets [15], neural networks [18,103], mathematical morphology [21], and wavelets [9,10].

1.4.2 Image Identification methods

From the available literature it could be said that restoration filters and algorithms have received a great deal of attention. However, the related field of research of image identification has received little emphasis, in spite of its importance and practicality.

The earliest work on blur identification started with estimating the point spread function (PSF) of the image using some analytic characteristics of the imaging system. An example of such an approach is the use of spectral and cepstral techniques to approximate the PSF. Since the location of poles and zeros uniquely determines the characteristic functions, in such techniques the PSF is reconstructed by observing the location of regular pattern of zeros on the unit bicircle [14]. Shortcomings of such methods include limitation to certain types of PSFs, and neglecting the presence of noise.

To overcome such limitations, more general approaches based on the maximum likelihood (ML) parameter estimation were extensively investigated. A class of image identification methods that can handle a wider range of PSFs was introduced in [85], in which a 2-D autoregressive moving average model (ARMA) was assumed. Solution techniques that identify the parameters of this model were proposed in several papers. These techniques are: 2-D recursive methods proposed by [85], parallel banks of 1-D ARMA processes [13], and gradient-based optimization algorithms proposed by [45]. Most of these techniques initially neglected the effect of noise which limit their use to images with high signal-to-noise ratio (SNR).

Lagendijk *et al.* [41,44] introduced identification methods that use the maximum likelihood approach and incorporate the effect of noise. Solution

algorithms based on gradient-based optimization algorithms [45], Kalman filtering [6], and the expectation-maximization (EM) method [16] were implemented to optimize the nonlinear ML function. The advantage of the latter is to avoid operating directly on the nonlinear likelihood function by alternating between a relatively simple identification problem and the restoration of the blurred image. It was shown by Lagendijk *et al.* [47] that most of these techniques are different implementations of the same maximum likelihood estimator resulting from different modeling assumptions and/or considerations about the computational complexity. New advances in the EM method included applications to the causal and semicausal AR models [97], MAP restoration using Gibbs prior density functions [23], implementation in the frequency domain [2,48]. Recently, Kim and Woods [38] proposed a modified EM model in the subband domain that is less sensitive to initial conditions.

In a recent work, Pavlovic´ and Tekalp [63] proposed a different formulation for the ML method blur identification problem, based on modeling the blur in the continuous domain. This method completely overcomes the major limitations encountered in the existing techniques which are exclusively based on discrete blur models, namely:

i) The ML estimates of the extents of the PSF have to be guessed in order to identify the parameters.

ii) The likelihood function (LF) to be maximized is highly nonlinear which requires numerical optimization to solve it. Moreover, convergence to the global maximum cannot be guaranteed.

We will review this formulation proposed by Pavlovic´ and Tekalp for the single channel case in chapter 4. This model forms the basis of our extension to the multichannel case.

10

Other techniques are based on residual spectral matching in which the PSF is chosen from a collection of candidate PSFs to provide the best match between the restoration and the expected residual spectra given that the candidate PSF is the true one [75]. Reeves and Mersereau in [71], extended the success of the generalized cross-validation technique in image restoration to the case of image and blur identification. A space-adaptive regularization approach for joint blur identification and image restoration is introduced in [98]. This approach effectively utilizes the piecewise smoothness of both the image and the PSF, however, the scaling problem inherent to the cost function can be unstable and sensitive to convergence parameters.

1.4.3 Multichannel Identification and Restoration

Multichannel images refer to the type of data obtained from multiple frequency bands, multiple time frames, or multiple sensors. Such images have numerous applications in practice. Their importance stems from the need for multiframe processing, and color or multispectral imaging in different fields such as medical diagnosis, forensic sciences, industrial automation, space and satellite imagery. It is important to note that filtering multispectral images and image sequences have certain similarities. Image sequences can have a time index to represent the temporal correlation rather than the spectral correlation. For the sake of terminology, we are going to use the term multichannel throughout this study to refer to an image obtained by an imaging system that uses more than one sensor for the same scene. Although our formulation will be applied to multispectral cases, it is also extendible to temporal cases.

Processing multichannel images, such as smoothing, restoration, and enhancement is an important step before any further use or analysis. The degradation sources for the single channel case, mentioned in section 1.3, apply to the multichannel case, too. However, an additional and important type of degradation that is natural to the multichannel imaging is cross-channel or cross-spectral degradation. The main cause of such distortion is the overlapping in the cutoff frequency characteristics of the detectors that result in cross-spectral mixing of adjacent spectral bands [20]. It is important to note that the amount of degradation may vary from one spectral component to the other. It has been shown by Bescos *et al.* [11] that chromatic aberrations produce different amounts of blur in the spectral components. However, it can be assumed that relative motion and out-of-focus blur result in equal amounts of blur in the spectral components [87]. These amounts need to be estimated for more reliable multichannel restoration.

As in the single channel case, the multichannel identification techniques have not received much attention as the restoration techniques have. As a matter of fact, even the restoration techniques for multichannel imaging have not received much attention. Although it seems a straightforward extension of the single channel methods, the lack of multichannel image processing theories, the complexity of the computation involved, and the consideration of the mutual relation of the cross-spectral effects between frames make the problem more difficult.

In general, restoring each channel independently does not necessarily produce useful results because of neglecting the information between the channels. Following this approach, Bescos *et al.* [11] applied conventional restoration techniques to individual color components without using the cross-channel information. Also, Angwin and Kaufman [5] presented adaptive filtering for color images without taking into account the correlation between the color components.

12

This resulted in a suboptimal solution. Thus, solutions which are optimal for the single channel case may be suboptimal for the multichannel image when restored independently. For example, a signal that is weak in one single image channel that may not be detected using single channel processing techniques can be detected using a multichannel scheme that incorporates the existence of that signal in the other channels [20].

Most of the available techniques in the literature today follow one of two approaches for optimal filtering of multichannel images. The first approach is to apply a spectral transformation that approximately uncorrelates the channels. Then, independent filtering in the transform domain can be applied. The second approach is to model the correlation between the channels, and incorporate this model explicitly into the filtering procedure [87].

One of the early works for multichannel restoration that follows the first approach was developed by Hunt and Kubler [27] using the Karhunen-Loeve transformation. In their scheme, it was assumed that the signal autocorrelation describing the between-channel (or spectral), and the within-channel (or spatial) relationship was separable. However, this procedure did not result in an optimal solution. Although it was assumed that the spectral and spatial correlation were separable, the transformation resulted in spectrally correlated noise. The independent filtering in the transform domain did not take this noise into account. Ohyama *et al.* [58] used the Hunt and Kubler approach by including only spatial blur and employing the least-squares filtering techniques.

Following the other approach, modeling the correlation between the channels and incorporating it explicitly into the filtering procedure, Pavlovic' and Tekalp [87] employed this approach using the Kalman filtering and least squares parameter identification of the image parameters. In an extensive study of this problem,

13

Galatsanos [19] presented and applied this approach using a very efficient and feasible computation algorithms including Wiener, Kalman, and least squares techniques. However, in this work, blur parameters were assumed to be known.

Katsaggelos in [33] modeled the image as an ideal one (using the AR model) with different blurs and used a least squares approach to estimate the ideal image. In [64], a multichannel AR model was introduced and experimented in segmenting texture images. A general framework for relating the single channel to the multichannel representation in the frequency domain was proposed in [36]. In [4], a multichannel Wiener filter was proposed in both the spatial and frequency domains that showed a reduction in computation over other methods.

Some other related work to multichannel imaging included color image enhancement and segmentation [65], structured regularization to reduce some artifacts [100], and use of cumulants (higher-order spectra) to identify color images [101,102]. In a recent paper [77], a Gibbs prior multispectral image model for use in Bayesian MAP estimation is proposed by incorporating spatial and spectral components. However, most of those papers discussed the restoration process and did not address the identification part fully.

1.5 Motivation and Research Objectives

Up-to-date techniques that study the multichannel identification problem are very limited and rare. Almost all of the above research deals with restoration techniques of multichannel images rather than the identification process. As mentioned above, the most extensive study of multichannel image restoration

14

available is by Galatsanos [19]. However, it does not address the identification issue, either. Thus, this area needs to be extensively studied.

In this research we will be considering blur identification of multichannel images using the ML parametric approach by modeling the process in the continuous spatial domain. Since this modeling overcame the limitations of the existing ML techniques in the monochrome case as demonstrated in [63,61], it is expected to behave the same in the multichannel one, thus improving the identification and the restoration process.

Considering the two familiar types of blur that can be represented in a closed form parametric description in the continuous domain, the 1-D uniform motion blur and the 2-D out of focus blur, we will be studying multichannel blur identification and restoration using synthetic and real images. In both cases, the effect of noise will be included.

By implementing some restoration methods available for multichannel imaging, the identified parameters will be used to restore the image and compare it to the case of applying the restoration techniques alone. Employing the cross-channel information will be an important factor in the modeling. The incorporation of this degradation will be investigated to see which approach should be used for better results.

The steps of the research and the organization of the thesis will be in the following order. First, the mathematical models will be developed in chapter 2 for the blurring effects, the noise, and the original image. Modeling the multichannel case will be discussed. Also, some computational considerations for the purpose of implementation will be reviewed.

In chapter 3, we will review some monochrome restoration techniques that will be used after the identification step, since the evaluation of the identification method

15

has to be in conjunction with the final restoration result. We will review two widely used restoration methods, namely, Wiener and Kalman filters.

In chapter 4, we will present the derivation for identifying blurred images in the single channel or monochrome case using the continuous spatial domain model in [63]. The identification of images blurred by uniform motion or out-of-focus degradations will be shown and the advantage of this method will be discussed. Applying this method to a linear motion in an orthogonal direction will be also investigated. We will show that general linear motion blur can be recovered by the identification of the blur in two orthogonal directions. Also, the effect of noise in the performance of the identification will be considered.

Some important concepts of the multichannel imaging will be considered in chapter 5. We will review different models used in color imaging and investigate the correlation between the channels. Independent and multichannel approaches that are used for restoring multichannel images will be also discussed.

In chapter 6, we will develop the formulation and derivations of blur identification for multichannel images following the models discussed in chapter 2 and extend the method used in the single channel case of chapter 4. The effects of noise and cross-channel components will be discussed. Experimental results using color images, for both the uniform motion and out-of-focus blur cases, will be given and compared with some existing methods.

Finally, in chapter 7, we will summarize the results and give some suggestions for future research.

العنوان:	CONTINUOUS SPATIAL DOMAIN IMAGE IDENTIFICATION AND RESTORATION WITH MULTICHANNEL APPLICATIONS
المؤلف الرئيسي:	Al Suwailem, Umar A.
مؤلفين آخرين:	Keller, James E.(super)
التاريخ الميلادي:	1996
موقع:	كولومبيا
الصفحات:	1 - 183
رقم MD:	616175
نوع المحتوى:	رسائل جامعية
اللغة:	English
الدرجة العلمية:	رسالة دكتوراه
الجامعة:	University of Missouri
الكلية:	The Graduate School
الدولة:	الولايات المتحدة الأمريكية
قواعد المعلومات:	Dissertations
مواضيع:	الهندسة الإلكترونية ، تطبيقات الحاسب ، ترميم الصور ، النمذجة ، الحركات الضبابية
رابط:	https://search.mandumah.com/Record/616175

CHAPTER 2

MODELING

Mathematical models that represent the real-world process involved in the generation, formation and recording of images are crucially needed to handle image identification and restoration problems. Normally, the imaging systems inherit some degradation in the form of blur and noise. Thus, formulating mathematical representations that reflect these degradations, as well as a statistical model of the ideal image, is the first step required before any further processing. It could be said that without such knowledge, the identification and restoration of a degraded image may not be accomplished.

In general, the determination of suitable analytical models is not a trivial task. It requires careful considerations of the level of abstraction that is acceptable for the application considered. Too simple a model may lead to a computationally elegant algorithm, but with no practical relevance. On the other hand, a very detailed model which does describe the real processes involved often requires complex algorithms that are impractical to compute [42].

17

In this chapter, we will review some modeling aspects of noisy, blurred images for the development of identification and restoration techniques. We first discuss the formulation of the autoregressive model and its properties in 1-D; then we extend this to the 2-D case. In section 2.3 we reflect this formulation onto image formation modeling. In sections 2.4 and 2.5 we discuss the modeling of blur and noise, respectively. The overall modeling of the observed image is given in section 2.6. Then, we develop, in section 2.7, modeling of image formation and observation in the multichannel case including cross-spectral effects. Some common types of blur are discussed in section 2.8. Finally, in section 2.9, some aspects for computation and implementation are considered.

2.1   Autoregressive (AR) Models in One Dimension (1-D)

A one-dimensional (1-D) shift invariant system is called causal if its output at any time is not affected by future inputs. A causal zero mean random sequence $s(n)$ is called an autoregressive of order p when it can be generated as the output of the following system

$$s(n) = \sum_{k=1}^{p} c(k)s(n-k) + \varepsilon(n) \quad \forall n \tag{2.1a}$$

$$E[\varepsilon(n)] = 0 , \quad E\{[\varepsilon(n)]^2\} = \sigma_\varepsilon^2 , \quad E[\varepsilon(n)s(m)] = 0 , \quad m < n \tag{2.1b}$$

where $\varepsilon(n)$ is a stationary zero mean input sequence that is independent of past outputs, and $s(n) = 0$ for $n \leq 0$. This system uses the most recent p outputs and the current input to generate recursively the next output as shown in Figure 2.1a [29,53].

18
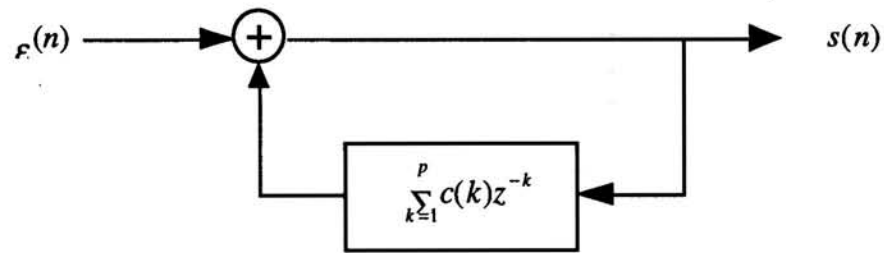
(a) AR Sequence Realization
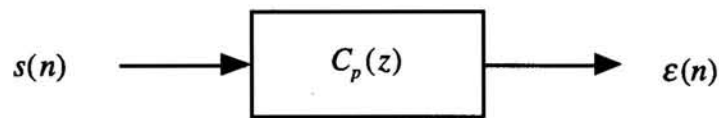
(b) Prediction Error Filter

Figure 2.1 pth Order AR Model

Autoregressive models have special significance in signal and image processing because they possess the following two important properties:

Property I: Causal minimum variance representation

The quantity defined by

$$\bar{s}(n) \underline{\Delta} \sum_{k=1}^{p} c(k)\, s(n-k) \qquad (2.2)$$

represents the best linear mean square prediction of $s(n)$ based on all its past values but depends only on the previous p samples. Thus, we may rewrite (2.1a) as

19

$$s(n) = \bar{s}(n) + \varepsilon(n) \tag{2.3}$$

which says that the sample at n is the sum of its minimum variance, causal, prediction estimate plus the prediction error $\varepsilon(n)$. Because of this property an AR model is sometimes called a causal minimum variance representation (MVR). The causal filter defined by

$$C_p(z) \triangleq 1 - \sum_{n=1}^{p} c(n) z^{-n} \tag{2.4}$$

is called the prediction error filter which generates the prediction error sequence $\varepsilon(n)$ from the sequence $s(n)$, as shown in Figure 2.1b. Also, $\varepsilon(n)$ is white, that is,

$$E[\varepsilon(n)\varepsilon(m)] = \sigma_\varepsilon^2 \, \delta(n-m) \tag{2.5}$$

Property II: Identification of AR models

The parameters $c(k)$ and σ_ε^2 can be easily identified by solving a set of equations. Multiplying both sides of (2.1a) by $\varepsilon(m)$ and taking expectations we have

$$E[s(n)\varepsilon(m)] = E\left[\left\{\sum_{k=1}^{p} c(k)s(n-k)\right\}\varepsilon(m)\right] + E[\varepsilon(n)\varepsilon(m)] \quad m \geq n \tag{2.6}$$

The first term to the right of the equal sign is equal to zero from (2.1b). Thus by using (2.5) we get

$$E[s(n)\varepsilon(m)] = E[\varepsilon(n)\varepsilon(m)] = \sigma_\varepsilon^2 \, \delta(n-m)$$

Now multiplying both sides of (2.1a) by $s(0)$ and taking expectations we have

20

$$E[s(n)s(0)] = E\left[\left\{\sum_{k=1}^{p} c(k)s(n-k)\right\}s(0)\right] + E[\varepsilon(n)s(0)]$$

Defining the covariance function of $s(n)$ as

$$r(n) \triangleq E[s(n)s(0)] \tag{2.7}$$

we get

$$r(n) - \sum_{k=1}^{p} c(k)r(n-k) = \sigma_\varepsilon^2 \delta(n) \qquad \forall n \geq 0 \tag{2.8}$$

since

$$E\left[\left\{\sum_{k=1}^{p} c(k)s(n-k)\right\}s(0)\right] = \sum_{k=1}^{p} c(k)r(n-k)$$

This result is important for identifying $c(k)$ and σ_ε^2 for a given set of covariances $\{r(n), -p \leq n \leq p\}$. In fact, solving (2.8) uniquely determines pth order AR model for $n = 0,1,...,p$ [29]. This formulation has powerful implications when applied to image modeling as we will see next.

2.2 AR Models in Two Dimension (2-D)

Extending the formulations in the previous section to 2-D case, we have [29,28,32]

$$s(m,n) = \sum_{(k,l) \in S_c} c(k,l)\, s(m-k,n-l) + w(m,n) \tag{2.9}$$

where $c(k,l)$ are called the modeling or predictor coefficients and S_c is a subset of the 2-D lattice called the prediction region, or the model support. Here, $w(m,n)$ is a zero

21

mean white Gaussian process with variance σ_w^2 independent of $s(m,n)$. Also, $c(k,l)$ denotes the minimum mean squared error (MMSE) which are computed by minimizing the variance of the noise process σ_w^2. From 2.9 we have

$$
\begin{aligned}
\sigma_w^2 &= E\left[w^2(m,n)\right] \\
&= E\left[\left\{s(m,n) - \sum_{(k,l)\in S_c} c(k,l)\; s(m-k,n-l)\right\}^2\right]
\end{aligned}
\tag{2.10}
$$

We need to minimize this with respect to $c(k,l)$ for $(k,l)\in \mathbf{S}_c$. This is according to the causal minimum variance representation property explained in the previous section. From the orthogonality principal [60], the MMSE is achieved when the error is orthogonal to the signal, i.e.,

$$
E\left[w(m,n)\; s(m-i,n-j)\right] = 0 \qquad \text{for} \qquad (i,j)\in S_c
\tag{2.11}
$$

Note that $E\left[w(m,n)\; s(m-i,n-j)\right]$ at $(i,j)=(0,0)$ is equal to σ_w^2, since

$$
\begin{aligned}
E\left[w(m,n)\; s(m-i,n-j)\right]\Big|_{i=j=0} &= E[w(m,n)s(m,n)] \\
&= E[w(m,n)\{\sum_{(k,l)\in S_c} c(k,l)\; s(m-k,n-l) + w(m,n)\}] \\
&= E[w^2(m,n)] + E[w(m,n)\sum_{(k,l)\in S_c} c(k,l)\; s(m-k,n-l)] \\
&= \sigma_w^2
\end{aligned}
\tag{2.12}
$$

Substituting from (2.9) into (2.11) we have

$$
E\left[\left\{s(m,n) - \sum_{(k,l)\in S_c} c(k,l)\; s(m-k,n-l)\right\}s(m-i,n-j)\right] = 0
\tag{2.13}
$$

or

22

$$E[s(m,n)s(m-i,n-j)] = E\left[\left\{\sum_{(k,l)\in S_c} c(k,l)\ s(m-k,n-l)\right\}s(m-i,n-j)\right]$$

Rewriting these equations we have

$$p_{ss}(i,j) = \sum_{(k,l)\in S_c} c(k,l)\ p_{ss}(i-k,j-l) \qquad \forall(i,j)\in S_c \qquad (2.14)$$

and using (2.12)

$$\sigma_w^2 = p_{ss}(0,0) - \sum_{(k,l)\in S_c} c(k,l)\ p_{ss}(k,l) \qquad (2.15)$$

where we have used the definition of the autocorrelation coefficients as

$$p_{ss}(i,j) = E[s(m,n)\ s(m-i,n-j)] \qquad (2.16)$$

Thus, from this set of linear equations, the modeling coefficients $c(k,l)$ and σ_w^2 can be determined [42].

2.3 Modeling the Ideal Image

Many image identification and restoration techniques make use of a priori knowledge about the ideal image. In some cases it is sufficient to characterize an image by its mean and covariance functions. For some other cases it is more convenient to characterize an image as the output of linear system driven by a white random field, i.e. AR model [61], as explained in the previous section.

In view of the experimental results obtained by many researchers in this field [28,29,42,61], AR models are commonly used as a powerful modeling characterization of the original image. As in equation (2.9),

$$s(m,n) = \sum_{(k,l) \in S_c} c(k,l) \, s(m-k,n-l) + w(m,n)$$

$$= c(m,n) * s(m,n) + w(m,n)$$

(2.17)

where ($*$) indicates convolution in 2-D and $c(k,l)$ denotes the MMSE image model coefficients which are computed by minimizing the noise variance σ_w^2. In this respect, $w(m,n)$ is viewed as the modeling error between a complex real-world image and the relatively simple autoregressive process fitted onto this data [42].

Different models result from different choices of the support S_c. Some common choices for the model support are:

1. Quarter plane (QP)

    $$S_{c1} = \{(k,l): (k \geq 0, l \geq 0) \cap (k+l > 0)\}$$

2. Non-symmetric half plane (NSHP)

    $$S_{c2} = \{(k,l): (k > 0, l \leq 0) \cup (k \geq 0, l > 0)\}$$

3. Semicausal half plane (HP)

    $$S_{c3} = \{(k,l): (k > 0, \forall l) \cup (k = 0, \forall l \neq 0)\}$$
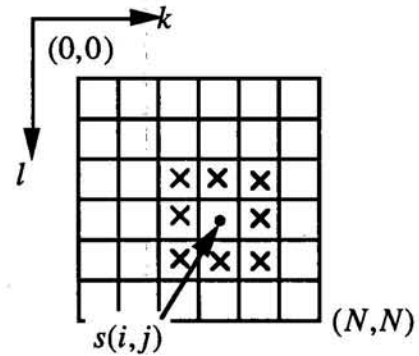
4. Non-causal full plane (FP)

    $$S_{c4} = \{(k,l): \forall(k,l) \neq (0,0)\}$$

    (2.18)

Experimental evidence shows that the order of the image model, i.e. the size of the support S_c, is not very critical in an image restoration setting. For this reason it is adequate to restrict the size to first order models, i.e. $k = l = 1$ [42]. Thus, the choice of certain support determines the number of modeling coefficients used which need to be evaluated from (2.14) and (2.15). Figure 2.2 shows the model support for $k = l = 1$.

24

Figure 2.2 Four different model supports of first order for the case of $k = l = 1$.

2.4   Modeling the Blur

Image recording systems are never perfect; both deterministic and statistical distortions are introduced in general. Deterministic degradations introduced by the imaging process may be very complex for several reasons. First of all, some 3-D features such as 3-D rotation of an object, parallax and 3-D geometry effects, may not be fully captured. Secondly, the transfer function of the imaging system may be very complex due to diffraction effects in optical systems, system aberrations, atmospheric turbulence, motion blurs and defocused lenses. Also, the severity of those imperfections may vary along the image (i.e. spatially varying blur). Finally, the non-linear behavior due to the response of the sensor may introduce further degradations [42]. We will restrict our discussion to 2-D degradation, since 3-D degradation are essentially impossible to model and restore.

Practically, the nonlinear behavior of the image sensor is ignored. This is not considered an oversimplification of the real problem for the following reasons. It has been shown that the linearization of the logarithmic behavior of a photographic medium is realistic when the image is of low contrast [3]. That is, if the image high frequency components (such as edges and line patterns) are considerably minimal, then the linear approximation of the sensor is practically acceptable. Sometimes this linearization is not possible; in such cases there are several ways to handle the nonlinearity.

The first approach is to incorporate the nonlinear response of the image sensor into the image observation model. In [3], Andrews and Hunt modeled the nonlinearity as a pointwise memoryless function D $\{\bullet\}$ of the image sensor. Unfortunately, such a model may yield complex, or even implementionally impossible restoration algorithms [92]. A second, but more practical, approach is to apply the inverse sensor response

26

(i.e. the inverse of the transfer function of the sensor response) to the observed image before any further processing is done. This means a pre-processing step that involves the elimination of the nonlinearity is applied when the characteristics of the sensor are given. Another approach is to use a more accurate model of the blur, such as using the principles of geometrical and physical optics [49,50]. However, Sezan, *et al.* [79] showed that restoration in the presence of noise does not benefit much from this higher accuracy representation.

From the above discussion we learn that in many practical cases it is justifiable to restrict the modeling of the image formation system to the usually dominant effects of blurring [42]. That is, it is acceptable to assume that the main factor of degradation, besides noise, is blurring and not system nonlinearity. Thus the entire process becomes a linear system characterized by a 2-D point spread function (PSF) $h(x,y;\xi,\eta)$ [3,29,42] and given by a 2-D superposition integral, i.e.,

$$r(x,y) = \int\limits_{-\infty}^{\infty} \int\limits_{-\infty}^{\infty} h(x,y;\xi,\eta)s(\xi,\eta) \, d\xi d\eta \qquad (2.19)$$

where $r(x,y)$ is the observed blurred image and $s(x,y)$ is the original image. Unfortunately this model is not very useful for processing purposes because of the complexity involved. It is computationally impractical to have a different PSF, $h(x,y;\xi,\eta)$, at each coordinate (x,y) of the image. Moreover, it is unrealistic to assume that one will be able to estimate these PSF's because of the lack of sufficient information for the estimation procedures. Therefore, it is generally assumed that the PSF of the image formation process is stationary or spatially invariant over (or at least a significant portion of) the image. Thus, (2.19) can be written as

$$r(x,y) = \int_{-\infty}^{\infty} \int_{-\infty}^{\infty} h(x-\xi, y-\eta) s(\xi, \eta) \, d\xi d\eta$$

$$= \int_{-\infty}^{\infty} \int_{-\infty}^{\infty} h(\xi, \eta) s(x-\xi, y-\eta) \, d\xi d\eta \qquad (2.20)$$

$$= h(x,y) * s(x,y)$$

where ($*$) denotes 2-D convolution. In discrete form we may write (2.20) as

$$r(m,n) = \sum_{k=-\infty}^{\infty} \sum_{l=-\infty}^{\infty} h(k,l) \, s(m-k, n-l) \qquad (2.21)$$

This is the general expression for a 2-D discrete convolution in which the PSF has infinite support. However, in real life, the observed image at the position (m,n) is only affected by values in a small neighborhood of (m,n). As a matter of fact, the correlation between image pixels drops significantly with distance [61]. Thus, without loss of generality, we may rewrite (2.21) with a finite PSF

$$r(m,n) = \sum_{k=-k_1}^{k_2} \sum_{l=-l_1}^{l_2} h(k,l) \, s(m-k, n-l)$$

$$= \sum_{(k,l) \in S_h} h(k,l) \, s(m-k, n-l) \qquad (2.22)$$

where S_h denotes the support of the PSF, i.e. the finite extent region where $h(k,l) \neq 0$ which may have any shape but is normally noncausal (see section 2.3). This implies that $r(m,n)$ is a function of both past and future pixels with respect to most definitions of causality in 2-D [96,95,42].

2.5 Modeling the Noise

Besides the deterministic distortions described in section 2.4, images are also degraded by stochastic degradations known as noise. There are many sources of observation noise in image processing. They could come from the sensing characteristics, quantizing, scanning, and/or recording. Pavlovic [61] provides an extensive discussion of this issue.

The digitization of images introduces quantization noise which reflects the error between the actual value and the quantized value. Normally, it is assumed that the quantization noise is an independent, additive, zero-mean, white Gaussian random process with power 40 dB below the image signal power [61].

The recording device, e.g. a charged-coupled device (CCD) camera, may also produce noise such as input photon noise and output amplifier thermal noise. Also, the recording medium, such as photographic films and papers, contribute some noise known as grain noise. Another type of noise is impulse noise. It is caused by small specks of dust on the film during exposure or scanning. The effect of this noise is most noticeable in the image after it has been restored.

For practical uses, the combined effects of these noise sources can be modeled in the domain where they are additive, by a white Gaussian random process, independent of the signal, with zero-mean and unknown variance [3,29,61]. This is a practical simplification since impulse noise and noise due to photon statistics are not uncorrelated and may not be additive. Nevertheless, such simplification leads to identification and restoration methods that apply to a wide class of problems [42].

In a recent paper [68], a parametric noise model was approximated by a generalized p-Gaussian family of probability density functions. However, this

more accurate modeling may produce better results for a small class of problems at the expense of more computations.

Noise constitutes an important limitation in the identification and restoration of images. The amount of noise present in an observed image is given by the (blurred) signal-to-noise ratio:

$$\text{SNR} = 10\log_{10}\frac{(\text{variance of the blurred image})}{(\text{variance of the noise})} \quad \text{in (dB)} \tag{2.23}$$

When images are digitally recorded and/or stored, the signal-to-noise ratio encountered in practice is at most 40 to 50 dB. In this case, the noise is not visible [42]. For very low SNR's the degradation effects of the noise is more prominent than those of the blurring. For the severe cases of 10 to 20 dB SNR, the regular image identification and restoration algorithms are no longer useful because, at these levels, the duty of the restoration becomes mainly smoothing out the noise rather than performing any restoration [42].

2.6 The Overall Observation Model

We may now formulate the overall observation model that describes and incorporates the blurring model (equation 2.22) and the additive noise model. Thus, the complete image observation model becomes

$$r(m,n) = \sum_{(k,l)\in S_h} h(k,l)\, s(m-k,n-l) + v(m,n) \tag{2.24}$$

where $r(m,n)$ and $s(m,n)$ represent the observed blurred image and the original image, respectively, $h(k,l)$ describes the blur function and $v(m,n)$ represents the

additive white Gaussian noise with variance σ_v^2. S_h denotes the support of the PSF where the value of $h(k,l)$ is nonzero. Figure 2.3 depicts the complete image observation model.
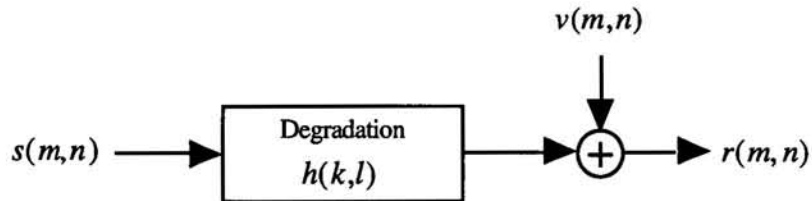
Figure 2.3 Discrete image observation model

2.7 Multichannel Modeling

Modeling in the multichannel case is an extension of the single channel modeling described in the above sections. However, there are components that need to be included in the model. These are the spectral correlation contributions in a multispectral image. Several recent studies [5,36,64,87,88,89] have proposed AR representation to describe multichannel image models. Here, we will only show the formulation of these models, then in a later stage of the research, chapters 5 and 6, we will make use of these models for multichannel identification and restoration.

The Multichannel Image Model

Consider the spectral channel p given by

$$s_p(m,n) = \sum_{q=1}^{N} \sum_{R_{pq}} c^{pq}(k,l)\, s_q(m-k,n-l) + w_p(m,n) \qquad (2.25)$$

where N is the number of spectral channels, $c^{pq}(k,l)$ represent the model coefficients coupling the pth and q^{th} channels, R_{pq} denotes the support of the coefficients $c^{pq}(k,l)$, $s_q(m,n)$ is the undistorted image for the qth channel and $w_p(m,n)$ is the zero mean white Gaussian noise for the pth channel [87]. Obviously, this is an extended form of equation (2.17). However, the model support $R_{pq}, p=1,2,...,N$ and $q=1,2,...,N$ plays an important role in describing the AR model. Pavlovic' and Tekalp [87] proposed two different sets of model support for (2.25).

1- For channel p, the supports, $q=1,2,...,N$, are NSHP. It is assumed that each $w_p(m,n)$ is independent of $s_q(m,n)$, $q=1,2,...,N$, and the spectral correlation between the modeling noise for channels p and q is given by $\mathbf{P}_w$ where the components of this matrix are given by $P_{w_{pq}} = E[w_p(m,n)w_q(m,n)]$. This configuration is depicted in Figure 2.4 for the case of $N=3$. In this figure, the diagonal elements represent the model coefficients for each channel alone, while the off-diagonal elements represent the cross-spectral contributions of the other channels.

2- For channel p, only the support R_{pp} is NSHP causal, the rest of the supports are noncausal, as shown in Figure 2.5 for the case of $N=3$. In this choice, it is assumed that each $w_p(m,n)$ is independent of $s_q(m,n)$, $q=1,2,...,N$, and the modeling noise for channels p and q are uncorrelated. This results in $\mathbf{P}_w$ being a diagonal matrix.

Clearly, other choices for the supports are possible. However, these two examples are presented here because of their relevance to the derivations of multichannel blur identification and restoration in chapters 5 and 6. For the time being, it is important to note that the first model is most suitable to Kalman restoration while the second one is useful in Wiener restoration [61].

The Multichannel Observation Model

The multichannel observation model can be expressed in a similar fashion by extending equation (2.24) as

$$r_p(m,n) = \sum_{q=1}^{N} \sum_{(k,l) \in S_h} h^{pq}(k,l) \, s_q(m-k,n-l) + v_p(m,n)$$

(2.26)

where $r_p(m,n)$ is the pth channel of the observed image, $h^{pq}(k,l)$ are the coefficients of the PSF for the pth channel, $s_q(m,n)$ is the undistorted image for the qth channel, and $v_p(m,n)$ is the observation noise for the qth channel with covariance $\sigma_{v_{pq}}^2$. Here, it is assumed that blur is space-invariant and the observation noise is additive zero mean white Gaussian that is independent of the image. It is worth mentioning here that the effect of blur on the cross-correlation is practically minimal. Therefore, it is normally assumed that there is no cross-spectral correlation due to the blur. We will elaborate on the details of this model when we handle multichannel restoration in chapter 5 and 6.
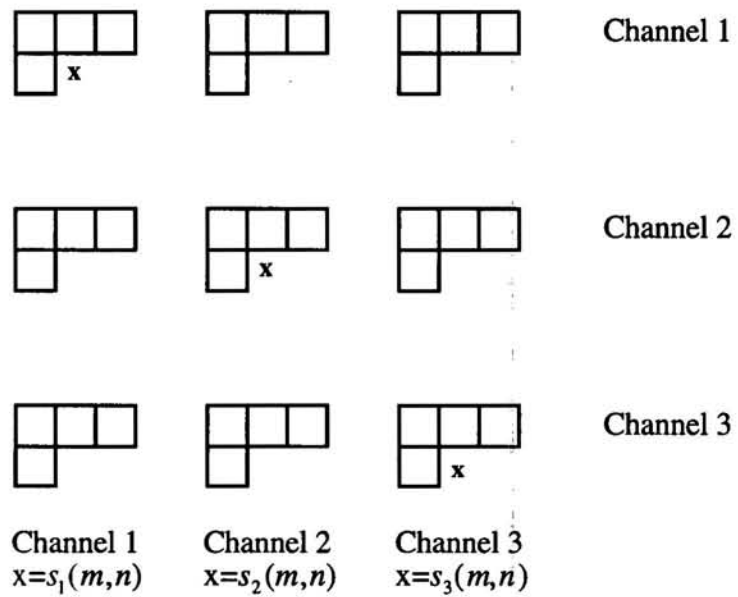
Figure 2.4 Multichannel AR model supports. Case I: R_{pq} are NSHP, $p,q = 1,2,...,N$ for $N = 3$.
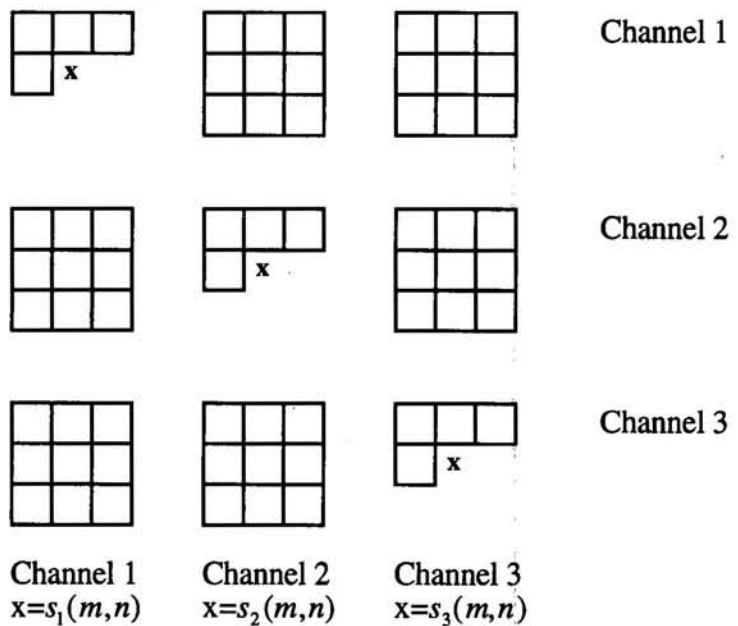
Figure 2.5 Multichannel AR model supports. Case II: R_{pp} are NSHP, and R_{pq}, $p \neq q$, are FP, $p,q = 1,2,...,N$ for $N = 3$.

34

2.8 Some Common Types of Blurs

As mentioned in chapter 1, there are several causes of blur that degrade the quality of the image. Among the common types of blur that are encountered in most practical cases is the uniform motion and out-of focus blurs. Here, we review the modeling of these two forms of blur and their PSF representation.

Blurring processes are essentially continuous functions. Thus, it is more logical to represent the PSF in the continuous context. However, in digital image processing, the discrete representation is needed to make use of the discrete image and observation models. In doing so, we assume that the sampling rate is chosen sufficiently high to avoid aliasing problems and to minimize modeling errors [42,73]. Also, we notice from the physics of the image formation process that the PSF of the blur needs to be nonnegative and real-valued and the energy preservation concept holds [42], i.e.,

$$\int_{-\infty}^{\infty} \int_{-\infty}^{\infty} h(x,y;\Theta)dxdy = 1.0 \tag{2.27}$$

where $h(x,y;\Theta)$ represent the parametric PSF of the blur and Θ describe the severity of the blur.

The mathematical description of the blur function is almost very complicated to be expressed in analytical form. Thus, most work in image processing relies on very simplified, but practical, approximations [49].

2.8.1 Uniform Motion Blur

Relative motion between the object and the recording device can be described as translational, rotational, curvilinear, a sudden change of scale, or a combination of them. We will consider here the important case of translation in one direction; known as uniform motion blur [42,25,73].

Let us assume that the object moves with a constant velocity in the x-direction; then the PSF of this process can be represented by a uniform function given by

$$h(x,y;\Theta) = \begin{cases} \frac{1}{a}, & \text{if } -\frac{a}{2} \leq x \leq \frac{a}{2} \\ 0, & elsewhere \end{cases} \tag{2.28}$$

as shown in Figure (2.6), where the parameter vector Θ in this case is $\Theta = a$ and a represent the extent of the blur, which is the only parameter that characterizes the blur. Physically, the extent of the blur depends on the relative velocity between the object and the imaging plane, and on the time of exposure. This results in smearing each point of the object over several pixels [61].
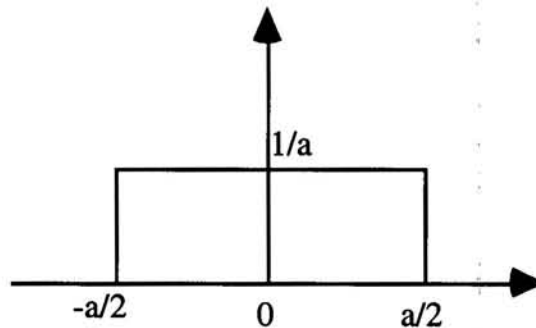
Figure 2.6 PSF for a uniform motion blur.

2.8.2 Out-Of-Focus Blur

In the ideal case, where the imaging system is properly focused, each point in the object results in a point in the imaging plane. However, in most practical cases, the imaging device becomes out of focus, which results in mapping each point in the object plane to a blur circle in the image plane, called circle of confusion (COC) [54,61,66]. For example, consider imaging a 3-D object onto a 2-D plane. This is an obvious out-of-focus setting since some parts of the object are in focus while some other parts are not [42].

The diameter of the circle of confusion for each point in the object that is not in-focus can be expressed using plane geometry and the lens law as follows. Let i_1 and i_2 be the image distances corresponding to object distances o_1 and o_2, respectively. The image at i_1 converges to a point on the image plane while the image at i_2 projects into a circle as it converges a distance $|i_2 - i_1|$ away, as illustrated in Figure 2.7. Using the lens law

$$\frac{1}{f} = \frac{1}{o} + \frac{1}{i}$$

where f is the focal length of the lens, o the object distance, and i the image distance, we have

$$\frac{1}{f} = \frac{1}{o_1} + \frac{1}{i_1} \quad \Rightarrow \quad i_1 = \frac{o_1 f}{o_1 - f} \qquad o_1 > f$$

and

$$\frac{1}{f} = \frac{1}{o_2} + \frac{1}{i_2} \quad \Rightarrow \quad i_2 = \frac{o_2 f}{o_2 - f} \qquad o_2 > f$$

Using the principles of plane geometry we notice that the triangles $\Delta 123$ and $\Delta 453$ in Figure 2.7 are similar. Thus, we may write

$$\frac{2a}{i_2} = \frac{2R}{i_2 - i_1}$$

Since the f-stop of the lens is defined as $F = \frac{f}{2a}$, the radius of the blur circle can be expressed as

$$R = \frac{f}{2F}\left(\frac{|i_2 - i_1|}{i_2}\right) \tag{2.29}$$

The PSF of uniform out-of-focus blur can be expressed as

$$h(x, y; \Theta) = \begin{cases} \dfrac{1}{\pi R^2}, & \text{if } x^2 + y^2 \leq R^2 \\ 0, & elsewhere \end{cases} \tag{2.30}$$

where the parameter vector Θ in this case is equal to R, R is the radius of the support [61]. Thus, if the imaging system is out-of-focus, each point in the object is mapped as a uniform disc of radius R. If some regions in an image are out-of-focus while others are not, then this mapping is performed on the out-of-focus segments only.

As we mentioned earlier, in section 2.4, that we are considering 2-D degradations only. The modeling of 3-D degradations is a different subject that is beyond the purpose of our work.
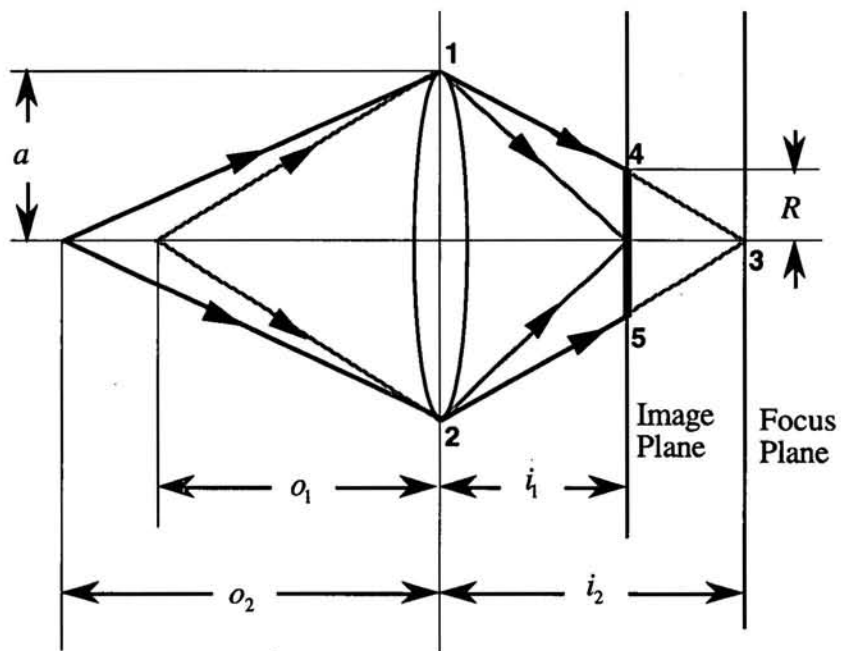
Figure 2.7 Geometry of Out-of-focus blur model.

2.9 Some Computational Considerations

In this section, we discuss some aspects of computation and implementation in digital image processing. We will review some techniques that are used for handling boundary value problems and for estimating the power spectrum and noise variance of images.

Boundary Value Problem

Boundary value problems result from the fact that images normally have finite spatial extent. In computing the convolutions required by restoration techniques, the computation extends beyond the available boundaries of the image. Thus, some manipulation and preprocessing of these boundaries are needed. It has been shown in [94] that this phenomena has global effects not only at the boundaries but on the entire image. To reduce these effects, several preprocessing techniques have been proposed [42,86,94,95,96] that substitute for the missing data at the boundaries using some approximations like:

1- Padding fixed values that represent the mean of the image.

2- Padding random values that have the same mean and variance as that measured from the image, or by model based extrapolation.

3- Repeating the values at all boundaries with the size needed by the convolution filter.

4- Reducing the size of the image at the boundaries such that the neglected boarders can be used as boundary values. This method is known as rectangular approximation.

5- Adding values at the boundaries in a way that interpolate the left and right, top and bottom boundaries linearly. This is known as circular approximation.

It has been shown [94] that rectangular and circular approximation are very successful in restorations. The choice of a certain method over the other depends on the restoration method used. In this thesis, both techniques will be used alternatively for the purpose of producing better quality restored images.

Estimation of Power Spectrum and Noise Variance

Estimation of power spectrum (PS) of the images is needed by many identification and restoration procedures [29,24,61,94] as we will see in the following chapters. To estimate the PS of the ideal image we may replace it by the estimate of the PS of a similar prototype image, or the PS of the noisy and blurred image. In iterative techniques, it can be replaced by the PS of the restored image at the beginning of each iteration, where the PS of the observed image is used as the initial estimate.

The PS of the observed image can be estimated using nonparametric approach such as Welch's method [29], or parametric approach by fitting an AR model to the observed image and using the computed parameters to find the PS. In most of the experiments in this thesis, we will use AR modeling to compute the PS of the image. It has been shown in [93] that the sensitivity of this approximation is minimal compared to other techniques.

The estimation of the noise variance of the observed image can be computed by selecting a uniform region in the image and computing its variance. Then, this can be used as the observation noise variance.

In most of the algorithms that we will be using, we must simulate a signal-to-noise ratio (SNR) at a certain dB level. This can be achieved by first computing the variance of the ($M \times N$) size original image, then solving for the corresponding noise variance from equation (2.23) at the dB level desired. Now, using a Gaussian random noise generator, we may compute a random sequence of $M \times N$ values with equivalent noise variance that can be added to the image.

العنوان:	CONTINUOUS SPATIAL DOMAIN IMAGE IDENTIFICATION AND RESTORATION WITH MULTICHANNEL APPLICATIONS
المؤلف الرئيسي:	Al Suwailem, Umar A.
مؤلفين آخرين:	Keller, James E.(super)
التاريخ الميلادي:	1996
موقع:	كولومبيا
الصفحات:	1 - 183
رقم MD:	616175
نوع المحتوى:	رسائل جامعية
اللغة:	English
الدرجة العلمية:	رسالة دكتوراه
الجامعة:	University of Missouri
الكلية:	The Graduate School
الدولة:	الولايات المتحدة الأمريكية
قواعد المعلومات:	Dissertations
مواضيع:	الهندسة الإلكترونية ، تطبيقات الحاسب ، ترميم الصور ، النمذجة ، الحركات الضبابية
رابط:	https://search.mandumah.com/Record/616175

www.manaraa.com

CHAPTER 3

IMAGE RESTORATION TECHNIQUES: A REVIEW

Image restoration is one of the important steps in image processing and analysis. The ultimate goal of restoration is to recover the original image from its degraded version. Restoration techniques assume that some statistical knowledge about the image and noise is available beforehand, in addition to knowledge of the blurring function. In the previous chapter, the modeling of image and noise that provide some *a priori* knowledge needed for restoration was discussed. The identification of the blur function will be discussed in the next chapter. In practice, the performance of the identification process must be combined with that of the restoration technique for an overall evaluation; however, in this chapter we will assume the blurring function to be known, for the purpose of illustrating the feasibility of the restoration methods.

There are several useful restoration techniques available in the literature that vary in performance. Among them are the ideal and pseudo inverse filter, LMMSE Wiener filter, recursive Kalman filter, maximum entropy approaches, and Bayesian methods

[3,22,29,34,42,73]. Some of those techniques perform well while the others either have poor performance or excessive computation. Moreover, some techniques are based on assumptions that limit their use in practice.

In this chapter, we will review two famous restoration techniques, namely , the Wiener and Kalman filters, that proved to be useful for a wide class of images. In section 3.1 we will review the mathematical derivation of the Wiener filter. In section 3.2, the formulation of the Kalman filter in 2-D is considered. The computation involved in implementing this filter is discussed to produce a slightly suboptimal filter called the reduced update Kalman filter (RUKF). Finally, in section 3.3 some experimental results for those filters are presented.

3.1 The Wiener Filter

The wiener filter is a linear minimum variance based estimator that minimizes the mean square error between the ideal image and the estimated one. To derive the filter equation, we use the observation model given by equation (2.24)

$$r(m,n) = \sum_{(k,l) \in S_h} h(k,l) \, s(m-k,n-l) + v(m,n) \qquad (3.1)$$

which can be written in a matrix form using lexicographical ordering as

$$\mathbf{r} = \mathbf{Hs} + \mathbf{v}$$

$$(3.2)$$

where $\mathbf{r}$, $\mathbf{s}$ and $\mathbf{v}$, correspond to $r(m,n)$, $s(m,n)$, and $v(m,n)$, respectively. $\mathbf{H}$ is the degradation or blur matrix of size $(MN \times MN)$.

As shown by Jain [29, section 8.6], the best linear estimate of the original image can be obtained using a Wiener filter $\mathbf{G}$ given by

44

$$\hat{s} = Gr \tag{3.3}$$

This minimizes the average mean square error given by

$$E[(s - \hat{s})'(s - \hat{s})] \tag{3.4}$$

which is obtained by the orthogonality relation

$$E[(s - \hat{s})r'] = 0 \tag{3.5}$$

Finally, the Wiener filter is computed as

$$\begin{aligned} G &= E[sr']\{E[rr']\}^{-1} \\ &= P_{ss}H'[HP_{ss}H' + Q_v]^{-1} \end{aligned} \tag{3.6}$$

where P_{ss} and Q_v are the correlation matrices of the image s and the noise v, respectively, which are assumed to be uncorrelated. For a stationary observation model, when the original image is stationary random field, the blur function is spatially invariant, and the noise is white, has zero mean and σ_v^2 variance, the Wiener filter reduces to [29]

$$G = [H'H + \sigma_v^2 P_{ss}^{-1}]^{-1}H' \tag{3.7}$$

We observe that (3.7) involves the inversion of a huge matrix, of size $O(MN \times MN)$, which makes direct computation of this equation impractical. However, under the stationarity assumptions mentioned above, P_{ss} and H become block Toeplitz. Thus, using a circulant-to-Toeplitz approximation and the DFT diagonalization properties [22], the Wiener filter can be computed efficiently [3,20].

3.2 The Kalman Filter

Kalman filtering is of fundamental importance in linear estimation theory. It is another form of a linear mean square error solution for image restoration. Moreover, it is recursive and overcomes the stationarity and space invariance restriction of the Wiener filter. The 2-D Kalman filter was first introduced by Woods and Radewan [96] as an extension of the 1-D version. We will follow their approach here.

In order to derive the 2-D Kalman filter equations, we need first to define the concept of a state in 2-D. The state of an image at coordinate (m,n), denoted as $s^{(m,n)}$, is defined as the minimum amount of information, pixel values, about the past and present estimates needed to determine an optimal causal estimate of future response, given future noisy observations [96]. Thus, for a first order NSHP image model, the state at location (m,n) can be represented by

$$
\begin{aligned}
s^{(m,n)} = [&s(m,n), s(m,n-1),....,s(m,0) \\
&s(m-1,N-1), s(m-1,N-2),...,s(m-1,n-1)]^t
\end{aligned}
\tag{3.8}
$$

Figure 3.1 illustrates this example, where the dimension of the state vector is $(N+2)$ and N is the number of columns in the image. Thus, we may write the image model of equation (2.17) in state-space representation as

$$
s^{(m,n)} = \mathbf{C} s^{(m-1,n)} + \mathbf{w}(m,n)
\tag{3.9}
$$

where $\mathbf{C}$ is the state transition matrix containing the appropriately arranged terms of the AR model coefficients $c(k,l)$. The dimension of $\mathbf{C}$ depends on the size of the state vector. For example, the first order NSHP model of Figure 3.1 results in $(N+2)\times(N+2)$ square $\mathbf{C}$ matrix.

46

Similarly, we may define the state observation model of equation (2.24) in state-space representation as

$$r(m,n) = \mathbf{H}^t \mathbf{s}^{(m,n)} + v(m,n) \tag{3.10}$$

where the state now includes all image rows which the PSF extends and $\mathbf{H}$ has the same size as the state vector. Figure 3.2 shows the pixel values included in the state for 1×5 blur PSF. The state-space equations of the image model (3.9) and observation model (3.10) are used to derive the Kalman filter equations.
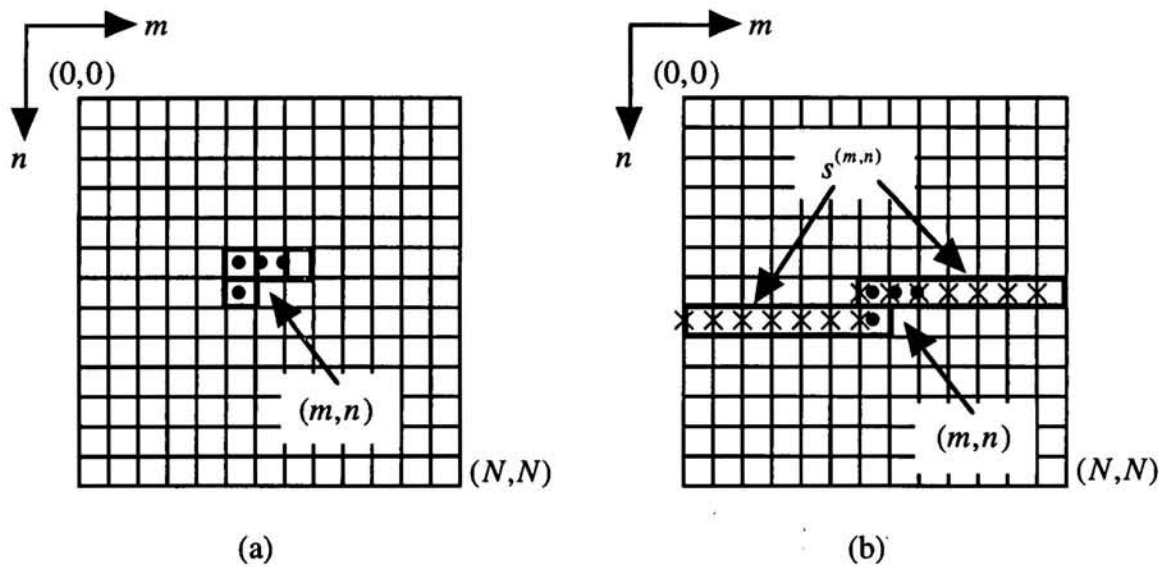
Figure 3.1 Illustration of the state definition for the image model.
(a) The 1st order NSHP model support
(b) The corresponding state vector of size $(N+2)$

47
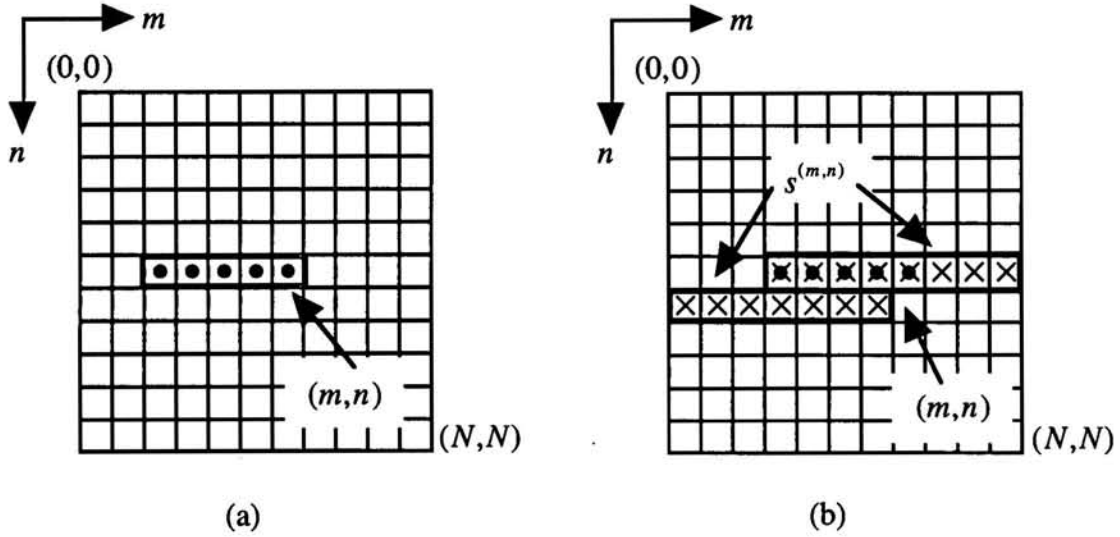
Figure 3.2 Illustration of the state definition for the blur function
(a) Support of 1×5 blur PSF (b) The pixels that are included in the state vector.

We may now construct the 2-D Kalman filter from the 1-D filter equations as developed in [96]. The filter consists of two processes; prediction and update steps, denoted as subscripts b and a, respectively, in the following set of equations

$$\hat{\mathbf{s}}_b^{(m,n)} = \mathbf{C}\hat{\mathbf{s}}_a^{(m-1,n)} \tag{3.11}$$

$$\hat{\mathbf{s}}_a^{(m,n)} = \hat{\mathbf{s}}_b^{(m,n)} + \mathbf{K}^{(m,n)}[r(m,n) - \mathbf{H}'\hat{\mathbf{s}}_b^{(m,n)}] \tag{3.12}$$

$$\mathbf{K}^{(m,n)} = \mathbf{U}_b^{(m,n)}\mathbf{H}[\mathbf{H}'\mathbf{U}_b^{(m,n)}\mathbf{H} + \sigma_v^2]^{-1} \tag{3.13}$$

$$\mathbf{U}_b^{(m,n)} = \mathbf{C}\mathbf{U}_a^{(m-1,n)}\mathbf{C}^t + \sigma_w^2[1,0,\ldots,0]'[1,0,\ldots,0] \tag{3.14}$$

$$\mathbf{U}_a^{(m,n)} = [\mathbf{I} - \mathbf{K}^{(m,n)}\mathbf{H}]\mathbf{U}_b^{(m,n)} \tag{3.15}$$

where $\mathbf{K}^{(m,n)}$ is the Kalman gain computed for the state at coordinates (m,n), and $\mathbf{U}_b^{(m,n)}$ and $\mathbf{U}_a^{(m,n)}$ represent the predicted and updated covariance matrices of the state at coordinates (m,n), respectively.

Direct evaluation of those equations involves tremendous computations and limits the practical implementation of this Kalman filter, especially when the size of the AR model support and/or the extent of the blur PSF function are large. Several attempts to overcome these problems are reported in literature [6,12,34,95, 96]. In [96], Woods and Radewan presented a slightly suboptimal but an efficient version called the reduced update Kalman filter (RUKF). In the RUKF formulation, updating the states in equation (3.12) is reduced to those elements of the state which are within a certain "effective" distance of the point (m,n) currently being processed. The support of the NSHP model was taken to be the "effective" update region. Omitting update of points far away should only minimally impact the performance, since the correlation between image pixels decreases drastically with distance [61].

Using this approach, the state vector is now partitioned into two vectors, $s_1^{(m,n)}$ which is the local state vector and $s_2^{(m,n)}$ that contains the remaining points (Figure 3.3) such that

$$s^{(m,n)} = \begin{bmatrix} s_1^{(m,n)} \\ s_2^{(m,n)} \end{bmatrix} \tag{3.16}$$

Thus, the state model (3.9) can be written as

$$s^{(m,n)} = C_{11}s_1^{(m-1,n)} + C_{12}s_2^{(m-1,n)} + w_1(m,n) \tag{3.17}$$

and the observation model (3.10) as

$$r(m,n) = H_1^t s_1^{(m,n)} + v(m,n) \tag{3.18}$$

where C_{11}, C_{12}, H_1, and w_1 are partitioned in an order that corresponds to the partition of the state vector $s^{(m,n)}$. Accordingly, the RUKF equations can be modified from the Kalman equations (3.11)-(3.15) as

state prediction:

$$\hat{s}_{1,b}^{(m,n)} = C_{11}\hat{s}_{1,a}^{(m-1,n)} + C_{12}\hat{s}_{2,a}^{(m-1,n)} \tag{3.19}$$

error covariance prediction:

$$U_b^{(m,n)} = CU_a^{(m-1,n)}C^t + \sigma_w^2[1,0,\ldots,0]^t[1,0,\ldots,0] \tag{3.20}$$

Kalman gain:

$$K_1^{(m,n)} = U_{11,b}^{(m,n)}H[H^tU_{11,b}^{(m,n)}H + \sigma_v^2]^{-1} \tag{3.21}$$

state update:

$$\hat{s}_{1,a}^{(m,n)} = \hat{s}_{1,b}^{(m,n)} + K_1^{(m,n)}[r(m,n) - H_1^t\hat{s}_{1,b}^{(m,n)}] \tag{3.22}$$

and, error covariance update:

$$U_{11,a}^{(m,n)} = [I - K_1^{(m,n)}H]U_{11,b}^{(m,n)}$$

$$(3.23a)$$

$$U_{12,a}^{(m,n)} = [I - K_1^{(m,n)}H]U_{12,b}^{(m,n)}$$

$$(3.23b)$$

It has been shown that the above formulation results in a huge reduction in computation as well as savings in the storage requirement [95,96].

50
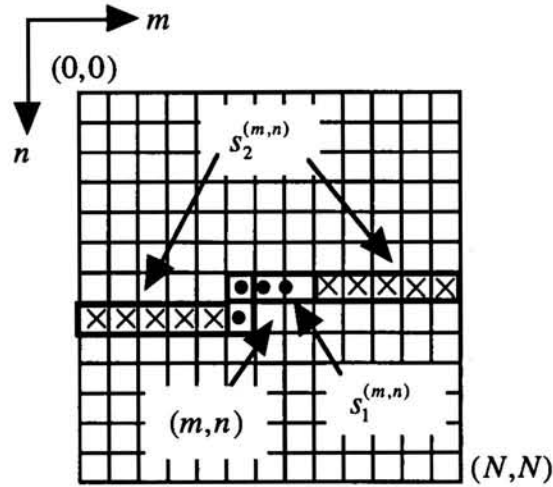
Figure 3.3 The partition of state vectors for RUKF implementation
using 1st order NSHP model support.

3.3 Experimental Results

In this section, we present some experimental results for the implementation of the
Wiener and Kalman filters. The "Man and House" image, Figure 3.4, was degraded by
three types of blur and by an additive zero mean white Gaussian noise of variance
corresponding to $SNR = 30$ dB as follows:

Case I: Uniform linear motion blur of extent $a=10$ pixels. Figure 3.5(a) shows
the blurred image, and Figures 3.5(b) and 3.5(c) show the restored images using the
Wiener and Kalman filters, respectively.

Case II: Out-of-focus blur of radius $R=9$. Figure 3.6(a) shows the blurred image, and Figures 3.6(b) and 3.6(c) shows the restored images using the Wiener and Kalman filters, respectively.

Case III: Blur mask of 5x5 box size. Figure 3.7(a) shows the blurred image, and Figures 3.7(b) and 3.7(c) shows the restored images using the Wiener and Kalman filters, respectively.

Examining the restoration results of these two filters one can conclude that Kalman filter performs better than the Wiener filter in the all of the three cases above. Considering the size of computation involved, the Kalman filter requires more computation and storage than the Wiener filter. However, this can be compensated for by the better performance gained. The noise effect is an important factor to both methods, since they perform poorly at very low SNR. In such severe degradation cases, enhancement techniques may result in better results than restoration.

As mentioned earlier in this chapter, Kalman and Wiener filters are widely used because of their practical implementation and good performance. Other existing techniques vary in their performance and some may have limitations. See Sezan and Tekalp [81] for a full review and comparison of restoration techniques.

Figure 3.4 The original " Man and House" image

Figure 3.5(a) The degraded "Man and House" image with linear
uniform motion blur of extent a=10 and SNR=30 dB.

(b)

(c)

Figure 3.5(b) and (c) The restored image of Figure 3.5(a).
(b) using Wiener filter (c) using Kalman filter

55

Figure 3.6(a) The degraded "Man and House" image with
Out-of-focus blur $R=9$ and $SNR=30$ dB.

(b)

(c)

Figure 3.6(b) and (c) The restored image of Figure 3.6(a).
(b) using Wiener filter (c) using Kalman filter

Figure 3.7(a) The degraded "Man and House" image
with a 5x5 mask blur and *SNR*=30 dB.

(b)

(c)

Figure 3.7(b) and (c) The restored image of Figure 3.7(a).
(b) using Wiener filter (c) using Kalman filter

العنوان:	CONTINUOUS SPATIAL DOMAIN IMAGE IDENTIFICATION AND RESTORATION WITH MULTICHANNEL APPLICATIONS
المؤلف الرئيسي:	Al Suwailem, Umar A.
مؤلفين آخرين:	Keller, James E.(super)
التاريخ الميلادي:	1996
موقع:	كولومبيا
الصفحات:	1 - 183
رقم MD:	616175
نوع المحتوى:	رسائل جامعية
اللغة:	English
الدرجة العلمية:	رسالة دكتوراه
الجامعة:	University of Missouri
الكلية:	The Graduate School
الدولة:	الولايات المتحدة الأمريكية
قواعد المعلومات:	Dissertations
مواضيع:	الهندسة الإلكترونية ، تطبيقات الحاسب ، ترميم الصور ، النمذجة ، الحركات الضبابية
رابط:	https://search.mandumah.com/Record/616175

www.manaraa.com

CHAPTER 4

MONOCHROME BLUR IDENTIFICATION

In the previous chapter, we assumed that the blur function is known and available for the implementation of restoration techniques. However, in practice, such information is often not available and has to be estimated from the received image. The purpose of this chapter is to present a successful method that can be used in identifying the PSF of the blur. We will study the formulation of the maximum likelihood (ML) blur identification problem in the single channel and monochrome case.

As proposed by Pavlovic and Tekalp [63], modeling the problem in the continuous spatial domain overcomes the major difficulties encountered in the discrete case. Unlike previous ML approaches [42, 47], this formulation enables us to estimate the extent of the blur as well as other parameters describing the blur function for some types of PSF's that admit closed-form description. As we will see later in this chapter, the nonlinearity of the likelihood function (LF) is overcome by using the continuous form of the autocorrelation function. First , in section 4.1, we will

introduce the likelihood estimation method and its application to the blur identification problem. Next, in section 4.2, the blur identification technique based on the continuous spatial domain model formulation is developed for both the uniform and out-of-focus blurs. Finally, in sections 4.3 and 4.3, the implementation and some experimental results will be presented and the method performance is evaluated.

4.1 The Maximum Likelihood Estimator

The method of maximum likelihood is a very general method for parameter estimation. This method was developed by Fisher (1912) although the essential ideas go back to Gauss (1809) [7]. The basic idea is to construct a function of the data and the unknown parameters called the likelihood function (LF), then the estimate is obtained as the parameter value which maximizes this function. The LF is effectively the probability density function (PDF) of the observations [7,42].

Applying this concept to the case of image blur identification problem, and assuming that the models given by equations (2.17) and (2.24) represent an appropriate abstraction of reality, the blur identification problem becomes as the estimation of a parameter vector Φ, from the observed image $r(m,n)$, defined as

$$
\begin{aligned}
\Phi &= (\phi_1, \phi_2, ..., \phi_M)^t \\
&= (h(i,j), c(k,l), \sigma_v^2, \sigma_w^2)
\end{aligned}
\tag{4.1}
$$

where, $h(i,j)$ represents the blur function, $c(k,l)$ are the coefficients of the ideal image model, σ_v^2 and σ_w^2 are the variances of the observation noise and modeling noise, respectively. The purpose of ML estimation procedures is to optimize the PDF of the observed image $r(m,n)$ with respect to the unknown parameters, in other words, to find a

61

Φ which most likely produced the blurred image that was observed. We will now show the derivation of the ML estimator.

Consider the image model given by (2.17) and the observation model (2.24). We may rewrite them in a matrix form, respectively, as

$$s = Cs + w \tag{4.2}$$

$$r = Hs + v \tag{4.3}$$

where s, r, w, and v, are the original image, $s(m,n)$, the observed image, $r(m,n)$, the modeling noise, $w(m,n)$, and the observation noise $v(m,n)$; all of size $(M \times N)$, respectively, but represented in lexicographical order as vectors, and where C is the image model matrix and H is the degradation or blur matrix both of size $(MN \times MN)$. Lexicographical order of an image x of size $(M \times N)$ is a $(MN \times 1)$ vector ordered as $x = [x(1,1), x(1,2), ..., x(M,N)]'$. We need now to find the PDFs of s and r which are needed for the formulation of the ML estimator. In order to do that, we use the following definition of multivariate joint Gaussian distribution.

Definition 4.1:

Let x be a k-dimensional Gaussian random vector with mean m and covariance matrix Γ, then the probability density function of x takes the form

$$p(x) = \frac{1}{\sqrt{(2\pi)^k |\Gamma|}} \exp\{-\frac{1}{2} J(x)\} \tag{4.4}$$

where

$m = E[x]$ is a $(k - \text{dimensional})$ mean vector

$\Gamma = E[(x - m)(x - m)']$ is a $(k \times k)$ covariance matrix

$J(x) = (x - m)' \Gamma^{-1} (x - m)$

and $|\bullet|$ and t denote the determinant and the transpose of a matrix, respectively.

To use this definition for finding the PDF of $\mathbf{s}$, we notice that the driving process, or modeling noise, $\mathbf{w}$ in (4.2) is a homogeneous Gaussian distribution white noise process with zero mean and covariance matrix $\mathbf{Q}_w = \sigma_w^2 \mathbf{I}$ $(\sigma_w^2 > 0)$ and is uncorrelated with $\mathbf{s}$. Hence, the PDF of $\mathbf{s}$ given the PDF of $\mathbf{w}$ and the model (4.2) is also a Gaussian of the form (4.4), Thus we may write the PDF of $\mathbf{w}$ as

$$p(\mathbf{w}) = \frac{1}{\sqrt{(2\pi)^{MN}|\mathbf{Q}_w|}} \exp\{-\frac{1}{2}\mathbf{w}^t \mathbf{Q}_w^{-1} \mathbf{w}\}$$

and the PDF of $\mathbf{s}$ as

$$p(\mathbf{s}; \mathbf{C}, \mathbf{Q}_w) = \frac{|\mathbf{I} - \mathbf{C}|}{\sqrt{(2\pi)^{MN}|\mathbf{Q}_w|}} \exp\{-\frac{1}{2}\mathbf{s}^t(\mathbf{I} - \mathbf{C})^t \mathbf{Q}_w^{-1}(\mathbf{I} - \mathbf{C})\mathbf{s}\} \qquad (4.5)$$

where we have used $\mathbf{w} = (\mathbf{I} - \mathbf{C})\mathbf{s}$ from (4.2)

and

$$\begin{aligned} \mathbf{w}^t \mathbf{Q}_w^{-1} \mathbf{w} &= [(\mathbf{I} - \mathbf{C})\mathbf{s}]^t \mathbf{Q}_w^{-1}(\mathbf{I} - \mathbf{C})\mathbf{s} \\ &= \mathbf{s}^t(\mathbf{I} - \mathbf{C})^t \mathbf{Q}_w^{-1}(\mathbf{I} - \mathbf{C})\mathbf{s} \end{aligned}$$

In a similar manner, we may write the PDF of the observation noise $\mathbf{v}$ using $\mathbf{v} = (\mathbf{r} - \mathbf{H}\mathbf{s})$ from (4.3), as

$$p(\mathbf{v}) = \frac{1}{\sqrt{(2\pi)^{MN}|\mathbf{Q}_v|}} \exp\{-\frac{1}{2}\mathbf{v}^t \mathbf{Q}_v^{-1} \mathbf{v}\}$$

and the PDF of the observed image $\mathbf{r}$, given the PDF of the observation noise $\mathbf{v}$, the model (4.3), and the original image $\mathbf{s}$, may be written as

$$p(\mathbf{r}/\mathbf{s}; \mathbf{H}, \mathbf{Q}_v) = \frac{1}{\sqrt{(2\pi)^{MN}|\mathbf{Q}_v|}} \exp\{-\frac{1}{2}(\mathbf{r} - \mathbf{H}\mathbf{s})^t \mathbf{Q}_v^{-1}(\mathbf{r} - \mathbf{H}\mathbf{s})\} \qquad (4.6)$$

Note that this PDF is conditional on both the original image (denoted by $\mathbf{r}/\mathbf{s}$) and on the deterministic $\mathbf{H}$ and $\mathbf{Q}_v$ (denoted by $\mathbf{r};\mathbf{H},\mathbf{Q}_v$) [42]. Now, we may write the PDF of $\mathbf{r}$ in terms of all the parameters that need to be optimized by first substituting (4.2) into (4.3) to get

$$
\begin{aligned}
\mathbf{r} &= \mathbf{Hs} + \mathbf{v} \\
&= \mathbf{H}(\mathbf{I} - \mathbf{C})^{-1}\mathbf{w} + \mathbf{v}
\end{aligned}
\tag{4.7}
$$

Since $\mathbf{r}$ is a sum of two Gaussian processes, namely $\mathbf{v}$ and $\mathbf{w}$, the PDF of $\mathbf{r}$ is also Gaussian with zero mean and covariance matrix $\mathbf{P}_{rr}$, and may be written using definition 4.1 as

$$
\begin{aligned}
p(\mathbf{r};\Phi) &= p(\mathbf{r};\mathbf{H},\mathbf{C},\mathbf{Q}_v,\mathbf{Q}_w) \\
&= \frac{1}{\sqrt{(2\pi)^{MN}|\mathbf{P}_{rr}|}} \exp\{-\frac{1}{2}\mathbf{r}'\mathbf{P}_{rr}^{-1}\mathbf{r}\}
\end{aligned}
\tag{4.8}
$$

where

$$
\begin{aligned}
\mathbf{P}_{rr} &= Cov(\mathbf{r};\Phi) = E[\mathbf{rr}'] \\
&= E[\{\mathbf{H}(\mathbf{I}-\mathbf{C})^{-1}\mathbf{w}+\mathbf{v}\}\{\mathbf{H}(\mathbf{I}-\mathbf{C})^{-1}\mathbf{w}+\mathbf{v}\}'] \\
&= E[\{\mathbf{H}(\mathbf{I}-\mathbf{C})^{-1}\mathbf{w}+\mathbf{v}\}\{(\mathbf{H}(\mathbf{I}-\mathbf{C})^{-1}\mathbf{w})'+\mathbf{v}'\}] \\
&= E[\{\mathbf{H}(\mathbf{I}-\mathbf{C})^{-1}\mathbf{w}\}\{\mathbf{H}(\mathbf{I}-\mathbf{C})^{-1}\mathbf{w}\}'] \\
&\quad + E[\mathbf{v}(\mathbf{H}(\mathbf{I}-\mathbf{C})^{-1}\mathbf{w})'] + E[(\mathbf{H}(\mathbf{I}-\mathbf{C})^{-1}\mathbf{w})\mathbf{v}'] + E[\mathbf{vv}']
\end{aligned}
$$

Because $\mathbf{v}$ and $\mathbf{w}$ are uncorrelated processes, the expected value of their product is zero, hence, the second and third terms vanish. Thus,

$$
\mathbf{P}_{rr} = \sigma_w^2[\mathbf{H}(\mathbf{I}-\mathbf{C})^{-1}(\mathbf{I}-\mathbf{C})^{-t}\mathbf{H}'] + \sigma_v^2\mathbf{I}
\tag{4.9}
$$

We note here that the structure of $\mathbf{H}$ and $\mathbf{C}$ is block Toeplitz [42]. However, if we consider the convolutions in the image model equation (2.9) and the observation model equation (2.24) to be circular, which effectively can be achieved using circular boundaries

64

as explained in section 2.9, then the block Toeplitz matrix can be approximated as block circulant matrix. Accordingly, $\mathbf{P}_{rr}$ is block circulant. Also, we notice that all the matrices in (4.9) commute because they are related to convolutions [42]. Furthermore, $\mathbf{P}_{rr}$ is positive definite if $\sigma_w^2 > 0$ which is satisfied due to the presence of noise in the blurred image.

Definition 4.2:

The maximum likelihood estimator, denoted by $\hat{\Phi}_{ml}$, of the parameter vector Φ is defined as [7,51,78]

$$\hat{\Phi}_{ml} = \arg\{ \max_{\phi \in \Re(\Phi)} \mathcal{L}^*(\Phi) \}$$
$$= \arg\{ \max_{\phi \in \Re(\Phi)} \log p(\mathbf{r};\Phi) \} \tag{4.10}$$

where $\mathcal{L}^*(\Phi)$ denotes the log likelihood function of Φ, $p(\mathbf{r};\Phi)$ denotes the *a priori* PDF of the observed image given Φ, and $\Re(\Phi)$ specifies the range of the parameters in Φ.

Using this definition along with equation (4.8), we can write the likelihood function (LF) as

$$\mathcal{L}^*(\Phi) = \log p(\mathbf{r};\Phi)$$
$$= -\{\log(|\mathbf{P}_{rr}|) + \mathbf{r}'\mathbf{P}_{rr}^{-1}\mathbf{r}\} \tag{4.11}$$

From which we can get the ML estimate, $\hat{\Phi}_{ml}$, that maximizes this LF.

65

4.2 Blur Identification Based on a Continuous Spatial Domain Model

In this section, we derive the equations for the ML estimator based on a continuous domain representation of the blur. As explained in section 2.4, blur formation can be modeled by a linear, space invariant system, equation (2.20), and the total observation model may be written in the continuous domain as

$$r(x,y) = \int_R h(\eta,\xi)s(x-\eta,y-\xi)d\eta d\xi + v(x,y) \qquad (4.12)$$

where $s(x,y)$ denotes the ideal image, $h(x,y)$ is the PSF of the blur, R denotes the support of the PSF, and $v(x,y)$ is the observation noise. Let us assume that the PSF can be expressed as a function of a small number of parameters, $\Theta = [\theta_1, \theta_2, ..., \theta_n]$:

$$h(x,y) = h(x,y;\Theta) \quad \text{for } (x,y) \in \Re(\Theta) \qquad (4.13)$$

where $\Re(\Theta)$ denotes the support of the PSF.

Substituting (4.13) into (4.12) and sampling (4.12) at the points $(x,y) = (m\Delta x, n\Delta y)$, where Δx and Δy denote the horizontal and vertical sampling distances, respectively, we may write

$$r(m,n) = \int_{\Re(\Theta)} h(\xi,\eta;\Theta)s(m\Delta x - \xi, n\Delta y - \eta)d\xi d\eta + v(m,n) \qquad (4.14)$$

where (m,n) denotes discrete spatial coordinates, and $r(m,n)$ are the observed samples of $r(x,y)$.

This is a more accurate model for the observation samples $r(m,n)$ than the well-known discrete spatial domain model given by equation (2.24), since the latter is valid only under the assumption that either the blur PSF or the image is bandlimitted as mentioned in section 2.4, i.e., the image at point (m,n) is affected by the values of a small neighborhood. Furthermore, this model enables us to obtain the ML estimate of the blur extent since we can differentiate with respect to a variable that appears in the integration limits.

We make the following modeling assumptions: 1) the samples $s(m,n)$ of the ideal image $s(x,y)$ are a realization of a 2-D homogeneous Gauss- random field characterized by the following 2-D AR model

$$s(m,n) = \sum_{(k,l) \in S_c} c(k,l)s(m-k,n-l) + w(m,n) \qquad (4.15)$$

where $c(k,l)$ are the image model coefficients, S_c is the nonsymmetric half plane (NSHP) image model support, and $w(m,n)$ is a zero mean white Gaussian noise with variance σ_w^2 that is independent of the image, and 2) the observation noise $v(m,n)$ is zero mean white Gaussian noise with variance σ_v^2. Then the probability density function (PDF) of the observed image, $\mathbf{r}$, is Gaussian, given by equation (4.8) as

$$p(\mathbf{r}; \Theta, c(m,n), \sigma_v^2, \sigma_w^2) = \frac{1}{\sqrt{(2\pi)^{N^2} |\mathbf{P}_{rr}|}} \exp\left(\frac{1}{2}\mathbf{r}'\mathbf{P}_{rr}^{-1}\mathbf{r}\right) \qquad (4.16)$$

where, $\mathbf{r}$ denotes a lexicographic ordering of the $N \times N$ samples of the observed image, and $\mathbf{P}_{rr}$ denotes the covariance matrix of $\mathbf{r}$. Note that the difference between equation (4.16) and (4.8) is the parameter vector Θ that represents the blur function in the continuous domain compared to $h(i,j)$ of the discrete case. From equations (4.10) and (4.11), the ML estimate of the parameters involved is obtained by maximizing the LF given by

$$\mathbf{L}(\Theta, c(m,n), \sigma_v^2, \sigma_w^2) = -\{\log(|\mathbf{P}_{rr}|) + \mathbf{r}'\mathbf{P}_{rr}^{-1}\mathbf{r}\} \qquad (4.17)$$

The inverse of $\mathbf{P}_{rr}$ and the logarithm of $|\mathbf{P}_{rr}|$ always exist, based on the explanation to equation (4.9). However, the dimension of $\mathbf{P}_{rr}$ is normally very large ($N^2 \times N^2$ where N is 128, 256, etc.), which makes it impractical to evaluate (4.17) directly. Thus, we can approximate the block Toeplitz matrix $\mathbf{P}_{rr}$ as a block circulant one, then the LF can be expressed in the discrete Fourier transform (DFT) domain as [Appendix B]

$$\begin{aligned}
\mathbf{L}(\Theta, c(m,n), \sigma_v^2, \sigma_w^2) &= -\{\log(|\mathbf{P}_{rr}|) + \mathbf{r}'\mathbf{P}_{rr}^{-1}\mathbf{r}\} \\
&= -\left\{ \log[\prod_{k=l} S_{rr}(k,l)] + \frac{1}{N^2} \sum_{k,l} \frac{|R(k,l)|^2}{S_{rr}(k,l)} \right\} \qquad (4.18) \\
&= -\sum_k \sum_l \left(\log S_{rr}(k,l) + \frac{1}{N^2} \frac{|R(k,l)|^2}{S_{rr}(k,l)} \right)
\end{aligned}$$

where k and l are integers corresponding to discrete frequency samples, $R(k,l)$ is the $N \times N$ point DFT of $r(m,n)$, and $S_{rr}(k,l)$ is the DFT of the autocorrelation function of the image (elements of one block of the autocorrelation matrix $\mathbf{P}_{rr}$) given as

$$P_{rr}(i,j) = E[r(m,n)r(m+i,n+j)] \qquad (4.19)$$

The novelty of the present formulation is to use (4.14) in computing $S_{rr}(k,l)$ when evaluating the LF and its derivatives. As stated earlier in this section, this is an important contribution which makes it possible to obtain the ML estimate of the blur extent. First, we evaluate $P_{rr}(i,j)$ and then compute its DFT analytically. By substituting (4.14) into (4.19) we have (see Appendix B)

$$P_{rr}(i,j) = \int_{\Re(\Theta)} \int_{\Re(\Theta)} h(\xi,\eta)h(\psi,\zeta)P_{ss}(i-\xi+\psi, j-\eta+\zeta)d\xi d\eta d\psi d\zeta + \delta(i,j)\sigma_v^2 \qquad (4.20)$$

68

where $P_{ss}(x,y) = E\{s(\xi,\eta)s(\xi+x,\eta+y)\}$ is the autocorrelation function of the ideal continuous domain image $s(m,n)$. Then, taking the DFT of (4.20), we have

$$
\begin{aligned}
S_{rr}(k,l) &= DFT\{P_{rr}(i,j)\} \\
&= \int_{\Re(\Theta)}\int_{\Re(\Theta)} h(\xi,\eta)h(\psi,\zeta)S_{ss}(k,l) \\
&\quad \cdot \exp\left[-j\frac{2\pi}{N}k(\xi-\psi)\right]\exp\left[-j\frac{2\pi}{N}l(\eta-\zeta)\right]d\xi d\eta d\psi d\zeta + \sigma_v^2 \qquad (4.21) \\
&= |H(k,l)|^2 S_{ss}(k,l) + \sigma_v^2
\end{aligned}
$$

where $S_{ss}(k,l)$ is the DFT of $P_{ss}(i,j)$ which denotes the samples of $P_{ss}(x,y)$, and $H(k,l)$ denotes the samples of the continuous Fourier transform of $h(x,y;\Theta)$ given by

$$
H(k,l) = \int_{\Re(\Theta)} h(x,y;\Theta)\exp\left(-j\frac{2\pi}{N}kx\right)\exp\left(-j\frac{2\pi}{N}ly\right)dxdy \qquad (4.22)
$$

The power spectrum of the ideal image $S_{ss}(k,l)$ can be obtained from the AR model of (4.15) (see Appendix B) as

$$
S_{ss}(k,l) = \frac{\sigma_w^2}{\left|1 - \displaystyle\sum_{(m,n)\in S_{\oplus+}} c(m,n)\exp\left(-j\frac{2\pi}{N}km\right)\exp\left(-j\frac{2\pi}{N}ln\right)\right|^2} \qquad (4.23)
$$

In order to keep the number of unknowns low, we will estimate the conditional ML estimate of Θ, where the conditional LF (CLF) will be denoted as $L(\Theta|c(m,n),\sigma_v^2,\sigma_w^2)$. Thus, the parameters $\{c(m,n)\}$, σ_v^2 and σ_w^2 will be estimated prior to blur identification. This procedure gives satisfactory results provided that we have a reasonable estimate of $\{c(m,n)\}$, σ_v^2 and σ_w^2 [63]. The vector Θ that maximizes the CLF can be computed from a set of equations obtained by setting the

derivatives of the CLF with respect to these parameters to zero. The derivative of the CLF with respect to θ_i can be computed for $i = 1, 2, \ldots, n$ from equation (4.18) as

$$\frac{\partial}{\partial \theta_i} L(\Theta | c(m,n), \sigma_v^2, \sigma_w^2) = -\sum_k \sum_l \left\{ \left(\frac{1}{S_{rr}(k,l)} - \frac{1}{N^2} \frac{|R(k,l)|^2}{S_{rr}^2(k,l)} \right) \frac{\partial}{\partial \theta_i} S_{rr}(k,l) \right\} \qquad (4.24)$$

The computation of the expression $(\partial / \partial \theta_i) S_{rr}(k,l)$ depends on the particular parametric form of the unknown PSF. Next, we will show how this is implemented for the two cases of linear motion blur and the out-of-focus blur. We will use the following relation in the derivation

$$\frac{\partial}{\partial \theta_i} S_{rr}(k,l) = \Im \left\{ \frac{\partial}{\partial \theta_i} P_{rr}(i,j) \right\} \qquad (4.25)$$

where $\Im\{\bullet\}$ denotes the DFT. Since we are dealing with only one parameter we use

$$\frac{d}{d\theta} S_{rr}(k,l) = \Im \left\{ \frac{d}{d\theta} P_{rr}(i,j) \right\}$$

Case I: Linear Uniform Motion Blur

We will show now how to compute $(d / d\theta) S_{rr}(k,l)$ for the case of uniform blur. The PSF for this type of blur is given by equation (2.28) as

$$h(x, y; \Theta) = \frac{1}{a}, \qquad \text{for } 0 \le x \le a \qquad (4.26)$$

where a represents the extent of the motion in one direction. Then the autocorrelation of the sampled observed image , using (4.20), can be written as

$$P_{rr}(i,j) = \frac{1}{a^2} \int\limits_0^a \int\limits_0^a P_{ss}(i - \xi + \eta, j) d\xi d\eta + \delta(i,j)\sigma_v^2 \qquad (4.27)$$

The derivative of $P_{rr}(i,j)$ with respect to the unknown parameter a can be computed as

$$\frac{d}{da} P_{rr}(i,j) = \frac{-2}{a^3} \int\limits_0^a \int\limits_0^a P_{ss}(i - \xi + \eta, j) d\xi d\eta$$

$$+ \frac{1}{a^2} \int\limits_0^a P_{ss}(i - \xi + a, j) d\xi + \frac{1}{a^2} \int\limits_0^a P_{ss}(i - a + \eta, j) d\eta \qquad (4.28)$$

Taking the DFT of (4.28) using (4.25) we get

$$\frac{d}{da} S_{rr}(k,l) = \frac{-2}{a^3} \int\limits_0^a \int\limits_0^a \exp\left[-j\frac{2\pi}{N}k(\xi - \eta)\right] S_{ss}(k,l) d\xi d\eta$$

$$+ \frac{1}{a^2} \int\limits_0^a \exp\left[-j\frac{2\pi}{N}k(\xi - a)\right] S_{ss}(k,l) d\xi$$

$$+ \frac{1}{a^2} \int\limits_0^a \exp\left[-j\frac{2\pi}{N}k(a - \eta)\right] S_{ss}(k,l) d\eta$$

$$= \left(\frac{1}{a}\right)\left\{\left(-2\int\limits_0^a \frac{1}{a}\exp\left[-j\frac{2\pi}{N}\xi k\right]d\xi\right)\left(\int\limits_0^a \frac{1}{a}\exp\left[+j\frac{2\pi}{N}\eta k\right]d\eta\right)\right.$$

$$+ \exp\left[+j\frac{2\pi}{N}ka\right]\int\limits_0^a \frac{1}{a}\exp\left[-j\frac{2\pi}{N}\xi k\right]d\xi$$

$$\left. + \exp\left[-j\frac{2\pi}{N}ka\right]\int\limits_0^a \frac{1}{a}\exp\left[+j\frac{2\pi}{N}\eta k\right]d\eta\right\} S_{ss}(k,l)$$

or

$$\frac{d}{da} S_{rr}(k,l) = \frac{1}{a}\left\{-2|H(k,l)|^2 + \exp\left[j\frac{2\pi}{N}ka\right]H(k,l)\right.$$

$$\left. + \exp\left[-j\frac{2\pi}{N}ka\right]H^*(k,l)\right\} S_{ss}(k,l) \qquad (4.29)$$

where we have used, from equation (4.22),

$$H(k,l) = \int_0^a (\frac{1}{a})\exp\left[-j\frac{2\pi}{N}kx\right]dx.$$

For the uniform blur $H(k,l)$ is computed as

$$H(k,l) = \left(-j\frac{2\pi}{N}k\frac{a-1}{2}\right)\frac{\sin\frac{2\pi}{N}k\frac{a}{2}}{\frac{2\pi}{N}k\frac{a}{2}} \tag{4.30}$$

Case II: Out-of-Focus Blur

For the case of out-of-focus blur, the PSF for this type of blur is given by equation (2.30) as

$$h(x,y;\Theta) = \begin{cases} \dfrac{1}{\pi R^2}, & \text{if } x^2 + y^2 \le R^2 \\ 0, & \text{elsewhere} \end{cases} \tag{4.31}$$

where the parameter vector Θ in this case is equal to R, R is the radius of the support. Then the autocorrelation function of the sampled observed image using (4.20) is given by

$$P_{rr}(i,j) = \frac{1}{(\pi R^2)^2}\int_{-R}^{R}\int_{-\sqrt{R^2-\xi^2}}^{\sqrt{R^2-\xi^2}}\int_{-R}^{R}\int_{-\sqrt{R^2-\psi^2}}^{\sqrt{R^2-\psi^2}} \tag{4.32}$$
$$\cdot P_{ss}(i-\xi+\psi, j-\eta+\zeta)d\xi d\psi d\eta d\zeta$$

Expressing this integral in polar coordinates, the derivative of $P_{rr}(i,j)$ with respect to the unknown parameter R may be written as

$$\frac{d}{dR}P_{rr}(i,j) = \frac{-4}{(\pi^2 R^5)}\int_0^R\int_0^{2\pi}\int_0^R\int_0^{2\pi}P_{ss}(r_1,r_2,\theta_1,\theta_2)r_1 dr_1 dr_2 d\theta_1 d\theta_2$$

$$+\frac{1}{(\pi R^2)^2}\int_0^{2\pi}\int_0^R\int_0^{2\pi}P_{ss}(R,r_2,\theta_1,\theta_2)Rd\theta_1 r_2 dr_2 d\theta_2 \qquad (4.33)$$

$$+\frac{1}{(\pi R^2)^2}\int_0^R\int_0^{2\pi}\int_0^{2\pi}P_{ss}(r_1,R,\theta_1,\theta_2)r_1 dr_1 d\theta_1 Rd\theta_2$$

where, $P_{ss}(r_1,r_2,\theta_1,\theta_2)\overset{\Delta}{=}P_{ss}(i-r_1\cos\theta_1+r_2\cos\theta_2, j-r_1\sin\theta_1+r_2\sin\theta_2)$. We may now find $\frac{d}{da}S_{rr}(k,l)$ by taking the DFT of (4.33) and using (4.22) and (4.25) to get

$$\frac{d}{dR}S_{rr}(k,l) = \Im\left\{\frac{d}{dR}P_{rr}(i,j)\right\}$$

$$= \left\{\frac{-4}{R}|H(k,l)|^2 + \frac{2}{R}J_0\left(\frac{2\pi}{N}R\sqrt{k^2+l^2}\right)(H(k,l)+H^*(k,l))\right\}S_{ss}(k,l) \quad (4.34)$$

where $H(k,l)$ for the out-of-focus blur can be computed as

$$H(k,l) = NR\frac{J_1\left(\frac{2\pi}{N}R\sqrt{k^2+l^2}\right)}{\sqrt{k^2+l^2}} \qquad (4.35)$$

and $J_0(\bullet)$ and $J_1(\bullet)$ are the zeroth and first order Bessel functions of the first kind, respectively.

4.3 Implementation of the ML Estimator

In order to compute the CLF by using (4.18) and the corresponding derivative expression along with (4.24), one needs to know the values of the parameters $\{c(m,n)\}$, σ_v^2 and σ_w^2. We will estimate the parameters $\{c(m,n)\}$ and σ_w^2 from the noisy image (taken as a prototype) using a least squares procedure. The observation noise, σ_v^2, is estimated as the variance of a uniform region selected from the image.

Using a simple gradient-based iterative optimization algorithm of the form

$$\hat{\theta}^{(k+1)} = \hat{\theta}^{(k)} - \beta \nabla_\theta \mathcal{L}(\hat{\theta}^{(k)}) \tag{4.36}$$

where the gradient of the likelihood function, $\nabla_\theta \mathcal{L}(\theta)$, is given by (4.24) at the k-th iteration

$$\nabla_\theta \mathcal{L}(\theta) = \frac{\partial \mathcal{L}(\theta)}{\partial \theta} \tag{4.37}$$

and β controls the convergence of the iterations [42], the Conditional ML algorithm can be summarized as follows :

1) Given $\{c(m,n)\}$ and σ_w^2 compute $S_{ss}(k,l)$ using (4.23).

2) Use the parametric form of the specific PSF, namely (4.26) or (4.31) and set the parameter, Θ, to some initial value.

DO UNTIL convergence criterion is satisfied

    3) Compute $|H(k,l)|^2$ using (4.30) or (4.35) depending on the parametric form chosen.

    4) Given σ_v^2, compute $S_{rr}(k,l)$ using (4.21).

    5) Compute the value of CLF using (4.18).

6) Compute the derivative of the CLF with respect to the unknown parameter using (4.24) and either (4.29) or (4.34), again depending on the parametric form chosen.

7) Update Θ using the gradient based numerical optimization technique (4.36).

END UNTIL

In the next section we will present some experimental results and the performance of the prescribed method.

4.4 Experimental Results

In this section, some experimental results are presented for the cases of linear uniform motion, out-of-focus, and angular motion. Also, the effect of image model support size, the noise sensitivity of this procedure, and the combined performance of the identification and restoration is discussed. The Restoretool package developed at the University of Rochester [83], will serve as the basis for these tests. This software package is designed for the monochrome case where several basic image processing functions are available. The following tests were performed on the "Man and House" image of Figure 4.1. The "Jets" image of Figure 4.12 will be used in the angular motion experiments.

Case I: Uniform linear motion blur

First we blurred the image with a uniform motion blur of extent a=10 in the horizontal direction and no noise was added, as shown in Figure 4.2. The computed values for the model coefficients and modeling noise were estimated using a least

squares procedure, as given in Table 4.1. Using the above algorithm, the negative of the conditional likelihood function, Figure 4.4, and its derivative were computed. As seen from the graph, the identified value of the extent a at which the negative of the likelihood function is minimum is approximately equals 10. Notice that this value is a global minimum of the LF. We restored the image using the identified parameter as $a=10$, using the Wiener filter. The result of restoration is given in Figure 4.3.

Next, we repeated the same experiment for $a=10$ and additive gaussian noise corresponding to 20 dB, as depicted in Figure 4.5. Table 4.2 shows the estimated values of $\{c(m,n)\}$ and σ_w^2. The values of the CLF and its derivatives as a function of the blur extent were computed. The identified value of the extent in this case is about 8.2, (see the minimum of the CLF in Figure 4.8). Using a rounded off value of the blur extent $a=8.0$, the restored image using the Wiener filter is shown in Figure 4.6, while the restored image using the actual value of the extent $a=10$ is shown in Figure 4.7, for the sake of comparison.

Figure 4.1 The original " Man and House" image

Figure 4.2 The degraded image with linear uniform motion blur of
extent $a=10$ and no noise added.

Figure 4.3 The restored image of Figure 4.2 using the identified
parameter of $a=10$.

Table 4.1: The modeling coefficients $c(k,l)$ and the modeling noise, σ_w^2 ,as estimated from the blurred image Figure 4.2.

$c(k,l)$	$k=1$	$k=0$	$k=-1$
$l=1$	-0.808	0.803	0.028
$l=0$	0.976		

$$\sigma_w^2 = 1.215$$
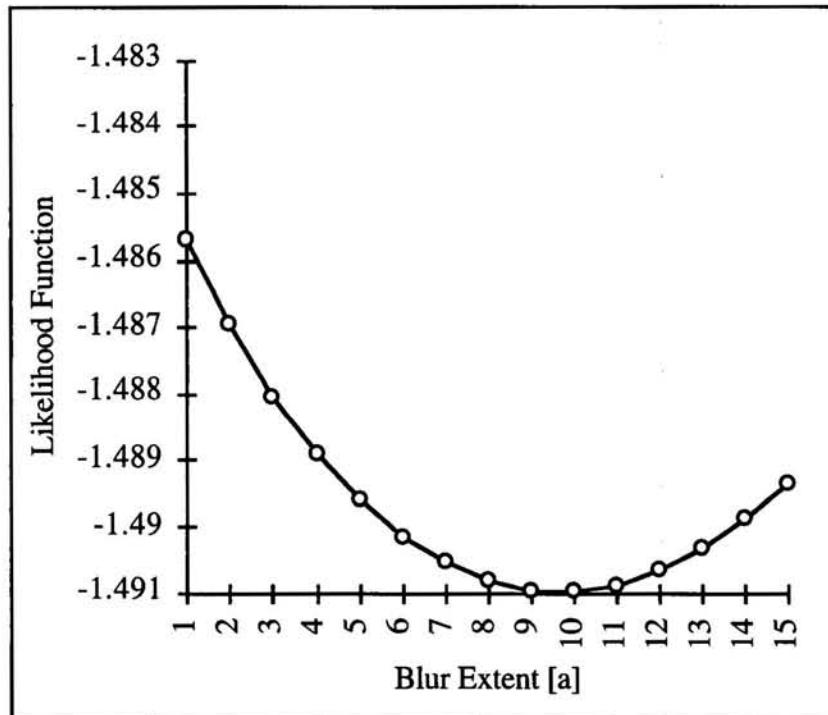
Figure 4.4 The CLF for the case of blur extent $a=10$ and with no noise added.

Figure 4.5 The degraded image with linear uniform motion blur of
extent $a=10$ and SNR=20 dB.

Figure 4.6 The restored image of Figure 4.5 using the identified parameter of $a=8$.

Figure 4.7 The restored image of Figure 4.5 using the actual parameter of $a=10$.

Table 4.2: The modeling coefficients $c(k,l)$ and the modeling noise, σ_w^2 ,as estimated from the blurred image Figure 4.5.

$c(k,l)$	$k=1$	$k=0$	$k=-1$
$l=1$	-0.815	0.794	0.032
$l=0$	0.988		

$$\sigma_w^2 = 1.215$$
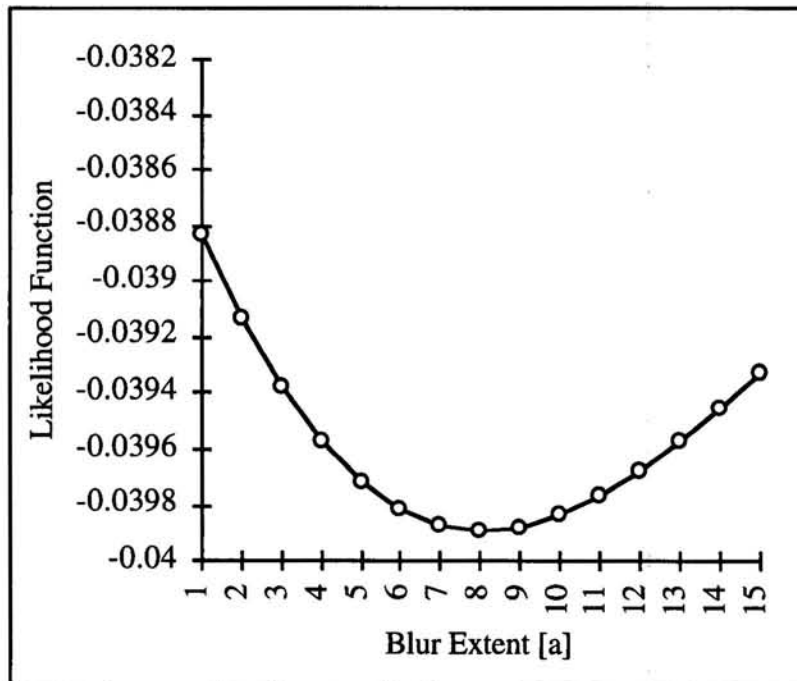
Figure 4.8 The CLF for the case of blur extent a=10 and SNR=20dB.

Case II: Out-of-focus blur

For the case of out-of-focus blur, we have blurred the Man and House image with a circular disc of size $R=7$, as given in Table 4.3 and added noise equivalent to 40 dB SNR. The resulting image is shown in Figure 4.9, and the estimated values of $\{c(m,n)\}$ and σ_w^2 are given in Table 4.4. The CLF, Figure 4.12, and its derivative were computed as a function of R. The identified value for R is about 5.8. Again, this shows the performance of this method even in the out-of-focus case. The restored images using the approximated value of $R=6.0$ and the actual value of $R=7.0$ are shown in Figure 4.10 and 4.11, respectively.

Figure 4.9 The degraded image with out-of-focus blur size of R=7, and SNR=40 dB.

Figure 4.10 The restored image of Figure 4.9 using the identified
parameter of $R=6$.

Figure 4.11 The restored image of Figure 4.9 using the actual
parameter of $R=7$.

85

Table 4.3 PSF for the out-of-focus blur with extent $R=7$
The blurred image is shown in Figure 4.9

$h(i,j)$		j						
		-3	-2	-1	0	1	2	3
	3	0	0.009138	0.02184	0.025674	0.02184	0.009138	0
	2	0.00913	0.02595	0.02598	0.02598	0.02598	0.02595	0.00913
	1	0.02184	0.02598	0.02598	0.02598	0.02598	0.02598	0.02184
i	0	0.02567	0.02598	0.02598	0.02598	0.02598	0.02598	0.02567
	-1	0.02184	0.02598	0.02598	0.02598	0.02598	0.02598	0.02184
	-2	0.00913	0.02595	0.02598	0.02598	0.02598	0.02595	0.00913
	-3	0	0.00913	0.02184	0.02567	0.02184	0.00913	0

Table 4.4: The modeling coefficients $c(k,l)$ and the modeling noise, σ_w^2 ,as estimated from the blurred image Figure 4.9.

$c(k,l)$	$k=1$	$k=0$	$k=-1$
$l=1$	-0.977	0.989	-0.004
$l=0$	0.991		

$$\sigma_w^2 = 1.215$$
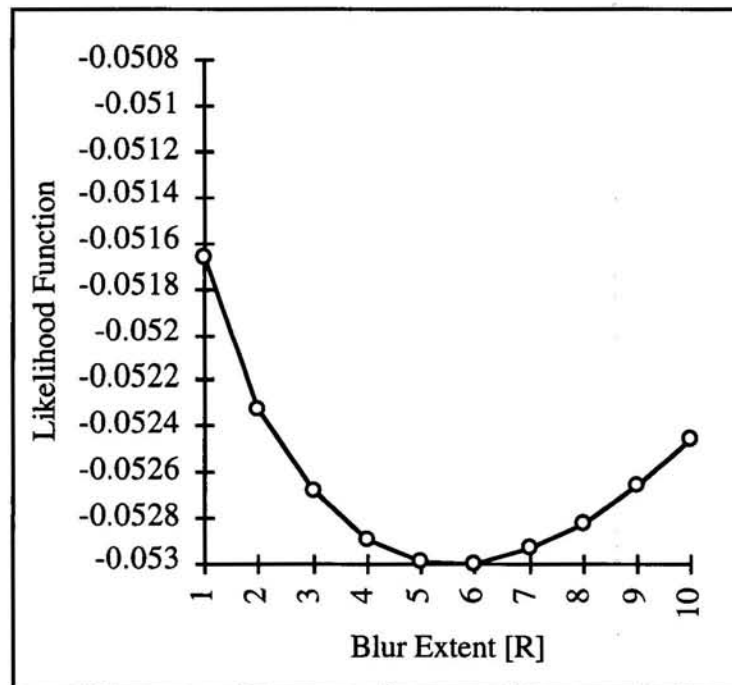
Figure 4.12 The CLF for the case of out-of-focus blur size of R=7, and SNR=40dB.

Case III: Angular linear motion blur

We consider now the case of general linear angular motion where the object image has been blurred in a direction of an angle $= \gamma$. For this case, the prescribed identification method can be modified to estimate the blur extent in two orthogonal directions. That is, given an image that is blurred in a diagonal direction, we first identify the horizontal (a_x) and vertical (a_y) blurs, then the resultant diagonal blur can be obtained using the simple geometrical relation $a = \sqrt{(a_x^2 + a_y^2)}$. The angle $\gamma = -\tan^{-1}\left[\frac{a_y}{a_x}\right]$ is needed to reconstruct the blur function for restoration.

This procedure has been successfully tested in the "Jets" image of Figure 4.13. We first blurred the image with diagonal blur of extent $a=10$ at angle $\gamma = 45$ degrees and added noise that is equivalent to 40 dB *SNR*, as seen in Figure 4.14. Next, we applied the identification procedure in both the x and y directions and recovered the parameters $a_x = 6.8$ and $a_y = 6.7$. The resultant extent $a = 9.6$ is of about 5% from the actual value and can be approximated by $a = 10$ to reconstruct the PSF for restoration. Figure 4.15 shows the result of restoring the blurred image with this value.

The same experiment was repeated for the value of $\gamma = 37$ degrees, $a=10$, and *SNR* = 40 dB. The values obtained from the likelihood function were $a_x = 4.8$ and $a_y = 8.3$, and $a = 9.6$. The blurred and the restored images are shown in Figures 4.16 and 4.17, respectively.
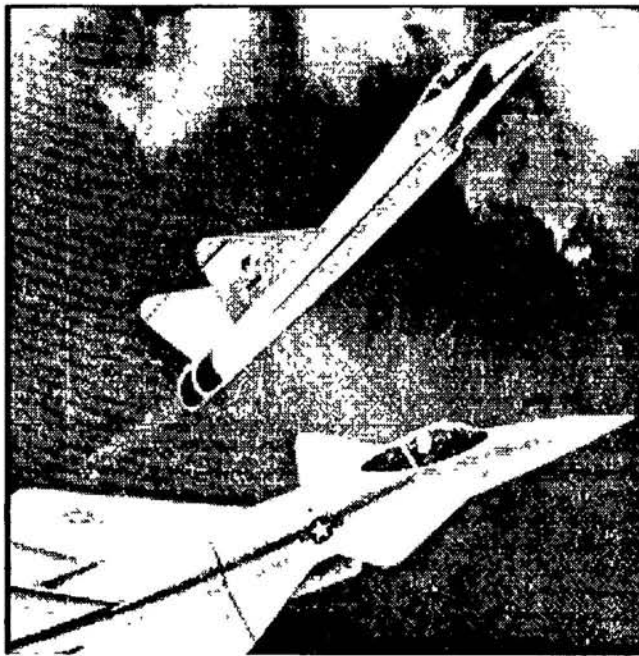
Figure 4.13 The original "Jets" image.

Figure 4.14 The diagonally blurred "Jets" image of Figure 4.13 with
a=10 at 45 degrees, and SNR=40dB.

Figure 4.15 The restored image of Figure 4.14 using the identified
parameter of a=10 in the 45 degrees direction.

Figure 4.16 The diagonally blurred "Jets" image of Figure 4.13 with
a=10 at 37 degrees, and SNR=40dB.
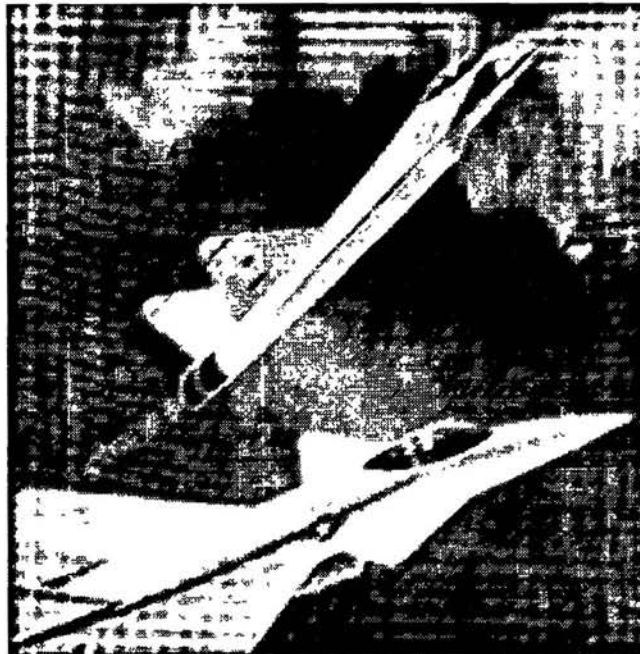
Figure 4.17 The restored image of Figure 4.16 using the identified
parameter of a=10 in the 37 degrees direction.

Effects of the Model Support Size

As stated in section 2.3, the size of the model support does not constitute a major factor in image restoration settings [42]. We have experimented this fact with the identification technique as follows. First, the modeling coefficients of the blurred Man and House image, with $a=10$ and $SNR=20$ dB, of Figure 4.5 were computed for support sizes of $k=l=2$ and $k=l=3$ as shown in Tables 4.5 and 4.6, respectively. Using the identification procedure for those two models resulted in a very slight improvement. The identified values for the blur extent a were 8.2 and 8.3 for the support sizes of $k=l=2$ and $k=l=3$, respectively. The identified value for the case $k=l=1$ was 8.2, as in Figure 4.8. Thus, a similar conclusion can be drawn from this experiment that the size of the model support is not very critical in both the restoration and identification settings.

Table 4.5 The Modeling coefficients estimated from Figure 4.5 with support size $k = l = 2$

$c(k,l)$	$k = 2$	$k = 1$	$k = 0$	$k = -1$	$k = -2$
$l = 2$	-0.067538	0.096462	0.125406	-0.263961	0.10658
$l = 1$	0.663171	-1.406765	0.58482	0.273594	-0.085394
$l = 0$	-0.791694	1.768369			

$$\sigma_w^2 = 2.612503$$

Table 4.6 The Modeling coefficients estimated from Figure 4.5 with support size $k = l = 3$

$c(k,l)$	$k = 3$	$k = 2$	$k = 1$	$k = 0$	$k = -1$	$k = -2$	$k = -3$
$l = 3$	-0.069618	0.223009	-0.161091	-0.203671	0.358262	-0.177479	0.036394
$l = 2$	0.103621	-0.34927	0.280258	0.292175	-0.579464	0.289153	-0.051082
$l = 1$	-0.090839	0.822648	-1.459834	0.525525	0.343239	-0.148433	0.026662
$l = 0$	0.110162	-0.991192	1.859833				

$$\sigma_w^2 = 3.325469$$

Noise Sensitivity

As reported in literature [42, 47], the performance of the identification techniques with respect to *SNR* varies from one to another. For example, the expectation maximization method (EM) [44,97], performs satisfactorily for *SNR* above 20 dB, beyond which the method provides poor results. The least square method [85], seems to perform satisfactorily for *SNR* above 40 dB and breaks down for *SNR* below that.

To test the performance of the technique at hand with respect to *SNR* variations, we have blurred the "Man and house" image with a linear uniform motion of extent $a=$ 10, and degraded it further with additive zero mean white noise with variances corresponding to *SNR* of 10, 15, 20, 30, 40, 50, and 60 dB. We applied the identification method to these blurred images and obtained different values for the extent a in Table 4.7. Next, we restored the images using those values as well as with the actual value of $a=$ 10. Figures 4.19 - 4.28 show the blurred and restored images at different *SNR* for the actual and identified parameters.

To incorporate the overall performance of identification and restoration, restored images are usually objectively evaluated using the following measure of improvement in *SNR* , α_{SNR}, as

$$\alpha_{SNR} = 10\log_{10} \frac{\sum_{m,n}[r(m,n)-s(m,n)]^2}{\sum_{m,n}[\hat{s}(m,n)-s(m,n)]^2} \qquad (4.38)$$

where $r(m,n)$ is the blurred image and $\hat{s}(m,n)$ represents the restored image using either the identified parameters or the actual one. Note that this evaluation can be studied for controlled experiments only since we have the original image $s(m,n)$. The maximally achievable *SNR* improvement depends on the content of the image, the type

of the blur, and the *SNR* of the blurred image [42]. The values of α_{SNR} obtained for the above experiments are given in Table 4.7.

Conclusion

From the above experiments, we observe that the parameters identified resulted in visually acceptable images. Also, the quantitative measures for the goodness of this estimation procedure prove its successful performance. These observations are in consistence with the results obtained by [63].

We observe from these results, that the method described in this chapter which is based on the continuous spatial domain model outperforms the other existing techniques, such as the one reported in [47], with regard to the noise factor. The noise sensitivity is tolerated for *SNR* levels above 20 dB at which the identified parameters are within 5% of the actual value. Moreover, the computation involved is much less than the one encountered in other techniques such as the EM method, for example.

Secondly, we did not need to guess the extent of the blur to get the maximum of the LF, as done in other methods, but rather we used the minimum value of the negative of the LF over a wide range of the extent values to identify the blur extent. Moreover, the behavior of the LF over the given range provides the novelty of this method to get a global minimum, which other methods are short to provide.

In the next chapter, we will extend the identification method presented in this chapter to the case of multichannel images.

Figure 4.19 The degraded "Man and House" image with linear
uniform motion blur of extent $a=10$ and SNR=10 dB.

(a)

(b)

Figure 4.20 The restored image of Figure 4.19
(a) using the identified parameter of $a=7.5$, (b) using the actual parameter of $a=10$

Figure 4.21 The degraded "Man and House" image with linear
uniform motion blur of extent a=10 and SNR=15 dB.

(a)

(b)

Figure 4.22 The restored image of Figure 4.21
(a) using the identified parameter of a=7.8, (b) using the actual parameter of a=10

Figure 4.23 The degraded "Man and House" image with linear
uniform motion blur of extent a=10 and SNR=20 dB.

(a)

(b)

Figure 4.24 The restored image of Figure 4.23
(a) using the identified parameter of $a=8$, (b) using the actual parameter of $a=10$

Figure 4.25 The degraded "Man and House" image with linear
uniform motion blur of extent $a=10$ and SNR=30 dB.

(a)

(b)

Figure 4.26 The restored image of Figure 4.25
(a) using the identified parameter of a=9.5, (b) using the actual parameter of a=10

105

Figure 4.27 The degraded "Man and House" image with linear
uniform motion blur of extent a=10 and SNR=40 dB.

Figure 4.28 The restored image of Figure 4.27
using the identified or actual parameter of a=10

Figure 4.29 The degraded "Man and House" image with linear
uniform motion blur of extent a=10 and SNR=50 dB.

Figure 4.30 The restored image of Figure 4.29
using the identified or actual parameter of a=10

Figure 4.31 The degraded "Man and House" image with linear
uniform motion blur of extent a=10 and SNR=60 dB.

Figure 4.32 The restored image of Figure 4.31
using the identified or actual parameter of a=10

Table 4.7 The improvement in SNR , α_{SNR} , for the restored images using the identified blur extents and the actual one, $a=10$

SNR	Identified	α_{SNR}	
(dB)	blur extent	Using identified extent	Using actual extent
10	7.5	3.4	3.61
20	8.2	3.52	3.82
30	9.5	4.35	4.71
40	9.8	4.9	5.15
50	10	5.33	5.46
60	10	5.54	5.68

العنوان:	CONTINUOUS SPATIAL DOMAIN IMAGE IDENTIFICATION AND RESTORATION WITH MULTICHANNEL APPLICATIONS
المؤلف الرئيسي:	Al Suwailem, Umar A.
مؤلفين آخرين:	Keller, James E.(super)
التاريخ الميلادي:	1996
موقع:	كولومبيا
الصفحات:	1 - 183
رقم MD:	616175
نوع المحتوى:	رسائل جامعية
اللغة:	English
الدرجة العلمية:	رسالة دكتوراه
الجامعة:	University of Missouri
الكلية:	The Graduate School
الدولة:	الولايات المتحدة الأمريكية
قواعد المعلومات:	Dissertations
مواضيع:	الهندسة الإلكترونية ، تطبيقات الحاسب ، ترميم الصور ، النمذجة ، الحركات الضبابية
رابط:	https://search.mandumah.com/Record/616175

www.manaraa.com

CHAPTER 5

MULTICHANNEL IMAGING

So far we have discussed the identification and restoration for single channel or monochrome images. This familiar class of images is encountered in many real life applications. However, another category of images that is of similar or even more importance is multichannel images. There are tremendous uses and applications in many fields for multichannel images, mainly because they provide more information than the monochrome ones.

Multichannel images refer to the data obtained from multiple sensors, time frames and sequences, and multiple spectral bands. For convenience, we will use the term multichannel to refer to images produced by imaging systems that use more than one sensor for the same scene. Although our formulation will emphasize and be applied to multispectral color images, it can be easily modified for other multichannel cases.

Restoration and identification research in the single channel case has almost reached a saturation level. However, its counterpart in multichannel case has not gained that much of attention. Previous related work in restoration was concentrated on three main areas,

113

namely, color correction due to imperfect recording [5,11,57,65,82], independent restoration of the channels or frames [5,8,11,27], and multichannel restoration techniques [9,20,27,33,58,59,87]. In all of these cases the issue of identification is not addressed.

The identification of the blur parameters and overall restoration of color images will be the topic of the next chapter. However, in this chapter, we review some related issues to multichannel imaging systems. In the next section, we will review the nature of color imaging and the relation between the different color models. In section 5.2 the correlation between spectral channels and the estimation of AR multichannel image model parameters are presented. Finally, in section 5.3 we will review image restoration techniques in independent and multichannel domains.

5.1 Nature of Color Images

Color is an important feature and has many useful implications in image processing. One of these advantages is that color serves as a reliable descriptor in image segmentation, object recognition, and feature extraction. Also, the human eye can distinguish thousands of colors but only a few dozen gray levels; hence, more visual information.

To the human eye, colors are visualized as the combination of different proportions of the primary colors red, green, and blue. There are several models for color representation that are widely used in practice, depending on the specific application. Among them are the, RGB (red, green, and blue) , YIQ (luminance, inphase, and quadrature) , CMY (cyan, magenta, and yellow) , and HSI (hue, saturation, and intensity) models. The transformation between the different models can be easily obtained from their corresponding definitions. References [22,29,31,39,74] provide the definitions and transformations between these models.

114

In our study, we will consider the RGB and YIQ models simply because they are frequently used in image processing and lend themselves to viewable display representation. Although the HSI representation is also suitable for image manipulation, it has to be converted at the end to a visual domain such as RGB or YIQ. The CMY model, which contains the three secondary colors, is oriented towards the design of color printing machines.

5.1.2 The RGB Model

In the RGB representation, different linear combinations of the primary spectral components, red, green and blue, constitute each color. This can be best understood if we can visualize the relation between colors, as represented in Figure 5.1. In this figure, it is assumed that the color values are normalized so that the cube is of unit size [22]. Black is located at the origin of the cube, white at the furthest corner from black and the line extending between them represent the gray scale. The color at any point P on or inside the cube is described by a vector extending from the origin and representing the different values of R, G, and B components.

Color images are normally represented as three different planes or frames, one for each of the primary colors. Thus, in color image processing we extract each of these spectral frames, process them independently or in a multichannel formulation, and finally put them back in their combined representation for visual and analysis purposes. Most visual systems and cameras used today utilize RGB representation, which makes this model suitable for image processing and display [22].
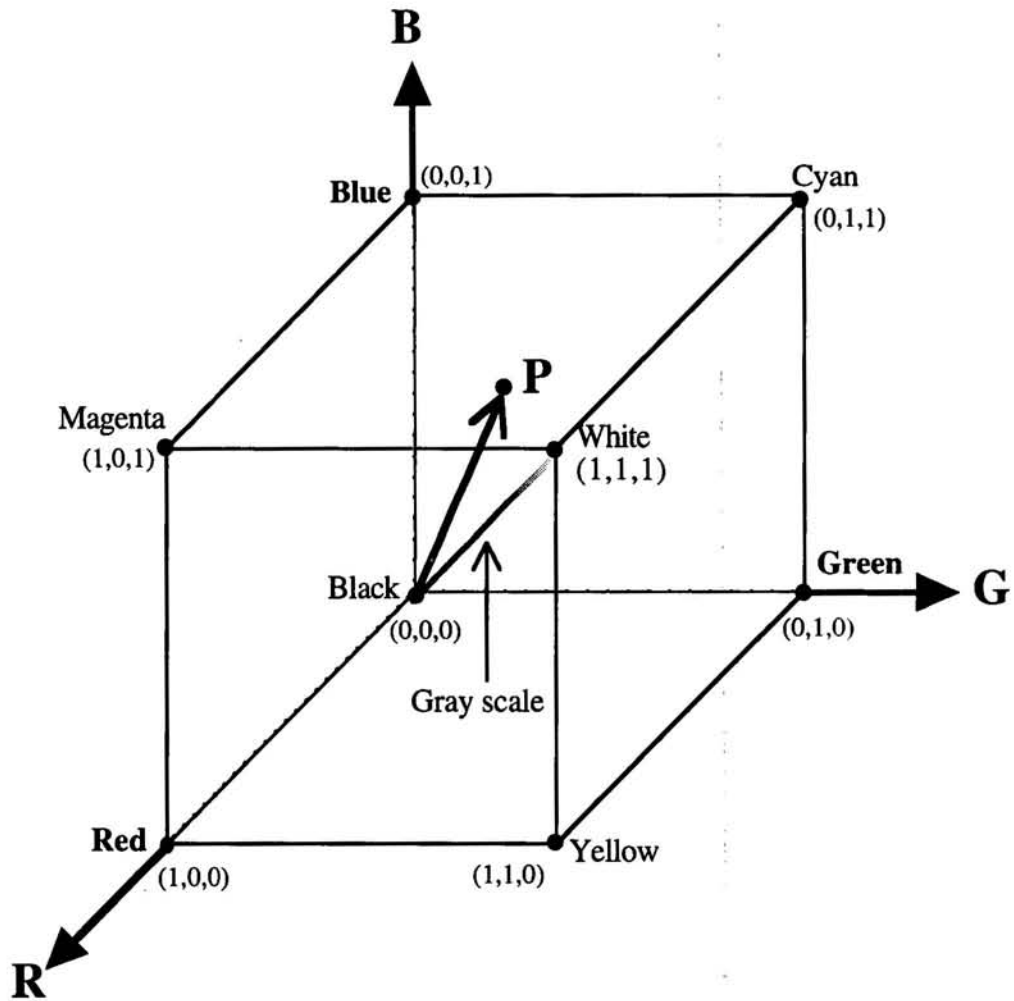
Figure 5.1 The relation between colors in the RGB domain. The color value at point P is the proportional combination of red, green, and blue. The gray scale extends between black and white colors.

5.1.2 The YIQ Model

The YIQ (luminance, inphase, and quadrature) model is a transformed model from the primary RGB model, mainly for the purpose of efficient transmission. It is also used in color television broadcasting because it is compatible with monochrome reception. Experimental evidence [27], suggests that the Y component, luminance, contains the significant part (85-95 percent) of the visual information in color imagery. The transformation between RGB and YIQ is defined as

$$\begin{bmatrix} Y \\ I \\ Q \end{bmatrix} = \begin{bmatrix} 0.299 & 0.587 & 0.114 \\ 0.596 & -0.275 & -0.321 \\ 0.212 & -0.523 & 0.311 \end{bmatrix} \begin{bmatrix} R \\ G \\ B \end{bmatrix} \qquad (5.1)$$

By matrix inversion we can get the RGB components from the YIQ ones.

One of the major advantages of the YIQ modeling is that the Y component can be easily decoupled from the I and Q components [27,22]. This procedure allows processing the Y component alone, without affecting the color content, then adding the I and Q components for color visibility. As we will see later in this chapter, this procedure is acceptable but has some drawbacks.

To illustrate the above discussion on color representation, we present the following examples. Figure 5.2 shows the original color image of a "Tank". The three primary planes or channels of red, green, and blue are extracted and shown in figure 5.3a-c, respectively. Next, the YIQ components were computed from their RGB counterparts which are shown in Figure 5.4a-c, respectively. Notice, as mentioned above, that the Y component has more definition about the image than the I and Q channels. These images will be used in the following sections for illustrating the identification and restoration techniques.
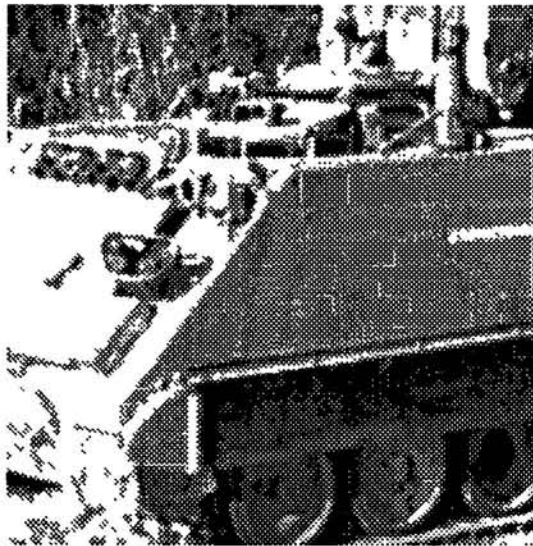
Figure 5.2 The original color "TANK" image.

(a)

(b)

(c)
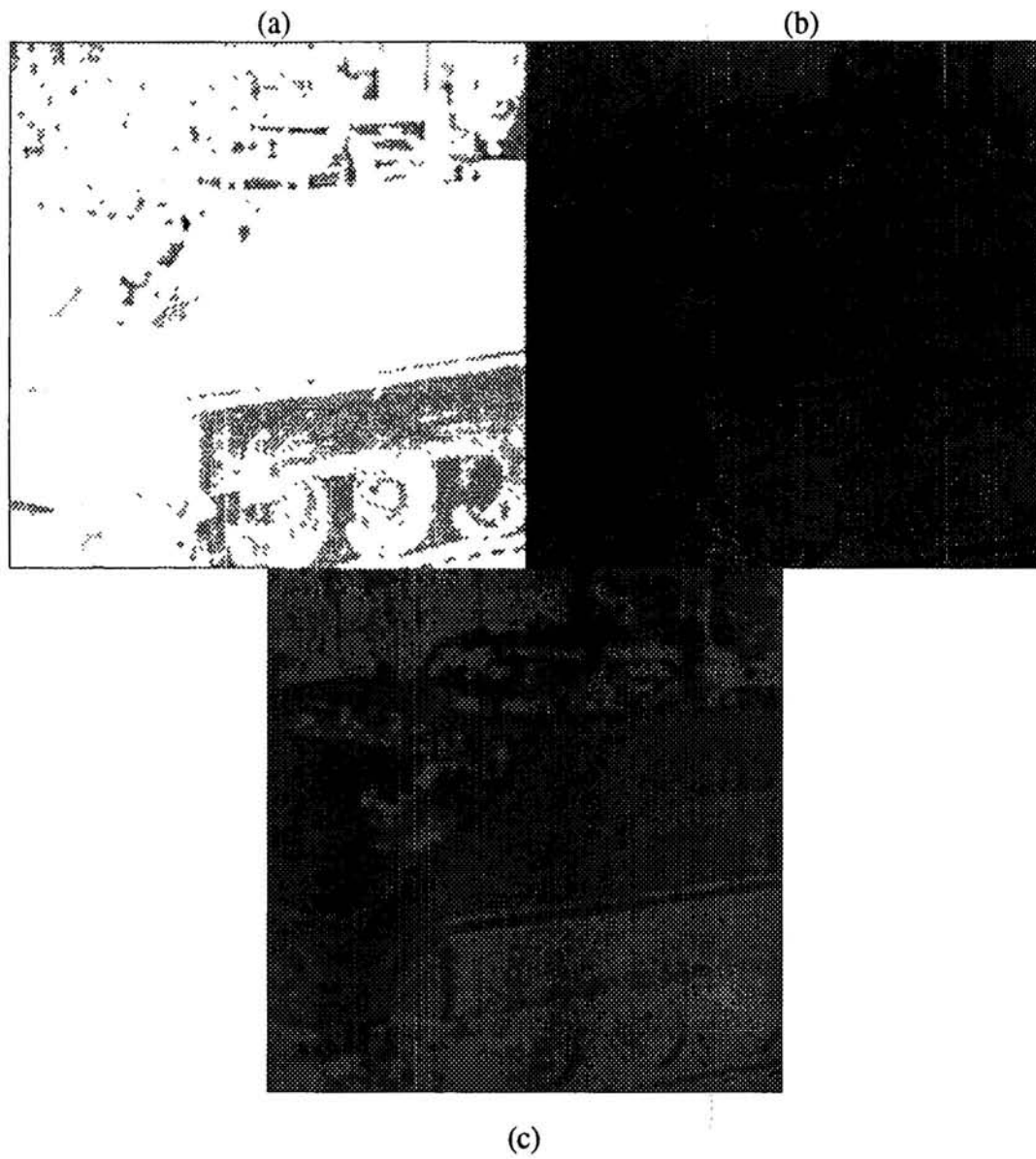
Figure 5.3 The extraxted primary color of the "TANK" image
(a) Red, (b) Green, and (c) Blue
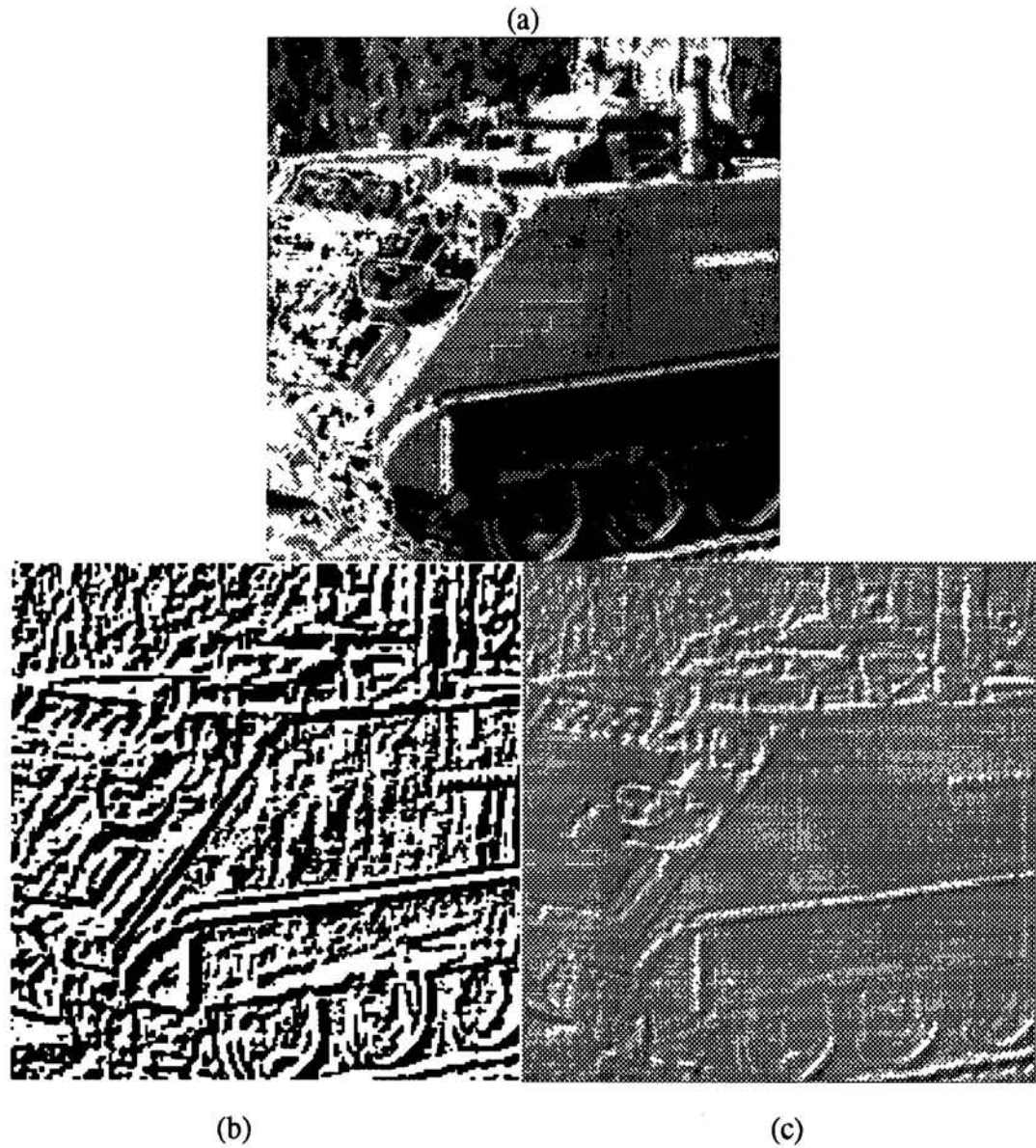
Figure 5.4 The extraxted spectral channels of the "TANK" image in the YIQ domain
(a) Y (luminance), (b) I (inphase), and (c) Q (quadrature)

5.2 Correlation Between Channels

In this section, we will discuss the correlation between channels or spectral images; since this factor contributes a major part in the performance of identification and restoration techniques, as we will see later in this chapter and the next chapter. Let us first consider the multichannel modeling proposed in section 2.7. The AR multichannel image model for the *pth* channel, equation (2.24), can be written as

$$s_p(m,n) = \sum_{q=1}^{N} \sum_{R_{pq}} c^{pq}(k,l) \, s_q(m-k,n-l) + w_p(m,n) \tag{5.2}$$

which can be expressed in a matrix form as

$$s(m,n) = C' s_1(m,n) + w(m,n) \tag{5.3}$$

where $s(m,n)$, $s_1(m,n)$, $w(m,n)$ represent the lexicographical order of the corresponding vectors as

$$s(m,n) = [\, s_1(m,n) \quad s_2(m,n) \quad ..... \quad s_N(m,n)\,]^t \tag{5.4}$$

$$s_1(m,n) = [\, s_{1,1}(m,n) \quad s_{1,2}(m,n) \quad ..... \quad s_{1,N}(m,n)\,]^t \tag{5.5}$$

$$w(m,n) = [\, w_1(m,n) \quad w_2(m,n) \quad ..... \quad w_N(m,n)\,]^t \tag{5.6}$$

$s_{1,q}$ is the vector formed from the pixels that correspond to the coupling coefficients in the model support R_{pq}, for $p = 1,2,...,N$, and C is the model parameters matrix. Note that the choice of the model support, R_{pq}, is as described in section 2.7 and Figures 2.4 and 2.5. Such representation allows us to estimate the model coefficients for the multichannel

case. To do so, we will use the least squares method as described in [37,61,87], (see Appendix C). The model parameters may be estimated as

$$\hat{C}' = [E\{s_i'(m,n)s_1(m,n)\}]^{-1} E\{s_i'(m,n)s(m,n)\} \tag{5.7}$$

and are estimated to minimize the trace of the matrix Q_{ww} given by

$$Q_{ww} = E[\{s(m,n) - \hat{C}'s_1(m,n)\}\{s(m,n) - \hat{C}'s_1(m,n)\}'] \tag{5.8}$$

Thus, the procedure for estimating those parameters can be described as follows:

1- Collect the pixel data over a representative data block, a sufficiently large region in the image or the whole image.

2- Form a set of index pairs (k,l) corresponding to the unknown coefficients.

3- Find the expectation, which is approximated by averaging the products over the data.

4- Solve for the components of $\hat{C}$ directly from equation (5.7)

5- Compute the fit error matrix Q_{ww} from equation (5.8)

We should note here that, in practice, the original image is not available to estimate the model coefficients from. Thus, the given degraded image is used for this purpose as a prototype image representing a realization of the ensemble of images for this model. Also, the expectations in (5.7) and (5.8) are replaced by the sample averages over one realization. It has been shown by Trussel *et al.* [93] that the sensitivity of this approximation in computing the model coefficients is minimal using least squares estimation when compared to other techniques such as the periodogram and windowing.

We have tested the least squares procedure, described above, for color images and estimated the AR multichannel model coefficients using the NSHP support model given in Figure 2.4. The "TANK" image of Figure 5.2 was used for these experiments in both the RGB and YIQ domains described in the previous section. First, in RGB domain, the model coefficients were identified for each of the three channels independently and the

122

result is shown in Table 5.1. Next, the multichannel procedure described above was applied to the same image and the result is given in Table 5.2. The same experiments were also repeated for the TANK image but now in the YIQ domain. The estimated parameters for the independent and multichannel estimation are given in Table 5.3 and 5.4, respectively.

From these tables, we observe that the use of multichannel AR model estimation reduces the fit error in the channels, given by Q_{ww}. For example, compare the values of σ_w^2 in Table 5.1 with those of Table 5.2 for the green, blue, and red components, the multichannel ones are smaller than those estimated independently. In the YIQ domain, we observe that the correlation between channels is minimal and the major contribution of the modeling is accounted for from the Y component. This confirms the findings in the previous section.

We will see next, and in the following chapter, the importance of incorporating the model parameters in the identification and restoration of multichannel images.

Table 5.1 The estimated AR model coefficients of the "TANK" image assuming independent RGB model.

	R			G			B		
R	0.11898	-0.32657	0.26746						
	0.90343								
			289.523						
G				0.11673	-0.32374	0.27462			
				0.91145					
						295.054			
B							0.12012	-0.34582	0.29016
							0.89954		
									298.739

The coefficients are arranged in this order

$c_{1,1}$	$c_{0,1}$	$c_{-1,1}$
$c_{1,0}$		
		$\sigma^2_{w_p}$

Table 5.2 The estimated AR model coefficients of the "TANK" image assuming multichannel RGB model.

	R			G			B		
R	0.10898	-0.30694	0.27702	0.0193	0.016624	0.00977	0.27613	-0.32761	0.11257
	0.91252			0.94932			0.93208		
			256.815			32.559			30.416
G	0.26072	-0.32779	0.11033	0.10294	-0.31231	0.28748	0.00569	0.023614	0.0227
	0.89538			0.9132			0.9536		
			32.559			268.337			32.613
B	0.04138	-0.0074	0.04884	0.30545	-0.35096	0.14311	0.12602	-0.35298	0.3061
	0.90607			0.8915			0.91231		
			30.416			32.613			270.523

The coefficients are arranged in this order

$c_{1,1}$	$c_{0,1}$	$c_{-1,1}$
$c_{1,0}$		
		$\sigma_{w_p}^2$

Table 5.3 The estimated AR model coefficients of the "TANK" image assuming independent YIQ model.

	Y			I			Q		
Y	-0.13902	0.45198	0.27692						
	0.84203								
			198.536						
I				-0.72351	-0.09762	0.01894			
				0.34781					
						31.208			
Q							-0.07298	-0.13274	0.07362
							0.05291		
									25.618

The coefficients are arranged in this order

$c_{1,1}$	$c_{0,1}$	$c_{-1,1}$
$c_{1,0}$		
		$\sigma^2_{w_p}$

Table 5.4 The estimated AR model coefficients of the "TANK" image assuming multichannel YIQ model.

	Y			I			Q		
Y	-0.15631	0.59326	0.25632	-0.06538	0.08395	0.00439	0.27613	0.08532	-0.03183
	0.86325			0.18321			0.08352		
			249.863			12.672			10.893
I	-0.05172	0.31132	0.03327	-0.81352	-0.11732	0.02315	-0.0119	0.02553	0.16213
	0.09117			0.03552			0.00781		
			12.672			41.571			15.562
Q	0.03519	-0.01428	0.0881	-0.1305	-0.05436	0.0315	-0.09328	-0.13325	0.06734
	0.05318			0.14421			0.06149		
			10.893			15.562			29.462

The coefficients are arranged in this order

$c_{1,1}$	$c_{0,1}$	$c_{-1,1}$
$c_{1,0}$		
		$\sigma^2_{w_p}$

5.3 Independent and Multichannel Restoration

In this section we review some of the techniques used in restoring multichannel images. Although our main objective is image identification, as in the single channel case, restoration is used in conjunction with identification for an overall evaluation of the combined process. Thus, we first discuss some of the available approaches in literature, namely, the independent and multichannel restoration. Then, in the next chapter we present the multichannel identification.

5.3.1 Independent Restoration

One approach to restore degraded multichannel images is to deblurr each channel separately. Assuming that the PSF of the blur and the statistics of noise are known, one can apply the available techniques of monochrome restoration to each channel or spectral component. Consider the formulation of a multichannel image as a lexicographical order of its N spectral components as

$$\boldsymbol{s}(m,n) = [\, \mathbf{s}_1(m,n) \quad \mathbf{s}_2(m,n) \quad \ldots \quad \mathbf{s}_N(m,n)]' \qquad (5.9)$$

Then, the autocorrelation matrix can be computed as

$$\boldsymbol{P}_{ss} = E[\mathbf{ss}'] = \begin{bmatrix} P_{ss}^{11} & P_{ss}^{12} & \cdots & P_{ss}^{1N} \\ P_{ss}^{21} & P_{ss}^{22} & \cdots & P_{ss}^{2N} \\ \cdot & \cdot & \cdot & \cdot \\ \cdot & \cdot & \cdot & \cdot \\ P_{ss}^{N1} & P_{ss}^{N2} & \cdots & P_{ss}^{NN} \end{bmatrix} \qquad (5.10)$$

128

where each of the components P_{ss}^{ij} is the correlation between the spectral components i and j. We note that, in general, the cross channel correlations are not the same since each channel is characterized by different properties. This means that P_{ss} is not block Toeplitz matrix and can not be diagonalized by the DFT to be used in the restoration filter . However, each P_{ss}^{ij} is a block Toeplitz as explained earlier in section 4.2.

In independent restoration, the channels are assumed to be uncorrelated, i.e. $P_{ss}^{ij} = 0$ for $i \neq j$, and only the diagonal elements of equation (5.3) exist. Thus, each channel is treated as a single entity and restored individually. This procedure was used in several studies [5,11,27]. Obviously, it produced suboptimal restoration results due to the fact that there exists some correlation between channels. Techniques that overcome this problem is discussed next.

5.3.2 Multichannel Restoration

Several attempts are reported in the literature to overcome the suboptimality problem of independent restoration by incorporating the cross spectral information and treating the multichannel image as one entity [4,19,20,27,33,36,87]. We will discuss here the development of two famous filters, namely, Wiener and Kalman multichannel filters.

Multichannel Wiener Filter Restoration

Consider the observation model given by equation (2.26), which can be represented in lexicographic order as

$$r = Hs + v \tag{5.11}$$

Then, the linear minimum mean square error (LMMSE) solution that describes the Wiener filter and recovers the image from its degraded version can be extended from the single channel case, equation (3.6), and is given by

$$\hat{s} = P_{ss}H'[HP_{ss}H' + Q_{vv}]^{-1}r \qquad (5.12)$$

where $\hat{s}$ represents the restored image [19,20]. The problem with this formulation, however, is the inversion of the huge matrix, $[HP_{ss}H' + Q_{vv}]$. For any practical image size, direct inversion is almost impossible. Note that the main factor that contributes to this difficulty is the correlation matrix given by P_{ss} where the cross spectral components are assumed to be incorporated. Taking advantage of the matrix structures in equation (5.12), Galatsenos *et al.* [20] and Angelopoulos *et al.* [4] proposed simplifications that reduce the computation to iterative inversion of small-sized matrices. Recently, Ozkan *et al.* [59] proposed a simplified inversion algorithm where inversion of the $NM^2 \times NM^2$ matrix is reduced to inverting $N \times N$ matrices M times. Considering a multichannel image of size $M \times M$ and N channels, this algorithm produce a great reduction in computation. We have used this simplification algorithm to implement the multichannel Wiener restoration filter that will be used following the identification procedure of the next chapter.

Multichannel Kalman Filter Restoration

In a recent paper [87], the development of Kalman filter for the multichannel case was presented. Following the formulation of 2-D reduced update Kalman filter (RUKF), as explained in chapter 3, the multichannel Kalman filter can be easily extended in the following manner.

Let us first consider the AR multichannel image model given by equation (2.25) and introduce its state representation of the N channels by stacking the state vectors of equation (3.8) for the 2-D Kalman filter. Next, we partition this state vector into a local vector, $s_1^{(m,n)}$, and a vector of the remaining elements, $s_2^{(m,n)}$, as defined in equation (3.16) of the RUKF. The resulting multichannel local state vector, assuming an NSHP model of order M, is given by

$$
\begin{aligned}
\mathbf{s}_1^{(m,n)} = [& s_1^{(m,n)}, s_1^{(m-1,n)}, \dots, s_1^{(m-M+1,n)}, \\
& s_1^{(m+M+1,n-1)}, \dots, s_1^{(m-M+1,n-M)}, \\
& s_2^{(m,n)}, s_2^{(m-1,n)}, \dots, s_2^{(m-M+1,n)}, \\
& s_2^{(m+M+1,n-1)}, \dots, s_2^{(m-M+1,n-M)}, \\
& \dots, \\
& \dots, \\
& s_N^{(m,n)}, s_N^{(m-1,n)}, \dots, s_N^{(m-M+1,n)}, \\
& s_N^{(m+M+1,n-1)}, \dots, s_N^{(m-M+1,n-M)},]^t
\end{aligned}
\tag{5.13}
$$

where $s_i^{(m,n)}$ is the state at location (m,n) of the i th channel. Thus, the AR multichannel image model can be expressed in state-space as

$$
s_1^{(m,n)} = C_{11} s_1^{(m-1,n)} + C_{12} s_2^{(m-1,n)} + w_1(m,n)
\tag{5.14}
$$

Similarly, the observation model of equation (2.26) can be represented as

$$
r(m,n) = H_1^t s_1^{(m,n)} + v(m,n)
\tag{5.15}
$$

Where the vectors $r(m,n)$, and $v(m,n)$ are the lexicographic orders of the corresponding terms in the N channels, and H_1 is given by

$$
H_1 = \begin{bmatrix}
\mathbf{H}_1^{11} & \mathbf{H}_1^{12} & . & \mathbf{H}_1^{1N} \\
\mathbf{H}_1^{21} & \mathbf{H}_1^{22} & . & \mathbf{H}_1^{2N} \\
. & . & . & . \\
\mathbf{H}_1^{N1} & \mathbf{H}_1^{N2} & . & \mathbf{H}_1^{NN}
\end{bmatrix}
\tag{5.16}
$$

We may now write the RUKF multichannel Kalman filter equations as an extension of the monochrome case as the following sequence of operations:

state prediction:

$$\hat{\mathbf{s}}_{1,b}^{(m,n)} = \mathbf{C}_{11}\hat{\mathbf{s}}_{1,a}^{(m-1,n)} + \mathbf{C}_{12}\hat{\mathbf{s}}_{2,a}^{(m-1,n)} \tag{5.17}$$

error covariance prediction:

$$\mathbf{U}_{b}^{(m,n)} = \mathbf{C}\mathbf{U}_{a}^{(m-1,n)}\mathbf{C}^{t} + \mathbf{Q}_{w} \tag{5.18}$$

Kalman gain:

$$\mathbf{K}_{1}^{(m,n)} = \mathbf{U}_{11,b}^{(m,n)}\mathbf{H}_{1}[\mathbf{H}_{1}^{t}\mathbf{U}_{11,b}^{(m,n)}\mathbf{H}_{1} + \boldsymbol{\sigma}_{v}]^{-1} \tag{5.19}$$

state update:

$$\hat{\mathbf{s}}_{1,a}^{(m,n)} = \hat{\mathbf{s}}_{1,b}^{(m,n)} + \mathbf{K}_{1}^{(m,n)}[r(m,n) - \mathbf{H}_{1}^{t}\hat{\mathbf{s}}_{1,b}^{(m,n)}] \tag{5.20}$$

and, error covariance update:

$$\mathbf{U}_{11,a}^{(m,n)} = [\mathbf{I} - \mathbf{K}_{1}^{(m,n)}\mathbf{H}_{1}]\mathbf{U}_{11,b}^{(m,n)} \tag{5.21a}$$

$$\mathbf{U}_{12,a}^{(m,n)} = [\mathbf{I} - \mathbf{K}_{1}^{(m,n)}\mathbf{H}_{1}]\mathbf{U}_{12,b}^{(m,n)} \tag{5.21b}$$

Where

$$\mathbf{Q}_{w} = E[w(m,n)w^{t}(m,n)]$$

$$= \begin{bmatrix} Q_{w_{11}} & Q_{w_{12}} & \cdots & Q_{w_{1N}} \\ Q_{w_{21}} & Q_{w_{22}} & \cdots & Q_{w_{2N}} \\ \cdot & \cdot & \cdot & \cdot \\ Q_{w_{N1}} & Q_{w_{N2}} & \cdots & Q_{w_{NN}} \end{bmatrix} \tag{5.22}$$

$$\sigma_v = E[\mathbf{v}(m,n)\mathbf{v}'(m,n)]$$

$$= \begin{bmatrix} \sigma_{v_{11}}^2 & \sigma_{v_{12}}^2 & \cdots & \sigma_{v_{1N}}^2 \\ \sigma_{v_{21}}^2 & \sigma_{v_{21}}^2 & \cdots & \sigma_{v_{2N}}^2 \\ \cdot & \cdot & \cdot & \cdot \\ \sigma_{v_{N1}}^2 & \sigma_{v_{N2}}^2 & \cdots & \sigma_{v_{NN}}^2 \end{bmatrix} \tag{5.23}$$

and

$$\mathbf{U}_b^{(m,n)} = E[(s^{(m,n)} - \hat{s}_b^{\ (m,n)})(s^{(m,n)} - \hat{s}_b^{\ (m,n)})^t] \tag{5.24}$$

This formulation of the multichannel Kalman filter is computationally efficient. To compute the Kalman gains, we need to invert the matrix $[\mathbf{H}_1^t \mathbf{U}_{11,b}^{(m,n)} \mathbf{H}_1 + \sigma_v]$ of size $N \times N$ at each pixel, where N is the number of channels. Also, for the case of block diagonal blur function where $\mathbf{H}_1^{pq} = 0$ for $p \neq q$, the need for matrix multiplications in $[\mathbf{H}_1^t \mathbf{U}_{11,b}^{(m,n)} \mathbf{H}_1 + \sigma_v]^{-1}$ can be reduced to

$$\sum_{kl} \sum_{ij} h_{kl}^{pp} h_{ij}^{qq} U_{b,pq}^{(m,n)}(m-k,n-l;m-i,n-j) + \sigma_{v_{pq}}^2 \tag{5.25}$$

In the next chapter, we will also use this filter for restoring the multichannel images in conjunction with the identification results.

العنوان:	CONTINUOUS SPATIAL DOMAIN IMAGE IDENTIFICATION AND RESTORATION WITH MULTICHANNEL APPLICATIONS
المؤلف الرئيسي:	Al Suwailem, Umar A.
مؤلفين آخرين:	Keller, James E.(super)
التاريخ الميلادي:	1996
موقع:	كولومبيا
الصفحات:	1 - 183
رقم MD:	616175
نوع المحتوى:	رسائل جامعية
اللغة:	English
الدرجة العلمية:	رسالة دكتوراه
الجامعة:	University of Missouri
الكلية:	The Graduate School
الدولة:	الولايات المتحدة الأمريكية
قواعد المعلومات:	Dissertations
مواضيع:	الهندسة الإلكترونية ، تطبيقات الحاسب ، ترميم الصور ، النمذجة ، الحركات الضبابية
رابط:	https://search.mandumah.com/Record/616175

CHAPTER 6

MULTICHANNEL BLUR IDENTIFICATION

In the previous chapter, the blur characteristics described by its PSF are assumed to be known prior to the restoration procedure. In some practical situations, this assumption may not be valid. In fact, in some other cases, the given blur PSF is far away from the actual one. Although multichannel restoration has been researched to some extent, multichannel identification has not, mainly because of its complexity and difficulty. Among the rare works in this area is that of Pavlovic *et al.* [62], where parameter identification was applied to multiframe image sequences. The purpose of this chapter is to develop a successful technique that can handle the identification issue in multichannel imaging.

In this chapter, we propose a multichannel blur identification technique for images degraded by the two types of blur that are mostly encountered in practice, namely, uniform linear motion and out-of-focus blurs. The successful formulation used in the single channel case of chapter 4 will be extended to the multichannel case. Again, the advantage of using the continuous spatial domain model will be employed here.

However, we should mention here that there is an important factor that needs to be incorporated in this extension, namely, the cross spectral interference. This degradation is additional to the one encountered in the single channel case. Identification and restoration have to include these factors for optimal solution; otherwise, the solution is suboptimal and in some situations the results may become of no practical use.

In the next section, we will show the formulation and derivations for multichannel identification. Based on the continuous spatial domain model, we will project the novelty and advantages of the single channel method of chapter 4 to the multichannel case. Finally, the experimental results for the proposed method of identification are presented.

6.1 Formulation for Multichannel Blur Identification

Following the AR image and observation models formulations given in [59,62,87,90], we consider here the multichannel modeling mentioned in section 2.7. The image and observation models for the pth channel are given by equations (2.24) and (2.25) as

$$s_p(m,n) = \sum_{q=1}^{N} \sum_{R_{pq}} c^{pq}(k,l) \, s_q(m-k,n-l) + w_p(m,n) \qquad (6.1)$$

$$r_p(m,n) = \sum_{q=1}^{N} \sum_{(k,l) \in S_h} h^{pq}(k,l) \, s_q(m-k,n-l) + v_p(m,n) \qquad (6.2)$$

respectively, which can be written in a matrix form as

$$\mathbf{s}_p = \mathbf{C}^{pq}\mathbf{s}_p + \mathbf{w}_p \qquad (6.3)$$

$$\mathbf{r}_p = \mathbf{H}^{pq}\mathbf{s}_p + \mathbf{v}_p \qquad (6.4)$$

135

where, $\mathbf{s}_p$, $\mathbf{r}_p$, $\mathbf{w}_p$, and $\mathbf{v}_p$ are the lexicographic order of the corresponding terms in equations (6.1) and (6.2), $\mathbf{C}^{pq}$ and $\mathbf{H}^{pq}$ represent the appropriate ordering of the model and blur coefficients, respectively. Further, we may write the set of equations (6.3) and (6.4) in lexicographic orders to get

$$s = Cs + w \tag{6.5}$$

$$r = Hs + v \tag{6.6}$$

where now, the $NM^2 \times 1$ vectors r, s, v, and w are the lexicographic order of $\mathbf{s}_p$, $\mathbf{r}_p$, $\mathbf{w}_p$, and $\mathbf{v}_p$, for $, p = 1,2,...,N$ and $q = 1,2,...,N$, respectively, and where C is the image model matrix and H is the degradation or blur matrix both of size $(NM^2 \times NM^2)$ having the following structure

$$H = \begin{bmatrix} \mathbf{H}^{11} & \mathbf{H}^{12} & ... & \mathbf{H}^{1N} \\ \mathbf{H}^{21} & \mathbf{H}^{22} & ... & \mathbf{H}^{2N} \\ ... & ... & ... & ... \\ \mathbf{H}^{N1} & \mathbf{H}^{N2} & ... & \mathbf{H}^{NN} \end{bmatrix} \tag{6.7}$$

$$C = \begin{bmatrix} \mathbf{C}^{11} & ... & ... & \mathbf{C}^{1N} \\ ... & \mathbf{C}^{22} & ... & ... \\ ... & ... & ... & ... \\ \mathbf{C}^{N1} & ... & ... & \mathbf{C}^{NN} \end{bmatrix} \tag{6.8}$$

both H and C are block matrices.

Following the procedure we used to derive the PDF of the observed image, we may now express the PDF of r, which is also Gaussian, as

$$p(r;\Theta) = \frac{1}{\sqrt{(2\pi)^{N^2}|P_{rr}|}} \exp\left(\frac{1}{2} r' P_{rr}^{-1} r\right) \tag{6.9}$$

where now, the vector Θ represents the unknown parameters, $h_{i,j}(k,l), c_{ij}(m,n), \sigma^2_{v_{ij}}, \sigma^2_{w_i},$ and the covariance matrix $\boldsymbol{P}_{rr}$ is structured as

$$\boldsymbol{P}_{rr} = \begin{bmatrix} \mathbf{P}^{11}_{rr} & \cdots & \cdots & \mathbf{P}^{1N}_{rr} \\ \cdots & \mathbf{P}^{22}_{rr} & \cdots & \cdots \\ \cdots & \cdots & \cdots & \cdots \\ \mathbf{P}^{N1}_{rr} & \cdots & \cdots & \mathbf{P}^{NN}_{rr} \end{bmatrix} \qquad (6.10)$$

Elements of each block of $\boldsymbol{P}_{rr}$ are computed as

$$\mathbf{P}^{ij}_{rr}(k,l) = E[r_i(m,n)r_j(m+k,n+l)] \qquad (6.11)$$

for $i,j = 1,2,...,N$ where N is the number of channels. Notice that $\boldsymbol{P}_{rr}$ is not a Toeplitz matrix because of the structure of $\boldsymbol{C}$ where cross-spectral components are not the same in each channel. However, each block element of $\boldsymbol{P}_{rr}$ is a Toeplitz matrix and $\mathbf{P}^{ij}_{rr} = [\mathbf{P}^{ij}_{rr}]'$. We may now express $\boldsymbol{P}_{rr}$ in terms of $\boldsymbol{C}$ and $\boldsymbol{H}$ as

$$\begin{aligned} \boldsymbol{P}_{rr} &= E[\boldsymbol{rr}^t] \\ &= E[\{\boldsymbol{H}(\boldsymbol{I} - \boldsymbol{C})^{-1}\boldsymbol{w} + \boldsymbol{v}\}\{\boldsymbol{H}(\boldsymbol{I} - \boldsymbol{C})^{-1}\boldsymbol{w} + \boldsymbol{v}\}^t] \end{aligned} \qquad (6.12)$$

which can be simplified as

$$\boldsymbol{P}_{rr} = \boldsymbol{H}(\boldsymbol{I} - \boldsymbol{C})^{-1}\boldsymbol{P}_{ww}(\boldsymbol{I} - \boldsymbol{C})^{-t}\boldsymbol{H}^t + \boldsymbol{P}_{vv} \qquad (6.13)$$

6.2 Maximum Likelihood Estimator

The maximum likelihood estimate is obtained by maximizing the LF given by definition (4.2). Using (6.9), (6.13) in that definition, dropping all terms independent of Θ and multiplying by 2, the ML identification problem can be expressed as

137

$$L(\Theta) = -\log\{p(\mathbf{r};\Theta)\}$$
$$= -\{\log(|\mathbf{P}_{rr}|) + \mathbf{r}^t \mathbf{P}_{rr}^{-1} \mathbf{r}\}$$

(6.14)

The parameters that maximize the LF can be obtained by equating all the partial derivatives of the LF to zero. However, this optimization problem is so extensive because of the number of unknowns involved. Therefore some simplifications are necessary. We will make the assumption that the model coefficients, $c_{ij}(m,n)$ and $\sigma_{w_i}^2$, are estimated using the least square procedure described in section 5.2. Also, the observation noise, $\sigma_{v_{ij}}^2$, will be estimated as the variance of a uniform region in the different channels. Further, we make the following practical assumption. We assume that the cross channel blur is not significant. This means that although the channels exhibit cross correlation, the contribution of the blur to this correlation is minimal or negligible. The major contributor to the cross correlation is the image signal. Our experimental results demonstrate this.

To be able to compute the conditional likelihood function, we make use of the structure of $\mathbf{P}_{rr}$ and apply the Toeplitz-to-circular approximation through the DFT (Appendix B) for each block element of $\mathbf{P}_{rr}$. Thus, the CLF can be written in the frequency domain as

$$L(\Theta) = -\sum_k \sum_l \left\{ \log(|\mathbf{S}_{r_p r_p}(k,l)|) + \frac{1}{M^2} \frac{|R_p(k,l)|^2}{\mathbf{S}_{r_p r_p}(k,l)} \right\}$$

(6.15)

Following the formulation in section 4.2, we first express the blur PSF as a function of parameters $\Theta = [\theta_1, \theta_2, ..., \theta_n]$ in the continuous domain for channel p, as

$$h_p(x,y) = h_p(x,y;\Theta) \quad \text{for} \ (x,y) \in \Re_p(\Theta)$$

(6.16)

138

where $\Re_p(\Theta)$ denotes the PSF support for channel p. The observed image in continuous domain can be written as

$$r_p(m,n) = \int_{\Re(\Theta)} h_p(\xi, \eta; \Theta) s(m\Delta x - \xi, n\Delta y - \eta) d\xi d\eta + v(m,n) \qquad (6.17)$$

by sampling at the points $(x,y) = (m\Delta x, n\Delta y)$, where Δx and Δy denote the horizontal and vertical sampling distances, respectively, (m,n) denotes discrete spatial coordinates, and $r_p(m,n)$ are the observed samples of $r_p(x,y)$. We may now write the crosscorrelation components, $P_{r_p r_q}(i,j)$, as

$$\begin{aligned}
P_{r_p r_q}(i,j) &= E[r_p(m,n)r_q(m+i,n+j)] \\
&= \int_{\Re_p(\Theta)} \int_{\Re_q(\Theta)} h_p(\xi, \eta) h_q(\psi, \zeta) P_{s_p s_q}(i-\xi+\psi, j-\eta+\zeta) d\xi d\eta d\psi d\zeta \qquad (6.18) \\
&\quad + \delta(i,j)\sigma_{v_p}\sigma_{v_q}
\end{aligned}$$

where $P_{s_p s_q}(x,y) = E\{s_p(\xi,\eta)s_q(\xi+x,\eta+y)\}$ is the crosscorrelation function of the ideal continuous domain image $s(m,n)$. Then, taking the DFT of (6.18), we have (See Appendix D)

$$\begin{aligned}
S_{r_p r_q}(k,l) &= DFT\{P_{r_p r_q}(i,j)\} \\
&= \int_{\Re_p(\Theta)} \int_{\Re_q(\Theta)} h_p(\xi, \eta) h_q(\psi, \zeta) S_{s_p s_q}(k,l) \\
&\quad . \exp\left[-j\frac{2\pi}{N}k(\xi-\psi)\right] \exp\left[-j\frac{2\pi}{N}l(\eta-\zeta)\right] d\xi d\eta d\psi d\zeta + \sigma_v^2 \qquad (6.19) \\
&= S_{s_p s_q}(k,l) H_p(k,l) H_q^*(k,l) + \sigma_{v_p}\sigma_{v_q}
\end{aligned}$$

where $S_{r_p r_q}(k,l)$ is the DFT of $P_{r_p r_q}(i,j)$ which denotes the samples of $P_{r_p r_q}(x,y)$, and $H_p(k,l)$ denotes the samples of the continuous Fourier transform of $h_p(x,y;\Theta)$ for the *pth* channel given by

139

$$H_p(k,l) = \int_{\Re_p(\Theta)} h_p(x,y;\Theta) \exp\left(-j\frac{2\pi}{N}kx\right)\exp\left(-j\frac{2\pi}{N}ly\right)dxdy \tag{6.20}$$

Thus, the power spectrum for each channel reduces to

$$S_{r_p r_p}(k,l) = S_{s_p s_p}(k,l)\left|H_p(k,l)\right|^2 + \sigma_{v_p}^2$$

The key point here is to incorporate the cross-spectral relation and to include them in the computation of the power spectrum of the ideal image, $S_{s_p s_q}(k,l)$, which can be obtained from the AR model of (6.1) as (See Appendix D)

$$S_{s_p s_p}(k,l) = \frac{\sigma_{w_p}^2 + \displaystyle\sum_{q, q \neq p}\sum_{(m,n)} C^{pq}(m,n)S_{s_p s_q}(k,l)}{\left|1 - \displaystyle\sum_{(m,n)} C^{pp}(m,n)\right|^2} \tag{6.21}$$

where $C^{pq}(k,l)$ are the DFT of the correlation coefficients computed as in section 5.2. Thus, for RGB color image the power spectrum for the red channel is computed using the power spectrum of the red spectral component and including the power spectra of the green and blue components.

We need now to compute the derivative of the CLF for each channel as

$$\frac{\partial}{\partial \theta_i} \mathsf{L}(\Theta|c_{i,j}(m,n),\sigma_{vi}^2,\sigma_{wi}^2) =$$

$$-\sum_k \sum_l \left\{ \left(\frac{1}{S_{r_p r_p}(k,l)} - \frac{1}{N^2}\frac{\left|R_p(k,l)\right|^2}{S_{r_p r_p}^2(k,l)} \right) \frac{\partial}{\partial \theta_i} S_{r_p r_p}(k,l) \right\} \tag{6.22}$$

140

Here, the derivative of the power spectrum component, $\frac{\partial}{\partial \theta_i} S_{r_p r_p}(k,l)$, can be computed depending on the particular parametric form of the unknown PSF. These expressions are given by equation (4.29) for the uniform motion blur as

$$\frac{\partial}{\partial \theta_i} S_{r_p r_p}(k,l) =$$

$$\frac{1}{a}\left\{-2|H_p(k,l)|^2 + \exp\left(j\frac{2\pi}{N}ka\right)H_p(k,l) + \exp\left(-j\frac{2\pi}{N}ka\right)H_p^*(k,l)\right\}S_{s_p s_p}(k,l) \qquad (6.23)$$

where $H_p(k,l)$ for this form is given by

$$H_p(k,l) = \left(-j\frac{2\pi}{N}k\frac{a-1}{2}\right)\frac{\sin\frac{2\pi}{N}k\frac{a}{2}}{\frac{2\pi}{N}k\frac{a}{2}} \qquad (6.24)$$

For the out-of-focus blur, $\frac{\partial}{\partial \theta_i} S_{r_p r_p}(k,l)$ is given by equation (4.34) as

$$\frac{d}{d\theta} S_{r_p r_p}(k,l) =$$

$$\left\{\frac{-4}{R}|H_p(k,l)|^2 + \frac{2}{R}J_0\left(\frac{2\pi}{N}R\sqrt{k^2+l^2}\right)(H_p(k,l) + H_p^*(k,l))\right\}S_{s_p s_p}(k,l) \qquad (6.25)$$

where in this case $H_p(k,l)$

$$H(k,l) = NR\frac{J_1\left(\frac{2\pi}{N}R\sqrt{k^2+l^2}\right)}{\sqrt{k^2+l^2}} \qquad (6.26)$$

6.3   Implementation of the ML Estimator

The multichannel estimation procedure can be described by the following algorithm:

1) Estimate $\{c^{pq}(m,n)\}$ and $\sigma^2_{w_i}$ for the different channels using least squares procedure of section 5.2.

2) Estimate σ^2_v from a uniform region in the different channels

3) Compute $S_{s_p s_p}(k,l)$ using (6.21) and employing the cross spectral components.

4) Use the parametric form of the specific PSF, namely (4.26) for uniform blur or (4.31) for out-of focus blur, and set the parameter, Θ, to some initial values.

DO UNTIL convergence criterion is satisfied

   5) Compute $\left|H_p(k,l)\right|^2$ using (6.24) or (6.26) depending on the parametric form

      chosen.

   6) Given σ^2_v , compute $S_{r_p r_p}(k,l)$ using (6.21).

   7) Compute the value of CLF using (6.15).

   8) Compute the derivative of the CLF with respect to the unknown parameter using

      (6.22) and either (6.23) or (6.25).   Again depending on the parametric form

chosen.

   9) Update Θ using a gradient based numerical optimization technique.

END UNTIL

In the next section we will present some experimental results and the performance of the prescribed method.

6.4 Experimental Results

Using the above procedure, the following experiments were conducted using the colored images of "TANK" for uniform motion blur, and "TEXT" for out-of-focus blur. The original " TANK" image is shown in Figure 6.1. We blurred this image by a uniform motion of size $a=10$ and noise was added to represent $SNR=40$ dB, shown in Figure 6.2. The identified parameter was computed without cross spectral correlation (i.e. independent channels) and the blur extent was estimated about $a=7.5$ for each channel. The blur extent estimated by the above multichannel procedure, i.e. including the cross spectral component was estimated as $a=9.1$ in each channel. The restoration results using the estimated parameters of the two cases are shown in figures 6.3 and 6.4, respectively. We note here that we are dealing with PSF that is expressed as a function of one parameter. The identified parameter a was computed for each channel while including the cross-spectral components of the other channels. Clearly, since the channels were blurred with the same PSF, we should expect the estimated extent a to be the same in all channels.

The same experiments were repeated on the "TEXT" image for the out-of-focus blur case of size $R=7$ and $SNR=40$ dB. The original and blurred images are shown in Figures 6.5 and 6.6 , respectively. The identified parameters were 5.1 and 6.2 for the independent and multichannel estimation, respectively. The restored images using the identified parameters are presented in Figure 6.7 and 6.8.

Performance of the method with noise

We will experiment now the performance of this method at different noise levels for both the uniform linear motion and the out-of-focus blurs. To do so, we blurred the "TANK" image with a uniform motion blur of extent $a=10$ and separately added Gaussian noise that corresponds to SNR of 10, 20, 30, 40, and 50 dB. Then, we estimated the blur extent using both the independent identification method and the multichannel approach described above. The results are shown in Table 6.1. In a similar fashion, we repeated these experiments for the case of out-of-focus blur using the "TEXT" image with blur size $R=7$. Table 6.2 shows the results for this case.

From the data in Table 6.1, we observe that the multichannel approach gives better results than the independent identification. Obviously, this improvement is due to the inclusion of the cross-spectral components in computing the likelihood function. Although at low SNR levels the improvement is moderate, the fact that cross-spectral component incorporation produce better results is still valid. The same conclusion can be also drawn from the results in Table 6.2.

To summarize, we may say that the novel approach outlined in this chapter is very useful in identifying blur extents of uniform motion or out-of-focus degradations and can be used satisfactory for SNR levels more than 20dB. This contribution is very important in the field of image restoration since there is no existing multichannel identification techniques that supply such results.
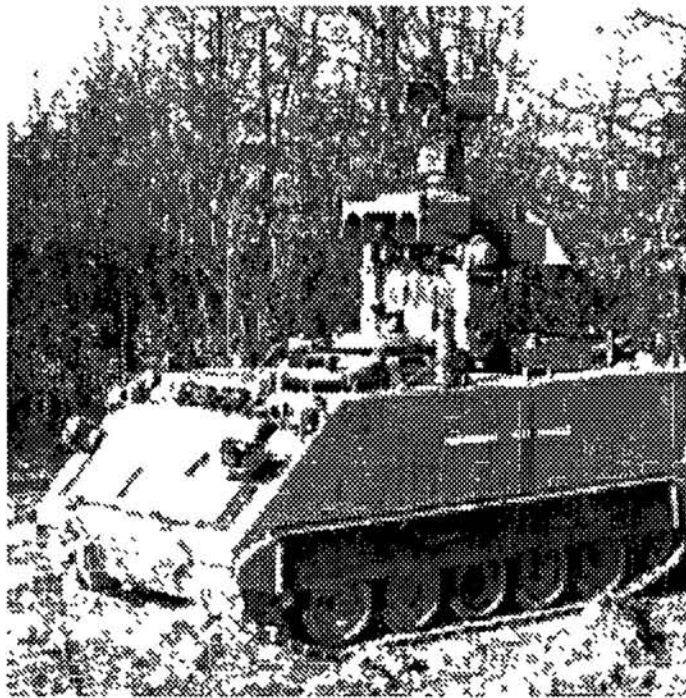
Figure 6.1 The original color "TANK" image.
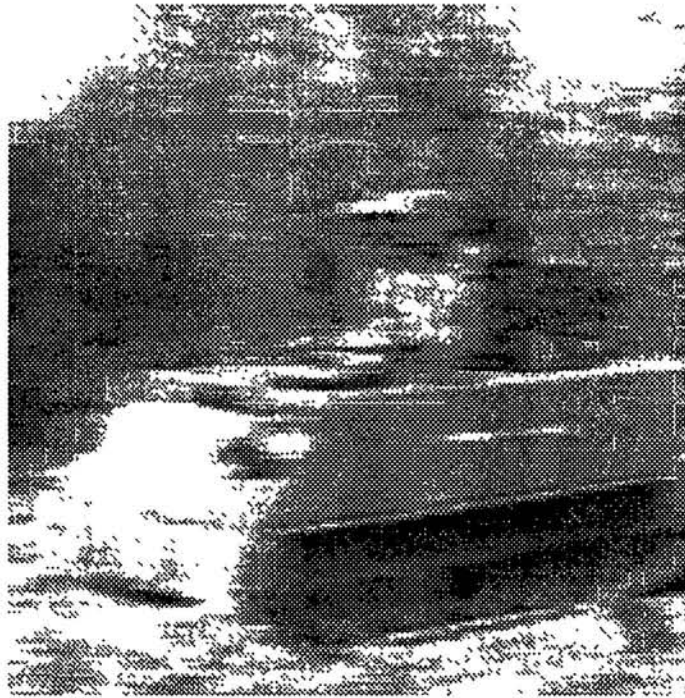
Figure 6.2 The blurred "TANK" image with
uniform motion blur of extent $a=10$
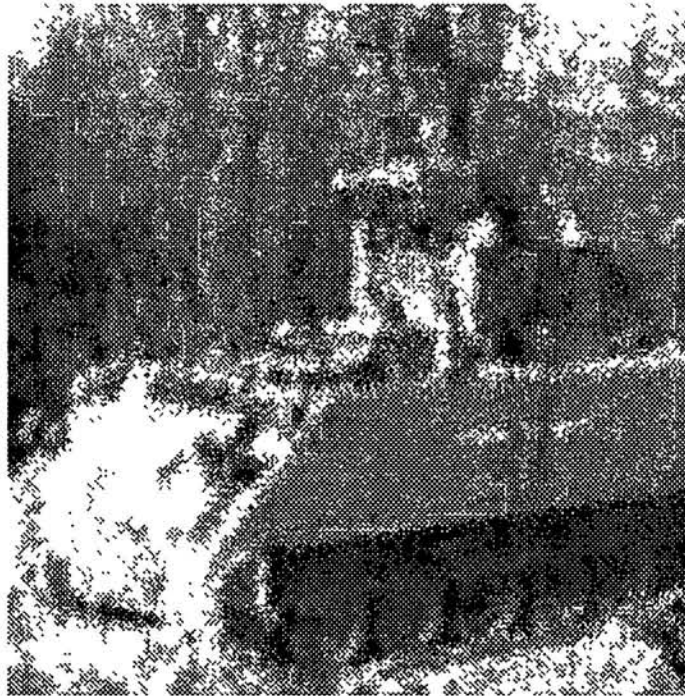
Figure 6.3 The restored "TANK" image using the identified parameter
of $a=7.5$ without using the cross-spectral information.
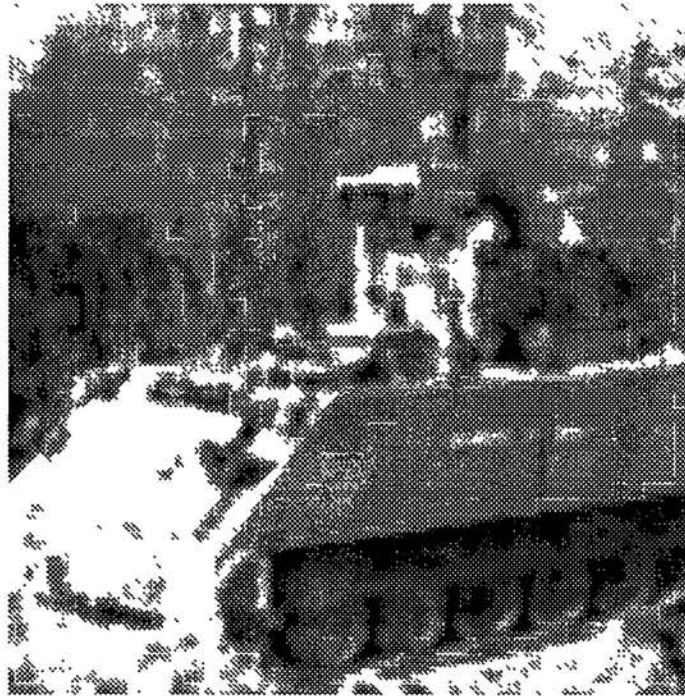
Figure 6.4 The restored " TANK" image using the identified paramter
of a=9 and including the cross spectral correlation.
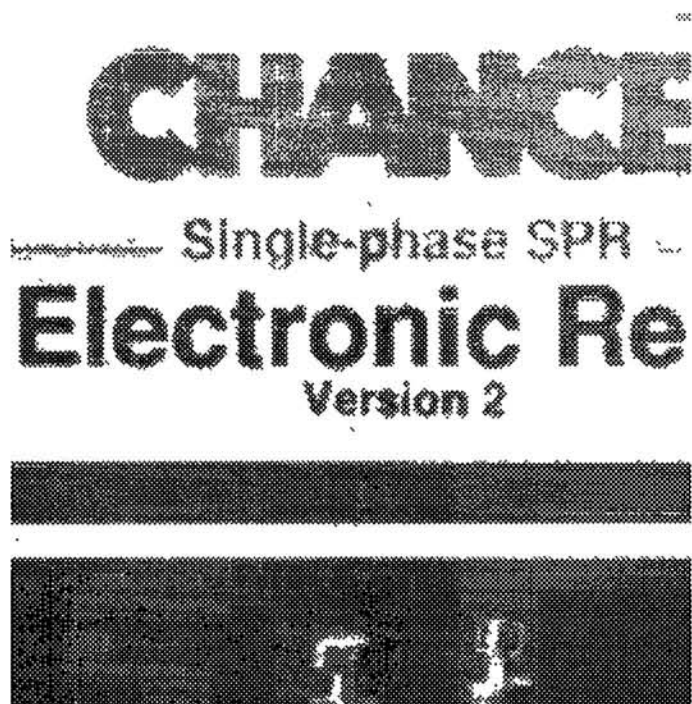
Figure 6.5 The original "TEXT" image.

Figure 6.6 The blurred region of the "TEXT" image with out-of-focus blur of extent $R=7$ and $SNR=40$ dB.
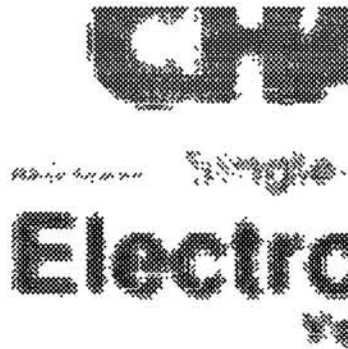
Figure 6.7 Restoration result using the estimated parameter of $R=5$ which is identified without cross spectral correlation.

Figure 6.8 The restored image using the estimated parameter of $R=7$ which is identified including cross spectral correlation.

150

Table 6.1 The identified blur extents for the TANK image that is degraded by uniform motion blur $a=10$ at different noise levels. The independent blur identification and the multichannel blur identification refer to estimating the blur from each channel without and with cross-spectral components, respectively.

SNR	Independent blur identification			Multichannel blur identification		
(dB)	Channel R	Channel G	Channel B	Channel R	Channel G	Channel B
10	7.1	7	7.1	7.5	7.5	7.6
20	7.2	7.3	7.2	8.2	8.1	8.1
30	7.3	7.3	7.3	8.5	8.5	8.5
40	7.5	7.4	7.5	9	8.9	9
50	7.8	7.8	7.9	9.3	9.3	9.4

Table 6.2 The identified blur extents for the TEXT image that is degraded by out-of-focus blur disk of size R=7 at different noise levels. The independent blur identification and the multichannel blur identification refer to estimating the blur from each channel without and with cross-spectral components, respectively.

SNR (dB)	Independent blur identification			Multichannel blur identification		
	Channel R	Channel G	Channel B	Channel R	Channel G	Channel B
10	4.5	4.6	4.6	5	4.9	5
20	4.8	4.8	4.8	5.2	5.2	5.3
30	5.1	5	5	5.7	5.8	5.8
40	5.1	5.1	5.2	6.2	6.2	6.1
50	5.3	5.2	5.3	6.3	6.2	6.2

العنوان:	CONTINUOUS SPATIAL DOMAIN IMAGE IDENTIFICATION AND RESTORATION WITH MULTICHANNEL APPLICATIONS
المؤلف الرئيسي:	Al Suwailem, Umar A.
مؤلفين آخرين:	Keller, James E.(super)
التاريخ الميلادي:	1996
موقع:	كولومبيا
الصفحات:	1 - 183
رقم MD:	616175
نوع المحتوى:	رسائل جامعية
اللغة:	English
الدرجة العلمية:	رسالة دكتوراه
الجامعة:	University of Missouri
الكلية:	The Graduate School
الدولة:	الولايات المتحدة الأمريكية
قواعد المعلومات:	Dissertations
مواضيع:	الهندسة الإلكترونية ، تطبيقات الحاسب ، ترميم الصور ، النمذجة ، الحركات الضبابية
رابط:	https://search.mandumah.com/Record/616175

CHAPTER 7

SUMMARY AND FURTHER RESEARCH

As a final chapter, we will give here a summary of our findings and contributions throughout this thesis. Also, we will conclude with some suggestions for further research in this field.

7.1 Summary

Image restoration and identification are two closely related processes that are extensively used in recovering images from their distorted versions. Initially, we reviewed and discussed some related research that has been done in this area. The importance of restoration and identification in the low-level stage of image processing was clearly established. Moreover, the necessity for studying the identification problem further, both in the single and multichannel cases, and the lack of research for this topic

was also outlined. As a result, we were motivated to make the emphasis of this study on blur identification for monochrome and multichannel images.

In chapter 2, we discussed modeling aspects of the image, blur, and noise for both the single and multichannel cases. In practice, there is a compromise between the accuracy and the complexity of the model. Following the leading research in this area, we found that the most successful models have represented the degraded image as an autoregressive process and the noise as a zero mean white Gaussian process. The blur representation is modeled according to the physical and/or geometrical description of the degradation. This modeling was extended to the multichannel case where the effect of cross-spectral information between the channels was incorporated. Also, some computational aspects of the power spectrum, observation noise, and boundary preprocessing were explained.

As both restoration and identification are related in the overall performance, we have revisited and experimented with some restoration techniques. In chapter 3, we have shown that both the Wiener and Kalman filters produce acceptable results; however, the Kalman filter performance is better than that of the Wiener filter. In practice, the restoration filters are used with prior knowledge of the blur and noise. However, such knowledge may not be available and has to be extracted from the received image. Such extraction of information is the main purpose of the identification techniques. We have discussed the identification problem in chapter 4.

We showed that by modeling the blur in the continuous spatial domain, we can overcome some of the limitations in the discrete representation and the difficulties in evaluating the maximum likelihood function. Expressing each of the two mostly encountered blurs in practice, uniform linear motion and out-of-focus blurs, as a function of one parameter, we were able to successfully identify the blur extent from the likelihood function. We have also tested this method in angular linear motion and discovered that the

154

blur extent can be recovered by identifying the blur in the horizontal and vertical directions.

Previous experimental evidence showed that the AR model support size is not critical in determining the performance of restoration techniques. Therefore, first order models are sufficient in most practical experiments. We have shown that this is also true for the identification technique we used in this research. It was found that by extending the support size to second or third order a very slight improvement was noticed.

To test the performance of the identification technique with respect to the noise factor, we have performed several experiments for the same image and the same blur at different noise levels. Using a measure for improvement in the SNR, it was observed that this method outperformed other existing techniques in its sensitivity to noise.

The successfulness of the identification method in the single channel case led us to extend the technique to the multichannel case. We first reviewed some aspects of multichannel imaging in chapter 5. Color image modeling and correlation between the spectral channels were discussed. The multichannel extension of the AR model was derived and the correlation coefficients were evaluated. It was shown that representation that included the cross-spectral components described the image model more accurately. The two famous restoration techniques, namely the Wiener and Kalman filters, were extended to include such modeling.

The identification of multichannel images was discussed in chapter 6. We have extended the single channel approach to the multichannel case using the modeling mentioned above. The likelihood function equations were derived where the cross-spectral components were included. The experimental results showed that incorporating the cross-channel components produced superior results over identifying each channel separately. The performance of this method was also tested with regard to noise effects. It has been observed that noise is a limiting factor for low SNR levels for both the

155

independent and multichannel identification. However, multichannel identification produced better results at all *SNR* levels.

7.2 Suggestions and Further Research

In this section we will give some suggestions and directions for further related research. Unlike the field of restoration which has been extensively studied, the field of blur identification is still a wide area of research that has not been fully explored, as we mentioned earlier in chapter 1. Some of the interesting research areas in this regard are the following:

Sequence of images

The multichannel identification approach prescribed in this thesis can be applied with modification to image sequences that are related by a certain parameter, such as time. The corresponding restoration filter should employ this modification, too [59,62].

Alternative computation of parameters

The estimation of the parameters in the likelihood function were computed throughout this thesis using the blurred image as a prototype. An alternative approach would be to simultaneously minimize the likelihood function with respect to those parameters [47,42].

Combination of blurs

The identification and restoration of images blurred by a combination of more than one type of blur is an important area that needs to be researched. This type of problem is encountered in some practical cases, e.g., taking the image of a moving object where the sensor is out-of-focus. This can be approached by expressing the combined effects of the

blur as one function. Also, the properties of the blur can be studied to see if it can be modeled as a linear combination, so that consecutive applications of the techniques can produce improved results.

Other Noise Models

Most of the restoration and identification methods assume additive Gaussian models for the noise. Other forms of noise, for example colored or multiplicative, may be applicable for certain situations. Thus, it would be of great importance to explore identification techniques for those cases [68].

Spatially varying images

In some cases, images may have spatial variation within the image contents. Therefore, it is of interest to develop identification techniques that can handle such cases. The image may be segmented and the blur parameters can be identified by region, or by using adaptive approach that take into consideration spatial variation [30]. Also, multiple model-based Kalman filter approach as in [40], may be used for this type of problem.

Artifact suppression

Artifacts are undesired patterns that are exhibited by image restoration techniques. It is an area that has been researched in restoration independently of identification [43,86]. The performance of identification techniques in combination with regularized restoration can be developed and studied as in [98]. [100] proposes an approach for the multichannel case.

Emerging techniques

There is an increasing interest in employing emerging techniques, such as neural networks [18], fuzzy rule-based systems [15], and morphological methods [21], in image

157

processing. It would be useful to incorporate these approaches in identification and restoration of images.

العنوان:	CONTINUOUS SPATIAL DOMAIN IMAGE IDENTIFICATION AND RESTORATION WITH MULTICHANNEL APPLICATIONS
المؤلف الرئيسي:	Al Suwailem, Umar A.
مؤلفين آخرين:	Keller, James E.(super)
التاريخ الميلادي:	1996
موقع:	كولومبيا
الصفحات:	1 - 183
رقم MD:	616175
نوع المحتوى:	رسائل جامعية
اللغة:	English
الدرجة العلمية:	رسالة دكتوراه
الجامعة:	University of Missouri
الكلية:	The Graduate School
الدولة:	الولايات المتحدة الأمريكية
قواعد المعلومات:	Dissertations
مواضيع:	الهندسة الإلكترونية ، تطبيقات الحاسب ، ترميم الصور ، النمذجة ، الحركات الضبابية
رابط:	https://search.mandumah.com/Record/616175

CONTINUOUS SPATIAL DOMAIN IMAGE IDENTIFICATION AND RESTORATION WITH MULTICHANNEL APPLICATIONS

Umar A. Al-Suwailem

Prof. James Keller, Dissertation Adviser

ABSTRACT

This research deals with the problem of identification and restoration of images. The field of image identification involves estimating the properties of an imperfect imaging system from an observed image prior to the restoration process, which is concerned mainly with the recovery or the original image from the corrupted one, given the properties of the imaging system. Thus, the two problems are related to each other in the sense that good restoration results depend on how accurate the identified parameters are to the actual situation. The purpose of this research is to investigate some novel identification techniques and their implementations in monochrome and multichannel image processing.

Using the maximum likelihood estimation (ML) approach, the image is represented as an autoregressive (AR) model and blur is described as a continuous spatial domain model. Such formulation overcomes some major limitations encountered in other ML methods. It is shown that blur extent can be optimally identified from noisy images that are degraded by uniform linear motion and out-of-focus blurs. Also, it is shown that angular linear motion can be recovered by identification in two orthogonal directions. The overall performance of this method in conjunction with restoration and noise sensitivity demonstrates its success.

Extending this approach to multichannel case, the image and blur are modeled to include cross-spectral and spatial components. Such components are inherent to multichannel imaging systems and degrade the image further. It is shown that by evaluating and incorporating those components in the identification and restoration techniques, the overall performance is improved significantly. Application of this method to color images and comparison to the independent restoration approach and other existing techniques are also investigated. The novelty of this approach in identifying the blur of multichannel images is a major contribution in producing visually acceptable results and is a significant step for higher processing levels.

العنوان:	CONTINUOUS SPATIAL DOMAIN IMAGE IDENTIFICATION AND RESTORATION WITH MULTICHANNEL APPLICATIONS
المؤلف الرئيسي:	Al Suwailem, Umar A.
مؤلفين آخرين:	Keller, James E.(super)
التاريخ الميلادي:	1996
موقع:	كولومبيا
الصفحات:	1 - 183
رقم MD:	616175
نوع المحتوى:	رسائل جامعية
اللغة:	English
الدرجة العلمية:	رسالة دكتوراه
الجامعة:	University of Missouri
الكلية:	The Graduate School
الدولة:	الولايات المتحدة الأمريكية
قواعد المعلومات:	Dissertations
مواضيع:	الهندسة الإلكترونية ، تطبيقات الحاسب ، ترميم الصور ، النمذجة ، الحركات الضبابية
رابط:	https://search.mandumah.com/Record/616175

LIST OF FIGURES

LIST OF TABLES

ABBREVIATIONS

For easy reference, we list the following abbreviations that are frequently used throughout this thesis:

AR	Autoregressive model
ARMA	Autoregressive moving average model
CCD	Charge coupled device camera
CLF	Conditional likelihood function
CMY	Cyan, magenta, and yellow components of a color image
DFT	Discrete Fourier Transform
EM	Expectation Maximization method
FFT	Fast Fourier Transform
FP	Full plane model support
HP	Half plane model support
HSI	Hue, saturation, and intensity components of a color image
LF	Likelihood function
LMMSE	Linear minimum square error
ME	Maximum Entropy
ML	Maximum Likelihood estimation method
MMSE	Minimum mean square error
MVR	Minimum variance representation
NSHP	Nonsymmetric half plane model support
PDF	Probability density function

RGB	Red, green, and blue components of a color image
PS	Power spectrum of the signal or image
PSF	Point spread function
RUKF	Reduced update Kalman filter
QP	Quarter plane model support
SNR	Signal-to-noise ratio
YIQ	Luminance, inphase, and quadrature components of a color image

SYMBOLS AND NOTATIONS

Unless otherwise stated, the following symbols and notations are used throughout this thesis as prescribed here:

$s(m,n)$	Discrete samples of source or original image
$r(m,n)$	Discrete samples of received or observed image
$v(m,n)$	Discrete samples of observation noise with variance σ_v^2
$w(m,n)$	Discrete samples of modeling noise with variance σ_w^2
$\mathbf{s}, \mathbf{r}, \mathbf{w}, \mathbf{v}$	Lexicographically ordered vectors of $s(m,n)$, $r(m,n)$, $w(m,n)$, and $v(m,n)$, respectively
$h(i,j)$	Degradation or blur function in discrete form
$H(k,l)$	DFT of the blur function $h(i,j)$
$H_p(k,l)$	DFT of the blur function for the pth channel
$c(k,l)$	Autoregressive model coefficients for the image
$C(m,n)$	DFT of the modeling coefficients $c(k,l)$
$C^{pq}(k,l)$	DFT of the Multichannel modeling coefficients
$\mathbf{H}$	$(MN \times MN)$ degradation or blur matrix of $h(i,j)$
$\mathbf{C}$	$(MN \times MN)$ image model coefficients matrix of $c(k,l)$
$\boldsymbol{H}$	Multichannel degradation or blur matrix
$\boldsymbol{C}$	Multichannel image model matrix
$s_p(m,n)$	Discrete samples of source or original image for the pth channel
$r_p(m,n)$	Discrete samples of received or observed image for the pth channel
$v_p(m,n)$	Discrete samples of observation noise for pth channel with $\sigma_{v_{pq}}^2$ variance

$w_p(m,n)$	Discrete samples of modeling noise for the pth channel with $\sigma^2_{w_{pq}}$ variance
$\mathbf{s}_p$, $\mathbf{r}_p$, $\mathbf{v}_p$, $\mathbf{w}_p$	Lexicographic order of the corresponding vectors $s_p(m,n)$, $r_p(m,n)$, $v_p(m,n)$, and $w_p(m,n)$, respectively
$\boldsymbol{r}$, $\boldsymbol{s}$, $\boldsymbol{v}$, $\boldsymbol{w}$	Lexicographic order of $\mathbf{r}_p$, $\mathbf{s}_p$, $\mathbf{v}_p$, and $\mathbf{w}_p$, for $,p=1,2,...,N$, respectively
S_c	Support for image model coefficients
S_h	Support for blur function coefficients
σ^2_v	Variance of observation noise
σ^2_w	Variance of modeling noise
$\mathbf{Q}_v$	Covariance matrix for the modeling noise $= \sigma^2_v \mathbf{I}$ $(\sigma^2_v > 0)$
$\mathbf{Q}_w$	Covariance matrix for the modeling noise $= \sigma^2_w \mathbf{I}$ $(\sigma^2_w > 0)$
$\sigma^2_{v_{pq}}$	Variance of observation noise for the pth channel
$\sigma^2_{w_{pq}}$	Variance of modeling noise for the pth channel
$c^{pq}(k,l)$	Model coefficients coupling the pth and qth channel
$h^{pq}(k,l)$	Blur coefficients for the pth channel
S_{pq}	Support of the multichannel blur function coefficients $h^{pq}(k,l)$
$\mathcal{R}_{pq}$	Support of the multichannel model coefficients $c^{pq}(k,l)$
Φ	Vector of parameters to be estimated
$\hat{\Phi}_{ml}$	Maximum likelihood estimator of the parameters vector Φ
$\Re(\Phi)$	Range of the parameters in Φ
$\mathcal{L}^*(\Phi)$	Log likelihood function of Φ
θ	Parameter describing the severity of the blur function
Θ	Vector of parameters describing the severity of the blur function
$\Re(\Theta)$	Range of the support for the blur function
$P_{ss}(i,j)$	Autocorrelation matrix of the original image $s(m,n)$

$S_{ss}(k,l)$	Power spectrum of $s(m,n)$ computed as the DFT of $P_{ss}(i,j)$
$\mathbf{P}_{rr}$	Covariance block matrix of the observed image $r(m,n)$
$P_{rr}(i,j)$	Elements of one block of $\mathbf{P}_{rr}$
$S_{rr}(k,l)$	Power spectrum of $r(m,n)$ computed as the DFT of $P_{rr}(i,j)$
$\dfrac{\partial}{\partial \theta_i} S_{rr}(k,l)$	Partial derivative of $S_{rr}(k,l)$ with respect to the parameter to be estimated
$R(u,v)$	DFT of the observed image $r(m,n)$
$\boldsymbol{P}_{rr}$	Multichannel block covariance matrix
$\boldsymbol{P}_{ww}$	Multichannel modeling noise matrix
$\boldsymbol{P}_{vv}$	Multichannel observation noise matrix
$P_{r_p r_q}(i,j)$	Autocorrelation components for the pth channel
$S_{r_p r_q}(k,l)$	Power spectrum of the observed image for pth channel
$J_0(\bullet),\ J_1(\bullet)$	Zeroth and first order Bessel functions of the first kind, respectively
$E[\bullet]$	Expected value of a random variable or process
$\lvert \mathbf{A} \rvert$	Determinant of matrix $\mathbf{A}$
$\mathbf{A}^t$	Transpose of matrix $\mathbf{A}$
$\mathbf{A}^*$	Conjugate of matrix $\mathbf{A}$
$s^{(m,n)}$	The state of an image at coordinate (m,n)
$\mathbf{K}^{(m,n)}$	Kalman gain computed for the state at coordinates (m,n)
$\mathbf{U}_b^{(m,n)}$	Predicted covariance matrices of the state at coordinates (m,n)
$\mathbf{U}_a^{(m,n)}$	Updated covariance matrices of the state at coordinates (m,n)

TABLE OF CONTENTS

العنوان:	CONTINUOUS SPATIAL DOMAIN IMAGE IDENTIFICATION AND RESTORATION WITH MULTICHANNEL APPLICATIONS
المؤلف الرئيسي:	Al Suwailem, Umar A.
مؤلفين آخرين:	Keller, James E.(super)
التاريخ الميلادي:	1996
موقع:	كولومبيا
الصفحات:	1 - 183
رقم MD:	616175
نوع المحتوى:	رسائل جامعية
اللغة:	English
الدرجة العلمية:	رسالة دكتوراه
الجامعة:	University of Missouri
الكلية:	The Graduate School
الدولة:	الولايات المتحدة الأمريكية
قواعد المعلومات:	Dissertations
مواضيع:	الهندسة الإلكترونية ، تطبيقات الحاسب ، ترميم الصور ، النمذجة ، الحركات الضبابية
رابط:	https://search.mandumah.com/Record/616175

CONTINUOUS SPATIAL DOMAIN
IMAGE IDENTIFICATION AND RESTORATION
WITH MULTICHANNEL APPLICATIONS

A Dissertation

presented to

the Faculty of the Graduate School

University of Missouri-Columbia

In Partial Fulfillment

of the Requirements for the Degree

Doctor of Philosophy

in Electrical and Computer Engineering

---

by

UMAR A. AL-SUWAILEM

Prof. James Keller, Dissertation Adviser

JULY, 1996

The undersigned appointed by the Dean of the Graduate School, have examined the dissertation entitled
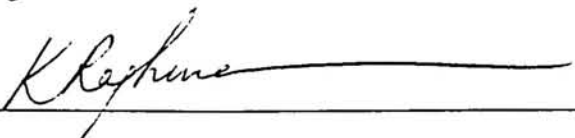
CONTINUOUS SPATIAL DOMAIN IMAGE
IDENTIFICATION AND RESTORATION
WITH MULTICHANNEL APPLICATIONS

presented by Umar A. Al-Suwailem
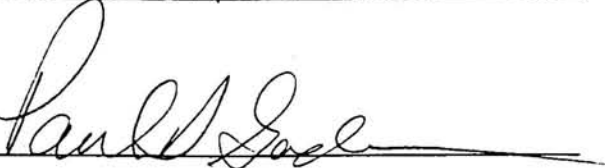
a candidate for the degree of Doctor of Philosophy in Electrical Engineering
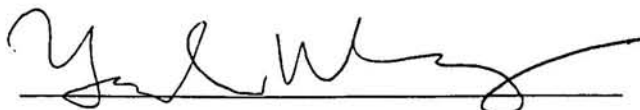
and hereby certify that in their opinion it is worthy of acceptance.

ACKNOWLEDGMENTS

CONTINUOUS SPATIAL DOMAIN IMAGE IDENTIFICATION AND RESTORATION WITH MULTICHANNEL APPLICATIONS

Umar A. Al-Suwailem

Prof. James Keller, Dissertation Adviser

ABSTRACT

This research deals with the problem of identification and restoration of images. The field of image identification involves estimating the properties of an imperfect imaging system from an observed image prior to the restoration process, which is concerned mainly with the recovery or the original image from the corrupted one, given the properties of the imaging system. Thus, the two problems are related to each other in the sense that good restoration results depend on how accurate the identified parameters are to the actual situation. The purpose of this research is to investigate some novel identification techniques and their implementations in monochrome and multichannel image processing.

Using the maximum likelihood estimation (ML) approach, the image is represented as an autoregressive (AR) model and blur is described as a continuous spatial domain model. Such formulation overcomes some major limitations encountered in other ML methods. It is shown that blur extent can be optimally identified from noisy images that are degraded by uniform linear motion and out-of-focus blurs. Also, it is shown that angular linear motion can be recovered by identification in two orthogonal directions. The overall performance of this method in conjunction with restoration and noise sensitivity demonstrates its success.

Extending this approach to multichannel case, the image and blur are modeled to include cross-spectral and spatial components. Such components are inherent to multichannel imaging systems and degrade the image further. It is shown that by evaluating and incorporating those components in the identification and restoration techniques, the overall performance is improved significantly. Application of this method to color images and comparison to the independent restoration approach and other existing techniques are also investigated. The novelty of this approach in identifying the blur of multichannel images is a major contribution in producing visually acceptable results and is a significant step for higher processing levels.

LIST OF FIGURES

viii

LIST OF TABLES

ABBREVIATIONS

For easy reference, we list the following abbreviations that are frequently used throughout this thesis:

AR	Autoregressive model
ARMA	Autoregressive moving average model
CCD	Charge coupled device camera
CLF	Conditional likelihood function
CMY	Cyan, magenta, and yellow components of a color image
DFT	Discrete Fourier Transform
EM	Expectation Maximization method
FFT	Fast Fourier Transform
FP	Full plane model support
HP	Half plane model support
HSI	Hue, saturation, and intensity components of a color image
LF	Likelihood function
LMMSE	Linear minimum square error
ME	Maximum Entropy
ML	Maximum Likelihood estimation method
MMSE	Minimum mean square error
MVR	Minimum variance representation
NSHP	Nonsymmetric half plane model support
PDF	Probability density function

RGB	Red, green, and blue components of a color image
PS	Power spectrum of the signal or image
PSF	Point spread function
RUKF	Reduced update Kalman filter
QP	Quarter plane model support
SNR	Signal-to-noise ratio
YIQ	Luminance, inphase, and quadrature components of a color image

SYMBOLS AND NOTATIONS

Unless otherwise stated, the following symbols and notations are used throughout this thesis as prescribed here:

$s(m,n)$	Discrete samples of source or original image
$r(m,n)$	Discrete samples of received or observed image
$v(m,n)$	Discrete samples of observation noise with variance σ_v^2
$w(m,n)$	Discrete samples of modeling noise with variance σ_w^2
$\mathbf{s}, \mathbf{r}, \mathbf{w}, \mathbf{v}$	Lexicographically ordered vectors of $s(m,n)$, $r(m,n)$, $w(m,n)$, and $v(m,n)$, respectively
$h(i,j)$	Degradation or blur function in discrete form
$H(k,l)$	DFT of the blur function $h(i,j)$
$H_p(k,l)$	DFT of the blur function for the pth channel
$c(k,l)$	Autoregressive model coefficients for the image
$C(m,n)$	DFT of the modeling coefficients $c(k,l)$
$C^{pq}(k,l)$	DFT of the Multichannel modeling coefficients
$\mathbf{H}$	$(MN \times MN)$ degradation or blur matrix of $h(i,j)$
$\mathbf{C}$	$(MN \times MN)$ image model coefficients matrix of $c(k,l)$
$\boldsymbol{H}$	Multichannel degradation or blur matrix
$\boldsymbol{C}$	Multichannel image model matrix
$s_p(m,n)$	Discrete samples of source or original image for the pth channel
$r_p(m,n)$	Discrete samples of received or observed image for the pth channel
$v_p(m,n)$	Discrete samples of observation noise for pth channel with $\sigma_{v_{pq}}^2$ variance

$w_p(m,n)$	Discrete samples of modeling noise for the pth channel with $\sigma^2_{w_{pq}}$ variance
$\mathbf{s}_p$, $\mathbf{r}_p$, $\mathbf{v}_p$, $\mathbf{w}_p$	Lexicographic order of the corresponding vectors $s_p(m,n)$, $r_p(m,n)$, $v_p(m,n)$, and $w_p(m,n)$, respectively
$\mathbf{r}$, $\mathbf{s}$, $\mathbf{v}$, $\mathbf{w}$	Lexicographic order of $\mathbf{r}_p$, $\mathbf{s}_p$, $\mathbf{v}_p$, and $\mathbf{w}_p$, for $,p=1,2,...,N$, respectively
S_c	Support for image model coefficients
S_h	Support for blur function coefficients
σ^2_v	Variance of observation noise
σ^2_w	Variance of modeling noise
$\mathbf{Q}_v$	Covariance matrix for the modeling noise $= \sigma^2_v \mathbf{I}$ $(\sigma^2_v > 0)$
$\mathbf{Q}_w$	Covariance matrix for the modeling noise $= \sigma^2_w \mathbf{I}$ $(\sigma^2_w > 0)$
$\sigma^2_{v_{pq}}$	Variance of observation noise for the pth channel
$\sigma^2_{w_{pq}}$	Variance of modeling noise for the pth channel
$c^{pq}(k,l)$	Model coefficients coupling the pth and qth channel
$h^{pq}(k,l)$	Blur coefficients for the pth channel
S_{pq}	Support of the multichannel blur function coefficients $h^{pq}(k,l)$
$\mathcal{R}_{pq}$	Support of the multichannel model coefficients $c^{pq}(k,l)$
Φ	Vector of parameters to be estimated
$\hat{\Phi}_{ml}$	Maximum likelihood estimator of the parameters vector Φ
$\mathfrak{R}(\Phi)$	Range of the parameters in Φ
$\mathcal{L}^{\ast}(\Phi)$	Log likelihood function of Φ
θ	Parameter describing the severity of the blur function
Θ	Vector of parameters describing the severity of the blur function
$\mathfrak{R}(\Theta)$	Range of the support for the blur function
$P_{ss}(i,j)$	Autocorrelation matrix of the original image $s(m,n)$

$S_{ss}(k,l)$	Power spectrum of $s(m,n)$ computed as the DFT of $P_{ss}(i,j)$
$\mathbf{P}_{rr}$	Covariance block matrix of the observed image $r(m,n)$
$P_{rr}(i,j)$	Elements of one block of $\mathbf{P}_{rr}$
$S_{rr}(k,l)$	Power spectrum of $r(m,n)$ computed as the DFT of $P_{rr}(i,j)$
$\dfrac{\partial}{\partial \theta_i} S_{rr}(k,l)$	Partial derivative of $S_{rr}(k,l)$ with respect to the parameter to be estimated
$R(u,v)$	DFT of the observed image $r(m,n)$
$\boldsymbol{P}_{rr}$	Multichannel block covariance matrix
$\boldsymbol{P}_{ww}$	Multichannel modeling noise matrix
$\boldsymbol{P}_{vv}$	Multichannel observation noise matrix
$P_{r_p r_q}(i,j)$	Autocorrelation components for the pth channel
$S_{r_p r_q}(k,l)$	Power spectrum of the observed image for pth channel
$J_0(\bullet),\ J_1(\bullet)$	Zeroth and first order Bessel functions of the first kind, respectively
$E[\bullet]$	Expected value of a random variable or process
$\lvert \mathbf{A} \rvert$	Determinant of matrix $\mathbf{A}$
$\mathbf{A}^t$	Transpose of matrix $\mathbf{A}$
$\mathbf{A}^*$	Conjugate of matrix $\mathbf{A}$
$s^{(m,n)}$	The state of an image at coordinate (m,n)
$\mathbf{K}^{(m,n)}$	Kalman gain computed for the state at coordinates (m,n)
$\mathbf{U}_b^{(m,n)}$	Predicted covariance matrices of the state at coordinates (m,n)
$\mathbf{U}_a^{(m,n)}$	Updated covariance matrices of the state at coordinates (m,n)

TABLE OF CONTENTS

Chapter

CHAPTER 1

INTRODUCTION

Images are produced for the purpose of recording, displaying, and analyzing useful information. Image processing is an essential and useful subject that has entered various fields in the real life today. It has important applications in the areas of education, medicine, industry, military, etc. The field of digital image processing can be divided into the following categories [73]:

1- Digitization and compression: Representing the image in a suitable and efficient format for further processing and manipulation.

2- Enhancement, identification, restoration, and reconstruction: Upgrading and improving the distorted data by reducing artifacts and corruption.

3- Matching, description, and recognition: Measuring properties and relationships between images or different parts of an image, and classifying image objects.

The subject of this thesis deals mainly with the second category, namely, blur identification and image restoration. The field of image restoration, sometimes

referred to as image deblurring, is concerned with the construction or estimation of the original image from a corrupted one. Basically, it tries to perform an inverting operation that will produce an image that is "as close as possible" to the original one. In doing so, the restoration methods assume that the characteristics of the degrading system and the noise are known *a priori*. However, in practice, one usually has hardly enough knowledge to obtain this information directly from the image formation process. The aim of the other related field, image identification, is to estimate the properties of the imperfect imaging system from the observed image itself prior to the restoration process [42]. Thus, the two problems are related to each other in the sense that good restoration results depend on how accurate the identified parameters are to the actual situation.

The available literature indicates that the field of image restoration has gained much more attention than the field of identification. Although this is true for the monochrome case, neither of the two fields has adequately been studied in the multichannel case, i.e., the parameter identification and restoration of, say, color or multispectral images. In fact, there is not any comprehensive study today that discusses the identification process in the multichannel case. One of the main purposes of this research is to investigate some novel identification techniques and their implementations in the monochrome and multichannel image processing.

1.1 Image Restoration

The process of image restoration is the process of obtaining the original image from a distorted and noisy one. This process involves using *a priori* knowledge available about the original image, mainly the point spread function (PSF) and the

العنوان:	CONTINUOUS SPATIAL DOMAIN IMAGE IDENTIFICATION AND RESTORATION WITH MULTICHANNEL APPLICATIONS
المؤلف الرئيسي:	Al Suwailem, Umar A.
مؤلفين آخرين:	Keller, James E.(super)
التاريخ الميلادي:	1996
موقع:	كولومبيا
الصفحات:	1 - 183
رقم MD:	616175
نوع المحتوى:	رسائل جامعية
اللغة:	English
الدرجة العلمية:	رسالة دكتوراه
الجامعة:	University of Missouri
الكلية:	The Graduate School
الدولة:	الولايات المتحدة الأمريكية
قواعد المعلومات:	Dissertations
مواضيع:	الهندسة الإلكترونية ، تطبيقات الحاسب ، ترميم الصور ، النمذجة ، الحركات الضبابية
رابط:	https://search.mandumah.com/Record/616175

REFERENCES

[1] F. Aghdasi and R. K. Ward, "Reduction of Boundary Artifacts in Image Restoration," *IEEE Trans. Image Processing*, vol. 5, no. 4, pp. 611-618, April 1996.

[2] E. Anarim, H. Uçar, and Y. Istefanopulos, "Identification of Image and Blur Parameters in Frequency Domain Using the Expectation-Maximization Algorithm," *IEEE Trans. Image Processing*, vol. 5, no. 1, pp. 159-164, January 1996.

[3] H.C. Andrews and B. R. Hunt, Digital Image Restoration, Prentice Hall, Inc., Englewood Cliffs, NJ, 1977.

[4] G. Angelopoulos and I. Pitas, "Multichannel Wiener Filters in Color Image Restoration," *IEEE Trans. Circ. Syst. for Video Technology*, vol. 4, no. 1, pp. 83-87, 1994.

[5] D. Angwin and H. Kaufman, "Effects of Modeling Domains on Recursive Color Image Restoration," in *Proc. 1987 IEEE Int. Conf. Acoust., Speech, and Signal Proc..* Dallas, Texas. April 1987.

[6] D. L. Angwin and H. Kaufman, " Image Restoration Using Reduced Order Models," *Signal Processing*, vol. 16, pp. 21-28, 1989.

[7] K. J. Åstrom, "Maximum Likelihood and Prediction Error," *Automatica* , vol. 16, pp. 551-574, 1980.

[8] A. A. Bales, *Multichannel Image Restoration of Motion Blurred Images*, M.Sc. Thesis, University of Missouri-Columbia, Dept. of Electrical Eng., 1990.

[9] M. R. Banham, N. P. Galatsanos, H. L. Gonzalez, and A. K. Katsaggelos, "Multichannel Restoration of Single Channel Images Using a Wavelet-based Subband Decomposition," *IEEE Trans. Image Processing*, vol. 3, no. 6, pp. 821-833, 1994.

[10] M. R. Banham and A. K. Katsaggelos,, "Wavelet-Based Multiscale Image Restoration," *IEEE Trans. Image Processing*, vol. 5, no. 4, pp. 619-634, April 1996.

[11] J. Bescos, I. Glaser, and A. A. Sawchuk, " Restoration of Color Images Degraded by Chromatic Aberrations," *Applied Optics*, vol. 19, pp. 3869-3876, November 1980.

[12] J. Biemond, J. Rieske and J. J. Gerbrands, "A Fast Kalman Filter for Image Degraded by Both Blur and Noise," *IEEE Trans. Acoustics, Speech and Signal Processing*, vol. 31, no. 5, pp. 1248-1256, 1983.

[13] J. Biemond, F. G. van der Putten and J. W. Woods, "Identification and Restoration of Images with Symmetric Noncausal Blurs," *IEEE Trans. Circuit and Systems*, vol. 23, no. 3, pp. 585-594, 1988.

[14] M. Canon "Blind Deconvolution of Spatially Invariant Image Blurs with Phase," *IEEE Trans. Acoustics, Speech and Signal Processing*, vol. 24, no. , pp. 58-63, 1976.

[15] M. R. Civanlar, and H. J. Trussell, "Digital Signal Restoration Using Fuzzy Sets," *IEEE Trans. Acoustics, Speech and Signal Processing*, vol. 34, no. 4, pp. 919-936, 1986.

[16] A. P. Dempster, N. M. Laird and D. B. Rubin, " Maximum Likelihood from incomplete Data," *J. Royal Statistic Soc. B*, vol. 39, pp. 1-38, 1977.

[17] H. W. Engl and C. W. Groetsch (Editors), *Inverse and Ill-Posed Problems* , Academic Press, Boston, MA, 1987.

[18] M. A. T. Figueiredo and J. M. N. Leitão, "Sequential and Parallel Image Restoration: Neural Networks Implementations," *IEEE Trans. Image Processing*, vol. 3, no. 11, pp. 789-801, November 1994.

[19] N. P. Galatsanos, *Multichannel Image Restoration*, Ph.D. Thesis, University of Wisconsin-Madison, Dept. of Electrical Engineering, 1989.

[20] N. P. Galatsenos and R. T. Chin, "Digital Restoration of Multichannel Images," *IEEE Trans. Acoustics, Speech and Signal Processing*, vol. 37 , no. 3, pp. 415-421, 1989.

[21] C. R. Giardina and E. R. Dougherty, *Morphological Methods in Image and Signal processing*, Englewood, NJ: Prentice-Hall, 1988.

[22] R. C. Gonzalez and R. E. Woods, *Digital Image Processing*, Addison-Wesley, Reading, MA, 1993.

[23] T. J. Hebert and K. Lu, "Expectation-Maximization Algorithm, Null Spaces, and MAP Restoration," *IEEE Trans. Image Processing*, vol. 4, no. 8, pp. 1084-1095, August 1995.

[24] A. D. Hillery and R. T. Chin, "Iterative Wiener Filters for Image Restoration," in *IEEE Int. Conf. Acoust., Speech, and Signal Proc.*. Albuquerque, New Mexico, pp.1901-1904, April 3-6,1990.

[25] T. S. Huang, W. F. Schreiber and O. J. Tretiak, "Image Modeling," *Proc. IEEE*, vol. 59, no. 11, pp. 1586-1609, 1972.

[26] B. R. Hunt, " The Application of Constrained least-squares Estimation to Image Restoration by Digital computer," *IEEE Trans. Computers*, vol. 22, no. 9, pp. 805-812, 1973.

[27] B. R. Hunt and O. Kubler, "Karhunen-Loeve Multispectral Image Restoration, Part I: Theory," *IEEE Trans. Acoustics, Speech and Signal Processing*, vol. 32, no. 3, pp. 592-600, 1984.

[28] A. K. Jain, "Advances in Mathematical Models for Image Processing," *Proc. IEEE*, vol. 69, no. 5, pp. 502-528, 1981.

[29] A. K. Jain, Fundamentals of Digital Image Processing, Prentice Hall, Inc., Englewood Cliffs, NJ, 1989.

[30] F. C. Jeng and J. W. Woods, "Inhomogeneous Gaussian Image Models for Estimation and Restoration," *IEEE Trans. Acoustics, Speech and Signal Processing*, vol. 36, no. 8 , pp. 1305-1312, 1988.

[31] B. Jähne, Digital Image Processing, Concepts, Algorithms, and Scientific Applications, Springer-Verlag, Berlin, 1993.

[32] R. L. Kashyap, " Image Models," in Handbook of Pattern Recognition and Image Processing, T. Y. Young and K.S. Fu (eds.), Academic Press, 1986.

[33] A. Katsaggelos, "Multiple Input Adaptive Iterative Image Restoration Algorithm," in *Proc. 1987 IEEE Int. Conf. Acoust., Speech, and Signal Proc.*. Dallas, Texas, pp. 1179-1182, April 1987.

[34] A. K. Katsaggelos (Editor), *Digital Image Restoration*, Springer-Verlag, Berlin, Germany, 1991.

[35] A. K. Katsaggelos, J. Biemond, R. M. Mersereau and R. W. Schafer, "An Iterative Method for Restoring Noisy Blurred Images," *Circ. Syst. Signal Processing*, vol. 3, no. 2, pp. 139-160, 1984.

[36] A. K. Katsaggelos, K. T. Lay, and N. P. Galatsanos, "A General Framework for Frequency Domain Multichannel Signal processing," *IEEE Trans. Image Processing*, vol. 2, no. 3, pp. 417-420, 1993.

[37] H. Kaufman, J. W. Woods, S. Dravida, and A. M. Tekalp, "Estimation and Identification of Two-Dimensional Images," *IEEE Trans. Auto. Control*, vol. AC-28, no. 7, pp. 745-756, 1983.

[38] J. Kim and J. W. Woods, "Image Identification and Restoration in the Subband Domain," *IEEE Trans. Image Processing*, vol. 3, no. 3, pp. 312-314, 1994. Erratum in *IEEE Trans. Image Processing*, vol. 3, no. 6, pp. 873, November 1994.

[39] G. J. Klinker, *A Physical Approach to Color Image Understanding*, A K Peters, , Wellesley, MA, 1993.

[40] S. Koch and J. Biemond, "Restoration of Spatially Varying Blurred Images Using Multiple Model-Based Extended Kalman Filters," *IEEE Trans. Image Processing*, vol. 4, no. 4, pp. 520-523, April 1995.

[41] R. L. Lagendijk, D. L. Angwin, H. Kaufman and J. Biemond, "Recursive and Iterative Methods for Image Identification and Restoration," in *Proc. Fourth European Signal Processing Conf. EUSIPCO'88,.*J.G. Lacoume (ed.), Grenoble, pp. 235-238.

[42] R. L. Lagendijk and J. Biemond, *Iterative Identification and Restoration of Images*, Kluwer Academic Publishers, Boston, 1991.

[43] R. L. Lagendijk, J. Biemond, and D. E. Boekee, "Regularized Iterative Image Restoration with Ringing Reduction," *IEEE Trans. Acoustics, Speech and Signal Processing*, vol. 36, no. 12, pp. 1874-1888, 1988.

[44] R. L. Lagendijk, J. Biemond, and D. E. Boekee, "Identification and Restoration of Noisy Images Using the Expectation Maximization Algorithm," *IEEE Trans. Acoustics, Speech and Signal Processing*, vol. 38, no. 7, pp. 1180-1191, 1990.

[45] R. L. Lagendijk, A. K. Katsaggelos and J. Biemond, "Iterative Identification and Restoration of images," in *Proc. 1988 IEEE Int. Conf. Acoust., Speech, and Signal Proc.*, New York, NY, USA, pp. 992-995.

[46] R. L. Lagendijk, R. M. Merseeau and J. Biemond, "On Increasing the Convergence Rate of Regularized Iterative Image Restoration Algorithms," in *Proc. 1987 IEEE Int. Conf. Acoust., Speech, and Signal Proc.*. Dallas, Texas, pp. 1183-1186.

[47] R. L. Lagendijk, A. M. Tekalp and J. Biemond, "Maximum Likelihood Image and Blur Identification: A unifying Approach," *J. Optical Engineering*, vol. 29, no. 5, pp. 422-435, 1990.

[48] K. T. Lay and A. K. Katsaggelos, "Image Identification and Restoration Based on the Expectation-Maximization Algorithm," *Optical Engineering*, vol. 29, no. 5, pp. 436-445, May 1990.

[49] H. Lee, "Review of Image-Blur Models in a Photographic System Using the Principles of Optics," *Optical Engineering*, vol. 29, no. 5, pp. 405-421, May 1990.

[50] J. S. Lee "Digital Image Enhancement and Noise Filtering by Use of Local Statistics," *IEEE Trans. Pattern Analysis, and Machine Intelligence*, vol. PAMI-2, pp. 165-168, 1980.

[51] L. Ljung and T. Söderström, *Theory and Practice of Recursive Identification*, The MIT Press, Cambridge, MA, 1986.

[52] B. Mahesh, W.-J. Song, and W. A. Pearlman, "Adaptive Estimators for Filtering Noisy Images," *Optical Engineering*, vol. 29, no. 5, pp. 488-494, May 1990.

[53] J. Makhoul, "Linear Prediction: A Tutorial Review," *Proc. IEEE*, vol. 63, no. 4, pp. 561-580, 1975.

[54] A. Marion (Editor), *An Introduction to Image Restoration*, Chapman and Hall, London, 1991.

[55] V. Z. Mesarovic', N. P. Galatsanos, and A. K. Katsaggelos, "Regularized Constrained Total Least Square Image Restoration," *IEEE Trans. Image Processing*, vol. 4, no. 8, pp. 1096-1108, 1995.

[56] V. A. Morozov, *Regularization Methods for Ill-Posed Problems* , CRC Press, Boca Raton, Florida, 1993.

[57] P. K. Nanda, K. Sunil Kumar, S. Ghokale and U. B. Desai, " A Multiresolution Approach to Color Image Restoration and Parameter Estimation Using Homotopy Continuation Method," in *Proc. Int. Conf. Image Proc.* Washington, DC, pp. 45-48, 1995.

[58] N. Ohyama, M. Yachida, E. Badique, J. Tsujiuchi, and T. Honda, "Least-Squares Filter for Color-Image Restoration," *J. Opt. Soc. Am. A*, vol. 5, no. 1, pp. 19-24, January 1988.

[59] M. K. Ozkan, A. T. Erdem, M. I. Sezan, and A. M. Tekalp, "Efficient Multiframe Wiener Restoration of Blurred and Noisy Image Sequences," *IEEE Trans. Image Processing*, vol. 1, no. 4, pp. 453-476, 1992.

[60] A. Papoulis, *Signal Analysis*, Mc Graw Hill, New York, 1977.

[61] G. M. Pavlovic, *Identification and Restoration of Images Based on Overall Modeling of the Imaging Process*, Ph.D. Thesis, University of Rochester, Dept. of Electrical Eng., 1991.

[62] G. Pavlovic' and Z. Kostic', "Multiframe Maximum Likelihood Parameter identification for Image Sequences," in *Proc. Conference on Information and Systems*, Princeton, New Jersey, 1992.

[63] G. Pavlovic´ and A. M. Tekalp, "Maximum Likelihood Blur Identification Based on a Continuous Spatial Domain Model," *IEEE Trans. Image Processing*, vol. 1, no. 4, pp. 496-504, 1992.

[64] I. Pitas and P. Kilindris, " Application of Multichannel Two-Dimensional AR Modeling to Color Image Processing," in Image Processing: Theory and Applications, G. Vernazza, A. N. Venetsanopoulos, and C. Braccini (eds.),pp. 193-196, Elsevier Science Publications, Amsterdam, 1993.

[65] I. Pitas and P. Kilindris, "Multichannel Techniques in Color Image Enhancement and Modeling," *IEEE Trans. Image Processing*, vol. 5, no. 1, pp. 168-171, January 1996.

[66] M. Potmesil and I. Chakravarty, "Synthetic Image Generation with a Lens and Aperture Camera Model," *AMC Trans. on Graphics*, vol. 1, no. 2, pp. 85-108, 1982.

[67] W. K. Pratt, "Vector Space Formulation of Two-Dimensional Signal Processing Operations," *Computer Graphics and Image Processing*, no. 4, pp. 1-24, 1975.

[68] W. H. Pun and B. D. Jeffs, "Adaptive Image Restoration Using A Generalized Gaussian Model for Unknown Noise," *IEEE Trans. Image Processing*, vol. 4, no. 10, pp. 1451-1456, October 1995.

[69] S. J. Reeves, "Optimal Space-Varying Regularization in Iterative Image Restoration," *IEEE Trans. Image Processing*, vol. 3, no. 3, pp. 319-324, May 1994.

[70] S. J. Reeves and R. M. Mersereau, "Optimal Estimation of the Regularization Parameter and Stabilizing Functional for Regularized Image Restoration," *Optical Engineering*, vol. 29, no. 5, pp. 446-454, May 1990.

[71] S. J. Reeves and R. M. Mersereau, "Blur Identification by the Method of Generalized Cross-Validation," *IEEE Trans. Image Processing*, vol. 1, no. 3, pp. 301-311, July 1992.

[72] Michael Rodriguez, " A Graphic ARTS Perspective on RGB-To-CMYK Conversion," in *Proc. Int. Conf. Image Proc..* Washington, DC, pp. 1995.

[73] A. Rosenfeld and A. C. Kak, *Digital Picture Processing (Volumes I and II)*, Academic Press, Orlando, FL, 1982.

[74] J. C. Russ, *The Image Processing Handbook*, CRC Press, Boca Raton, Florida, 1992.

[75] A. E. Savakis and H. J. Trussell, "Blur Identification by Residual Spectral Matching," *IEEE Trans. Image Processing*, vol. 2, no. 2, pp. 141-151, 1993.

[76] J. Schoukens and R. Pintelon, *Identification of Linear Systems: A practical Guideline to Accurate Modeling* , Pergamon Press, Oxford , Great Britain, 1991.

[77] R. R. Schultz and R. L. Stevenson, "Stochastic Modeling and Estimation of Multispectral Image Data," *IEEE Trans. Image Processing*, vol. 4, no. 8, pp. 1109-1119, August 1995.

[78] F. C. Schweppe, *Uncertain Dynamic Systems*, Printice Hall, New Jersey, 1973.

[79] M. I. Sezan, G. Pavlovic, A. M. Tekalp, and A. T. Erdem, "On Modeling the Focus Blur in Image Restoration," in *IEEE Int. Conf. Acoust., Speech, and Signal Proc..* (Toronto, Canada), pp. 2486-2489, May, 1991.

[80] M. I. Sezan and H. Stark, "Image Restoration by the Method of Convex Projections: Part 2 - Application and Numerical Results," *IEEE Trans. Medical Imaging*, vol. 1, no. 2, pp. 95-101, 1982.

[81] M. I. Sezan and A. M. Tekalp, "Survey of Recent Developments in Digital Image Restoration," *Optical Engineering*, vol. 29, no. 5, pp. 393-404, May 1990.

[82] K. Tang, J. Astola, and Y. Neuvo, "Multichannel Edge Enhancement in Color Image Processing," *IEEE Trans. Circuits and Systems for Video Technology*, Vol. 4, No. 5, pp. 775-781, 1994.

[83] A. M. Tekalp, "Restoretool 2.0: Image Processing Package," University of Rochester, Electrical Engineering Department, 1991.

[84] A. M. Tekalp, H. Kaufman, "Adaptive Image Restoration Using Control Theoretic Principles," *IEEE Control Syst. Mag.*, vol. 11, no. 1, pp. 29-32, January 1991.

[85] A. M. Tekalp, H. Kaufman, and J. W. Woods, "Identification of Image and Blur Parametres for the Restoration of Noncausal Blurs," *IEEE Trans. Acoustics, Speech and Signal Processing*, vol. 34, no. 4, pp. 963-972, 1986.

[86] A. M. Tekalp, H. Kaufman, and J. W. Woods, "Edge-Adaptive Kalman Filtering for Image Restoration with Ringing Suppression," *IEEE Trans. Acoustics, Speech and Signal Processing*, vol. 37, no. 6, pp. 892-899, 1989.

[87] A. M. Tekalp and G. Pavlovic, "Multichannel Image modeling and Kalman Filtering for Multispectral Image Restoration," *Signal Processing*, vol. 19, no. 3, pp. 221-232, March 1990.

[88] C. W. Therrien and H. T. El-Shaer, "Methods for Multichannel 2-D Spectrum Analysis: Description and Comparison," in *Proc. 1987 IEEE Int. Conf. Acoust., Speech, and Signal Proc.*. Dallas, Texas, pp. 1179-1182, April 1987.

[89] C. W. Therrien and H. T. El-Shaer, "A Direct Algorithm for Computing 2-D AR Power Spectrum Estimates," *IEEE Trans. Acoustics, Speech and Signal Processing*, vol. 37, no. 11, pp. 1795-1798, 1989.

[90] C. W. Therrien and H. T. El-Shaer, "Multichannel 2-D AR Spectrum Estimation," *IEEE Trans. Acoustics, Speech and Signal Processing*, vol. 37, no. 11, pp. 1798-1800, 1989.

[91] H. J. Trussell and M. R. Civanlar, "Signal Deconvolution by Projections onto çonvex Sets," in *Proc. 1984 IEEE Int. Conf. Acoust., Speech, and Signal Proc.*. San Diego, California, 1984.

[92] H. J. Trussell and B. R. Hunt, " Improved Methods of maximum A Posteriori Restoration," *IEEE Trans. Computers*, vol. 27, no. , pp. 57-62, 1979.

[93] H. J. Trussell, M. I. Sezan, and D. Tran, 'Sensitivity of Color LMMSE Restoration of Images to the Spectral Estimate," *IEEE Trans. Acoustics, Speech and Signal Processing*, vol. 39, no. 1, pp. 248-252, 1991.

[94] J. W. Woods, J. Biemond and A. M. Tekalp, " Boundary Value Problem in Image Restoration," in *Proc. 1985 IEEE Int. Conf. Acoust., Speech, and Signal Proc..* Tampa, Florida, pp. 692-695.

[95] J. W. Woods and V. K. Ingle, "Kalman Filtering in Two-Dimension: Further Results," *IEEE Trans. Acoustics, Speech and Signal Processing*, vol. 29, no. 2 ,pp. 188-197, 1981.

[96] J. W. Woods and C. H. Radewan, "Kalman Filtering in Two-Dimension," *IEEE Trans. Information Theory*, vol. 23, no. 4, pp. 473-482, 1977.

[97] Y. Yemez, E. Anarim, and Y. istefanopulos, "Causal and Semicausal AR Image Model Identification Using the EM Algorithm," *IEEE Trans. Image Processing*, vol. 2, no. 4, pp. 523-528, 1993.

[98] Y. -L. You and M. Kaveh, "A Regularization Approach to Joint Blur Identification and Image Restoration," *IEEE Trans. Image Processing*, vol. 5, no. 3, pp. 416-428, March 1996.

[99] D. C. Youla, and H. Webb, "Image Restoration by the Method of Convex Projections: Part 1 - Theory," *IEEE Trans. Medical Imaging*, vol. 1, no. 2, pp. 81-94, 1982.

[100] M. E. Zervakis, "A structured Regularized Approach in Multichannel Image Restoration," in Image Processing: Theory and Applications, G. Vernazza, A. N. Venetsanopoulos, and C. Braccini (eds.),pp. 255-258, Elsevier Science Publications, Amsterdam, 1993.

[101] X. Zhang, Y. Song, and Y. Li, "Adaptive Identification of Nonminimum Phase ARMA Models Using Higher Order Cumulants Alone," *IEEE Trans. Signal Processing*, vol. 44, no. 5, pp. 159-164, May 1996.

[102] Y. Zhang, D. Hatzinakos, and A. Venetsanopoulos, "Identification of Multichannel and Multidimensional Systems Using Cumulants: Application to Colour Images," in Image Processing: Theory and Applications, G. Vernazza, A. N. Venetsanopoulos, and C. Braccini (eds.),pp. 255-258, Elsevier Science Publications, Amsterdam, 1993.

[103] Yi-Tong Zhou, R. Chellappa, A. Vaid, and B. K. Jenkins "Image Restoration Using a Neural Network," *IEEE Trans. Acoustics, Speech and Signal Processing*, vol. 36, no. 7, pp. 1141-1151, July 1988.

العنوان:	CONTINUOUS SPATIAL DOMAIN IMAGE IDENTIFICATION AND RESTORATION WITH MULTICHANNEL APPLICATIONS
المؤلف الرئيسي:	Al Suwailem, Umar A.
مؤلفين آخرين:	Keller, James E.(super)
التاريخ الميلادي:	1996
موقع:	كولومبيا
الصفحات:	1 - 183
رقم MD:	616175
نوع المحتوى:	رسائل جامعية
اللغة:	English
الدرجة العلمية:	رسالة دكتوراه
الجامعة:	University of Missouri
الكلية:	The Graduate School
الدولة:	الولايات المتحدة الأمريكية
قواعد المعلومات:	Dissertations
مواضيع:	الهندسة الإلكترونية ، تطبيقات الحاسب ، ترميم الصور ، النمذجة ، الحركات الضبابية
رابط:	https://search.mandumah.com/Record/616175

www.manaraa.com

APPENDIX A

DEFINITIONS

In this appendix we will give definitions for some of the mathematical terminology used throughout this study.

Definition A.1: Toeplitz Matrix

A matrix $\mathbf{A}$ is called Toeplitz if it has constant elements along the main diagonal and the subdiagonals, i.e., $a_{(m,n)} = a_{m-n}$. Thus, $\mathbf{A}$ has the following structure:

$$\mathbf{A} = \begin{bmatrix} a_0 & a_{-1} & a_{-2} & \cdot & \cdot & a_{-N+1} \\ a_1 & a_0 & a_{-1} & \cdot & \cdot & a_{-N+2} \\ a_2 & \cdot & \cdot & \cdot & \cdot & \cdot \\ \cdot & \cdot & \cdot & \cdot & \cdot & \cdot \\ \cdot & \cdot & \cdot & \cdot & a_0 & a_{-1} \\ a_{N-1} & \cdot & \cdot & a_2 & a_1 & a_0 \end{bmatrix} \tag{A.1}$$

Definition A.3: Circulant Matrix

A matrix **A** is called circulant if each row (column) is a circular shift of the pervious row (column). A circulant matrix **A** should have the following structure:

$$\mathbf{A} = \begin{bmatrix} a_0 & a_1 & a_2 & \cdot & & \cdot & a_{N-1} \\ a_{N-1} & a_0 & a_1 & \cdot & & \cdot & a_{N-2} \\ a_{N-2} & \cdot & \cdot & \cdot & & \cdot & \cdot \\ \cdot & \cdot & \cdot & \cdot & & \cdot & \cdot \\ a_2 & \cdot & \cdot & a_{N-1} & a_0 & a_1 \\ a_1 & a_2 & \cdot & a_{N-2} & a_{N-1} & a_0 \end{bmatrix} \tag{A.2}$$

Note that circulant matrices are Toeplitz but not vise versa.

Definition A.4: Block Matrix

A matrix **A** is called block matrix if its elements are matrices too, i.e.

$$\mathbf{A} = \begin{bmatrix} \mathbf{A}_{11} & \mathbf{A}_{12} & \cdot & \mathbf{A}_{1N} \\ \mathbf{A}_{21} & \mathbf{A}_{22} & \cdot & \cdot \\ \cdot & \cdot & \cdot & \cdot \\ \mathbf{A}_{1N} & \cdot & \cdot & \mathbf{A}_{MN} \end{bmatrix} \tag{A.3}$$

If each element $\mathbf{A}_{ij}$ has a dimension $p \times q$, then **A** is called $M \times N$ block matrix of basic dimension $p \times q$. However, if each $\mathbf{A}_{ij}$ is a square matrix of dimension $p \times p$ then **A** is called $M \times N$ block matrix of basic dimension p.

Definition A.5: Block Toeplitz and Block Circulant Matrices

A block Toeplitz matrix $\mathbf{A}$ is a block matrix whose elements are ordered in a Toeplitz form such that $\mathbf{A}_{i,j} = \mathbf{A}_{i-j}$

$$\mathbf{A} = \begin{bmatrix} \mathbf{A}_0 & \mathbf{A}_{-1} & \mathbf{A}_{-2} & \cdot & \cdot & \mathbf{A}_{-N+1} \\ \mathbf{A}_1 & \mathbf{A}_0 & \mathbf{A}_{-1} & \cdot & \cdot & \mathbf{A}_{-N+2} \\ \mathbf{A}_2 & \mathbf{A}_1 & \mathbf{A}_0 & \cdot & \cdot & \cdot \\ \cdot & \cdot & \cdot & \cdot & \cdot & \cdot \\ \cdot & \cdot & \cdot & \cdot & \mathbf{A}_0 & \mathbf{A}_{-1} \\ \mathbf{A}_{N-1} & \cdot & \cdot & \cdot & \mathbf{A}_1 & \mathbf{A}_0 \end{bmatrix}$$

Similarly, a block circulant matrix $\mathbf{A}$ is a block matrix whose elements are ordered in a Toeplitz form such that $\mathbf{A}_{i,j} = \mathbf{A}_{(j-i)}$ modulo N

$$\mathbf{A} = \begin{bmatrix} \mathbf{A}_0 & \mathbf{A}_1 & \mathbf{A}_2 & \cdot & \cdot & \mathbf{A}_{N-1} \\ \mathbf{A}_{N-1} & \mathbf{A}_0 & \mathbf{A}_1 & \cdot & \cdot & \mathbf{A}_{N-2} \\ \mathbf{A}_{N-2} & \mathbf{A}_1 & \mathbf{A}_0 & \cdot & \cdot & \cdot \\ \cdot & \cdot & \cdot & \cdot & \cdot & \cdot \\ \cdot & \cdot & \cdot & \cdot & \mathbf{A}_0 & \mathbf{A}_1 \\ \mathbf{A}_1 & \mathbf{A}_2 & \cdot & \cdot & \mathbf{A}_{N-1} & \mathbf{A}_0 \end{bmatrix}$$

We should know that although each block is in Toeplitz or circulant forms, $\mathbf{A}$ need not be Toeplitz or circulant with regard to the order of its blocks. If the order of the blocks in $\mathbf{A}$ is Toeplitz or circulant order, then $\mathbf{A}$ is called doubly Toeplitz or doubly circulant, respectively.

APPENDIX B

DERIVATIONS OF EQUATIONS IN CHAPTER 4

Frequency Domain Representation of the Likelihood Function: Equation (4.18)

In section 4.2, the likelihood function in its spatial domain representation, equation (4.17), is expressed in the frequency domain, equation (4.18), for implementation purposes. In this appendix we show the derivation for this transformation. Consider the LF given by (4.17) as

$$\mathbf{L}(\Theta, c(m,n), \sigma_v^2, \sigma_w^2) = -\{\log(|\mathbf{P}_{rr}|) + \mathbf{r}'\mathbf{P}_{rr}^{-1}\mathbf{r}\} \tag{B.1}$$

The block Toeplitz autocorrelation matrix $\mathbf{P}_{rr}$ is approximated by a block circulant matrix and then diagonalized by 2-D Fourier transform through the $N \times N$ operator $\mathbf{W}$ defined as

$$\mathbf{W} = [\mathbf{w}(0), \mathbf{w}(1), \dots, \mathbf{w}(N-1)] \tag{B.2}$$

where each of the components $\mathbf{w}(k)$ is describes the kernel of the transform as follows

$$\mathbf{w}(k) = [1, e^{j\frac{2\pi}{N}k}, e^{j\frac{2\pi}{N}2k}, e^{j\frac{2\pi}{N}3k}, ..., e^{j\frac{2\pi}{N}(N-1)k}]^t \qquad \text{(B.3)}$$

Thus, we may construct a matrix $\mathbf{W}$ that diagonalizes the block circulant matrix $\mathbf{P}_{rr}$ by arranging $\mathbf{W}$ in N rows and N columns so that the size of $\mathbf{W}$ is $N^2 \times N^2$ [22].

Using the following properties of $\mathbf{W}$

$$\mathbf{I} = \mathbf{W}\mathbf{W}^{-1}$$
$$\mathbf{W}^{-1} = \frac{1}{N^2}\,\mathbf{W}^*$$
$$\left|\mathbf{W}\mathbf{W}^{-1}\mathbf{P}_{rr}\right| = \left|\mathbf{W}^{-1}\mathbf{P}_{rr}\mathbf{W}\right|$$

and
$$(\mathbf{W}^{-1}\mathbf{P}_{rr}\mathbf{W})^{-1} = \mathbf{W}^{-1}\mathbf{P}_{rr}^{-1}\mathbf{W}, \qquad \text{(B.4)}$$

we may write (B.1) as

$$\mathbf{L}(\Theta, c(m,n), \sigma_v^2, \sigma_w^2) = -\{\log(\left|\mathbf{W}\mathbf{W}^{-1}\mathbf{P}_{rr}\right|) + \mathbf{r}'\mathbf{W}\mathbf{W}^{-1}\mathbf{P}_{rr}^{-1}\mathbf{W}\mathbf{W}^{-1}\mathbf{r}\} \qquad \text{(B.5)}$$

or

$$\mathbf{L}(\Theta, c(m,n), \sigma_v^2, \sigma_w^2) = -\{\log(\left|\mathbf{W}^{-1}\mathbf{P}_{rr}\mathbf{W}\right|) + (\mathbf{W}'\mathbf{r})'(\mathbf{W}^{-1}\mathbf{P}_{rr}\mathbf{W})^{-1}(\frac{1}{N^2}\mathbf{W}^*\mathbf{r})\} \qquad \text{(B.6)}$$

We notice that the DFT diagonalization of the autocorrelation matrix $\mathbf{P}_{rr}$ results in the power spectrum $\mathbf{S}_{rr}$, i.e. $\mathbf{S}_{rr} = \mathbf{W}^{-1}\mathbf{P}_{rr}\mathbf{W}$. Thus, (B.6) can be written as

$$\mathbf{L}(\Theta, c(m,n), \sigma_v^2, \sigma_w^2) = -\{\log(\left|\mathbf{S}_{rr}\right|) + \frac{1}{N^2}\mathbf{R}'\mathbf{S}_{rr}^{-1}\mathbf{R}^*\} \qquad \text{(B.7)}$$

163

where $\mathbf{R}$ is the Fourier Transform of $\mathbf{r}$ given by $\mathbf{R} = \mathbf{W}\mathbf{r}$. Since $\mathbf{S}_{rr}$ is a diagonal matrix, then its inverse is also a diagonal matrix with each element equals the reciprocal of the corresponding element of $\mathbf{S}_{rr}$. Thus, we may write the LF (B.7) as

$$\mathbf{L}(\Theta, c(m,n), \sigma_v^2, \sigma_w^2) = -\sum_k \sum_l (\log S_{rr}(k,l) + \frac{1}{N^2} \frac{|R(k,l)|}{S_{rr}(k,l)}) \qquad (B.8)$$

which is the same as equation (4.18). Note that the $S_{rr}(k,l)$'s are the diagonal elements of $\mathbf{S}_{rr}$

Autocorrelation and Power Spectrum Representation in the Continuous Domain: Equations (4.20) and (4.21)

We will show here the derivations for equations (4.20) and (4.21). The autocorrelation P_{rr} can be computed by substituting (4.14) into (4.19) to get

$$
\begin{aligned}
P_{rr}(i,j) &= E[r(m,n)r(m+i,n+j)] \\
&= E[\{ \iint_{R(\Theta)} h(\psi,\zeta)s(m\Delta x - \psi, n\Delta y - \zeta)d\psi d\zeta + v(m,n)\} \\
&\quad \{ \iint_{R(\Theta)} h(\xi,\eta)s(m\Delta x + i - \xi, n\Delta y + j - \eta)d\xi d\eta + v(m+i,n+j)\}]
\end{aligned}
\qquad (B.9)
$$

The products of the noise and signal terms drop because of independence between them. Thus, we end up with the following terms

$$
\begin{aligned}
P_{rr}(i,j) &= E[\{ \iint_{R(\Theta)} h(\psi,\zeta)s(m\Delta x - \psi, n\Delta y - \zeta)d\psi d\zeta\} \\
&\quad \{ \iint_{R(\Theta)} h(\xi,\eta)s(m\Delta x + i - \xi, n\Delta y + j - \eta)d\xi d\eta\}] \\
&\quad + E[v(m,n)v(m+i,n+j)]
\end{aligned}
\qquad (B.10)
$$

164

or

$$P_{rr}(i,j) = \iint_{R(\Theta)} \iint_{R(\Theta)} h(\psi,\zeta)h(\xi,\eta)P_{ss}(i - \xi + \psi, j - \eta + \zeta)d\psi d\zeta d\xi d\eta\}$$

$$+ \delta(i,j)\sigma_v^2 \tag{B.11}$$

where we have used the definition of the autocorrelation of the original image as

$$P_{ss}(x,y) = E[s(\xi,\eta)s(\xi + x, \eta + y)] \tag{B.12}$$

To get the power spectrum equation (4.21), we take the DFT of (4.20), which is (B.11) too, as follows

$$S_{rr}(k,l) = DFT[P_{rr}(i,j)]$$

$$= DFT[\iint_{R} \iint_{R} h(\psi,\zeta)h(\xi,\eta)P_{ss}(i - \xi + \psi, j - \eta + \zeta) \tag{B.13}$$

$$d\psi d\zeta d\xi d\eta] + \sigma_v^2$$

Using the definition of the power spectrum as $S_{ss}(k,l) = DFT[P_{ss}(i,j)]$, we may write (B.13) with the shift factor as

$$S_{rr}(k,l) = S_{ss}(k,l)[\iint_{R(\Theta)} \iint_{R(\Theta)} h(\psi,\zeta)h(\xi,\eta)$$

$$\exp[-j\tfrac{2\pi}{N}k(\psi - \xi)]\exp[-j\tfrac{2\pi}{N}l(\zeta - \eta)]d\psi d\zeta d\xi d\eta] + \sigma_v^2 \tag{B.14}$$

which can be written, using the separability property of the DFT, as

$$S_{rr}(k,l) = S_{ss}(k,l)[\{\iint_{R(\Theta)} h(\psi,\zeta)\exp[-j\tfrac{2\pi}{N}k\psi]\exp[-j\tfrac{2\pi}{N}l\zeta]d\psi d\zeta\}$$

$$\{\iint_{R(\Theta)} h(\xi,\eta)\exp[j\tfrac{2\pi}{N}k\xi]\exp[j\tfrac{2\pi}{N}l\eta]d\xi d\eta\}] + \sigma_v^2 \tag{B.15}$$

We note that the first double integral is the transfer function of the blur and the second is its conjugate. Thus, we may write

$$S_{rr}(k,l) = S_{ss}(k,l)[H(k,l)H^*(k,l)] + \sigma_v^2$$

$$= S_{ss}(k,l)|H(k,l)|^2 + \sigma_v^2 \tag{B.16}$$

which is identical to equation (4.21).

Power Spectrum of the Ideal Image: Equation (4.23)

Equation (4.23) computes the power spectrum of the ideal image, S, as derived from the ideal image formation model equation, (4.15). We will give that derivation here .

From equation (4.15), the ideal image formation model is given by

$$s(m,n) = \sum_{(k,l) \in \mathbf{S}_c} c(k,l)s(m-k,n-l) + w(m,n) \tag{B.17}$$

We may write the autocorrelation function as

$$
\begin{aligned}
P_{ss}(i,j) &= E[s(\xi,\eta)s(\xi+i,\eta+j)] \\
&= E[s(\xi,\eta)\{ \sum_{(k,l) \in \mathbf{S}_c} c(k,l)s(\xi+i-k,\eta+j-l) \\
&\quad + w(\xi+i,\eta+j)\}] \\
&= E[\sum_{(k,l) \in \mathbf{S}_c} c(k,l)s(\xi,\eta)s(\xi+i-k,\eta+j-l)] \\
&\quad + E[s(\xi,\eta)w(\xi+i,\eta+j)]
\end{aligned}
\tag{B.18}
$$

166

Since $E[s(\xi,\eta)s(\xi+i-k,\eta+j-l)] = P_{ss}(i-k,j-l)$, and the last term in equation (B.18) contributes only to the zeroth term of the noise autocorrelation (the autocorrelation is a delta function), we may write the previous equation in a simplified form as

$$P_{ss}(i,j) = \sum_{(k,l)\in\mathbf{S}_c} c(k,l)P_{ss}(i-k,j-l) + \sigma_w^2\delta(i,j) \qquad (B.19)$$

Noting that the first term in the right hand side of this equation represents convolution in the discrete domain, then by taking the DFT of equation (B.19) and using $S_{ss}(k,l) = DFT[P_{ss}(i,j)]$ we have

$$S_{ss}(k,l) = \left[\sum_{(m,n)\in S_c} c(m,n)\exp\left(-j\frac{2\pi}{N}km\right)\exp\left(-j\frac{2\pi}{N}ln\right)\right]S_{ss}(k,l) + \sigma_w^2 \qquad (B.20)$$

or we may get an identical expression to equation (4.23) as

$$S_{ss}(k,l) = \frac{\sigma_w^2}{\left|1 - \sum_{(m,n)\in S_c} c(m,n)\exp\left(-j\frac{2\pi}{N}km\right)\exp\left(-j\frac{2\pi}{N}ln\right)\right|^2} \qquad (B.21)$$

APPENDIX C

DERIVATIONS OF EQUATIONS IN CHAPTER 5

Least Squares Estimation of the Model Coefficients: Equations (5.7) and (5.8)

The model coefficients can be computed using a least squares procedure as given in equations (5.7) and (5.8). We will show here the derivation for this approach.

Consider the multichannel AR image model given by equation (5.3) as

$$s(m,n) = C's_1(m,n) + w(m,n) \qquad (C.1)$$

where $s(m,n)$, $s_1(m,n)$, $w(m,n)$ and C are as defined in section 5.2. We now perform a least square fit over the whole image or over a representative block of data, B. Then, the estimated coefficients $\hat{C}$ can be computed as to minimize the error function given by

$$Q_{ww} = \sum_{(m,n)\in B} \left[s(m,n) - \hat{C}' s_1(m,n) \right]^2$$

$$= \sum_{(m,n)\in B} [s(m,n)]^2 - 2\hat{C}' s_1(m,n)s(m,n) + [\hat{C}' s_1(m,n)]^2 \qquad (C.2)$$

Taking the gradient of Q_{ww} with respect to C and setting the it to zero, we have

$$-2\sum_{(m,n)\in B} s_1(m,n)s(m,n) + 2\hat{C}' \sum_{(m,n)\in B} s_1(m,n)s_1^t(m,n) = 0$$

or

$$\hat{C}' = [\sum_{(m,n)\in B} s_1(m,n)s_1^t(m,n)]^{-1} \sum_{(m,n)\in B} s_1(m,n)s(m,n) \qquad (C.4)$$

If we regard the summations in this expression as expectation approximation, then equation (C.4) may be written as

$$\hat{C}' \cong E[s_1(m,n)s_1^t(m,n)]^{-1} E[s_1(m,n)s(m,n)] \qquad (C.5)$$

and equation (C.2) as

$$Q_{ww} = E[s(m,n) - \hat{C}' s_1(m,n)]^2$$

$$= E[\{s(m,n) - \hat{C}' s_1(m,n)\}\{s(m,n) - \hat{C}' s_1(m,n)\}'] \qquad (C.6)$$

which are identical to equations (5.7) and (5.8), respectively.

We note here that in the actual situation we have the observed image $r(m,n)$ rather than the original one, $s(m,n)$, which is not available. This raises the question of bias in the estimate of the model coefficients C. Kaufman, *et al.* [37], show that this can be corrected and compensated for by the following expression

$$\hat{C}' = [E\{r_1^t(m,n)r_1(m,n) - IN_B Q_v\}]^{-1} E\{r_1^t(m,n)r(m,n)\} \qquad (C.7)$$

where N_B represents the number of pixels in the data and $\boldsymbol{Q}_v$ is the covariance of the observation noise.

APPENDIX D

DERIVATIONS OF EQUATIONS IN CHAPTER 6

Multichannel Power Spectrum of the Observed Image: Equation (6.19)

In this section, we will give the derivation of equation (6.19) which describes the power spectrum of the ideal image in the multichannel case. Note that this is a generalization to the derivation in Appendix B. From equation (6.18) we have the autocorrelation components $P_{r_p r_q}(i, j)$ as

$$
\begin{aligned}
P_{r_p r_q}(i, j) &= E[r_p(m,n) r_q(m+i, n+j)] \\
&= \int_{\Re_p(\Theta)} \int_{\Re_q(\Theta)} h(\xi, \eta) h(\psi, \zeta) P_{s_p s_q}(i - \xi + \psi, j - \eta + \zeta) d\xi d\eta d\psi d\zeta \\
&\quad + \delta(i, j) \sigma_{v_p} \sigma_{v_q}
\end{aligned}
\tag{D.1}
$$

Taking the DFT of this expression results in

$$S_{r_p r_q}(k,l) = DFT\{P_{r_p r_q}(i,j)\}$$

$$= \int_{\Re_p(\Theta)} \int_{\Re_q(\Theta)} h_p(\xi,\eta) h_q(\psi,\zeta) \sum_k \sum_l P_{s_p s_q}(i-\xi+\psi, j-\eta+\zeta)$$

$$.\exp\left[-j\frac{2\pi}{N}k(i-\xi+\psi)\right]\exp\left[-j\frac{2\pi}{N}l(j-\eta+\zeta)\right]d\xi d\eta d\psi d\zeta$$

$$+\sigma_{v_p}\sigma_{v_q} \qquad (D.2)$$

which can be rearranged as

$$S_{r_p r_q}(k,l) = \int_{\Re_p(\Theta)} \int_{\Re_q(\Theta)} h_p(\xi,\eta) h_q(\psi,\zeta) \sum_k \sum_l P_{s_p s_q}(i,j)\exp\left[-j\frac{2\pi}{N}ki\right]\exp\left[-j\frac{2\pi}{N}lj\right]$$

$$.\exp\left[-j\frac{2\pi}{N}k(\psi-\xi)\right]\exp\left[-j\frac{2\pi}{N}l(\zeta-\eta)\right]d\xi d\eta d\psi d\zeta + \sigma_{v_p}\sigma_{v_q} \qquad (D.3)$$

Simplifying, we get

$$S_{r_p r_q}(k,l) = S_{s_p s_q}(k,l)\left\{\int_{\Re_p(\Theta)} h_p(\xi,\eta)\exp\left[j\frac{2\pi}{N}k\xi\right]\exp\left[j\frac{2\pi}{N}l\eta\right]d\xi d\eta\right.$$

$$\left.\int_{\Re_q(\Theta)} h_q(\psi,\zeta)\exp\left[-j\frac{2\pi}{N}k\psi\right]\exp\left[-j\frac{2\pi}{N}l\zeta\right]d\psi d\zeta\right\} + \sigma_{v_p}\sigma_{v_q} \qquad (D.4)$$

Which reduces to

$$S_{r_p r_q}(k,l) = S_{s_p s_q}(k,l)H_p^*(k,l)H_q(k,l) + \sigma_{v_p}\sigma_{v_q}$$

$$(D.5)$$

as in equation (6.19)

Multichannel Power Spectrum of the Ideal Image, Equation (6.21)

We will give here the derivation of equation (6.21)

$$s_p(m,n) = \sum_{q=1}^{N} \sum_{R_{pq}} c^{pq}(k,l)\, s_q(m-k,n-l) + w_p(m,n)$$ (D.6)

We may write the autocorrelation function as

$$
\begin{aligned}
P_{s_p s_p}(i,j) &= E[s_p(\xi,\eta)s_p(\xi+i,\eta+j)] \\
&= E[s_p(\xi,\eta)\{\sum_q \sum_{(k,l)\in \mathbf{S}_c} c^{pq}(k,l)s_p(\xi+i-k,\eta+j-l) + w_p(\xi+i,\eta+j)\}] \\
&= E[\sum_q \sum_{(k,l)\in \mathbf{S}_c} c^{pq}(k,l)s_p(\xi,\eta)s_p(\xi+i-k,\eta+j-l)] \\
&\quad + E[s_p(\xi,\eta)w_p(\xi+i,\eta+j)]
\end{aligned}
$$ (D.7)

which can be expanded as

$$
\begin{aligned}
P_{s_p s_p}(i,j) = E\Bigg[&\sum_{(k,l)\in \mathbf{S}_c} c^{p1}(k,l)s_p(\xi,\eta)s_1(\xi+i-k,\eta+j-l) \\
&+ \sum_{(k,l)\in \mathbf{S}_c} c^{p2}(k,l)s_p(\xi,\eta)s_2(\xi+i-k,\eta+j-l) \\
&\quad \cdots \\
&+ \sum_{(k,l)\in \mathbf{S}_c} c^{pN}(k,l)s_p(\xi,\eta)s_N(\xi+i-k,\eta+j-l) \Bigg] \\
&+ E[s_p(\xi,\eta)w_p(\xi+i,\eta+j)]
\end{aligned}
$$ (D.8)

$$P_{s_p s_p}(i,j) = \left[\sum_{(k,l) \in \mathbf{S}_c} c^{p1}(k,l) P_{s_p s_1}(i-k, j-l) \right.$$

$$+ \sum_{(k,l) \in \mathbf{S}_c} c^{p2}(k,l) P_{s_p s_2}(i-k, j-l)$$

$$\cdots$$

$$\left. + \sum_{(k,l) \in \mathbf{S}_c} c^{pN}(k,l) P_{s_p s_N}(i-k, j-l) \right]$$

$$+ \sigma_p^2 \delta(i,j)$$

(D.9)

Taking the DFT of this expression, we have

$$S_{s_p s_p}(k,l) = DFT[P_{s_p s_p}(i,j)]$$

$$S_{s_p s_p}(i,j) = \sum_{m,n} C^{p1}(m,n) S_{s_p s_1}(i-m, j-n)$$

$$+ \sum_{m,n} C^{p2}(m,n) S_{s_p s_2}(i-m, j-n)$$

$$\cdots$$

$$+ \sum_{m,n} C^{pN}(m,n) S_{s_p s_N}(i-m, j-n) + \sigma_p^2$$

(D.10)

where

$$\sum_{m,n} C^{pq}(m,n) = DFT\{ \sum_{(k,l) \in \mathbf{S}_c} c^{pq}(k,l)\}$$

(D.11)

Thus, we may express equation (D.10), as in equation (6.21), as

$$S_{s_p s_p}(k,l) = \frac{\sigma_{w_p}^2 + \sum\limits_{q, q \neq p} \sum\limits_{(m,n)} C^{pq}(m,n) S_{s_p s_q}(k,l)}{\left| 1 - \sum\limits_{(m,n)} C^{pp}(m,n) \right|^2}$$

(D.12)

174